This is to certify that the

dissertation entitled

A KINETIC MODEL OF THE OXIDIZING SIDE
OF CHLOROPLAST PHOTOSYSTEM II USING
TIME RESOLVED EPR SPECTROSCOPY
presented by

Christine Thompson Yerkes

has been accepted towards fulfillment
of the requirements for

Ph.D. degree in Chemistry

Gerald T. Babcock
Major professor

Date Aug 27, 1982

A KINETIC MODEL OF THE OXIDIZING SIDE OF CHLOROPLAST PHOTOSYSTEM II USING TIME RESOLVED EPR SPECTROSCOPY

By

Christine Thompson Yerkes

A DISSERTATION

Submitted to
Michigan State University
in partial fulfillment of the requirements
for the degree of

DOCTOR OF PHILOSOPHY

Department of Chemistry

1981

ABSTRACT

A KINETIC MODEL OF THE OXIDIZING SIDE OF CHLOROPLAST PHOTOSYSTEM II USING TIME RESOLVED EPR SPECTROSCOPY

By

Christine Thompson Yerkes

This is a study of the reduction kinetics of an EPR detectable free-radical arising from the photo-induced oxidation of Z, the primary donor to the Photosystem II (PS II) reaction center chlorophyll, P680. The rise time of the Z^{+} radical, corresponding to its oxidation by $P680^{+}$, cannot be resolved by conventional EPR spectroscopy but its decay kinetics become accessible upon inhibition of the water oxidizing reaction.

We have observed a strong pH dependence in the reduction rate of Z^{+} by ascorbate. It is hypothesized that the reaction rate between Z^{+} and anionic donors is mediated by the negative membrane potential, arising from charged membrane bound groups, near Z. This has been tested by altering the surface potential, and so the reaction rate, by changing the ionic strength of the medium. Cationic detergents, which modify the outer membrane surface charge density by adsorption to the membrane, show no effect on

the kinetics of $Z^{+\cdot}$ reduction by anionic donors. It is concluded that the mediating potential arises from the inner membrane surface.

The re-oxidation of the primary stable PS II acceptor, Q, by anionic oxidants has been shown to depend on the outer membrane surface potential. Through use of the Guoy-Chapman diffuse double layer model, the magnitude of both the inner and outer membrane surface potentials have been calculated. Under dark adapted conditions ($\Delta pH=0$ in bulk phases) it is estimated that a trans-membrane surface charge asymmetry exists, giving rise to a static electric field across the membrane. This field is of an orientation and magnitude to stabilize the forward charge separation reaction ($P680^{+}Q^{-}$) over the deleterious back reaction by a factor of two.

Addition of low (mM) concentrations of Ca^{2+} to the medium leads to a non-surface charge enhancement in the $Z^{+\cdot}$ decay rate. Lower concentrations (μM) of Mn^{2+} lead to a similar enhancement, although mechanisms appear to be different. These results are discussed in terms of divalent cation stabilization or activation of a high potential donor to PS II, possibly cytochrome b_{559}. Finally, the effects of ADRY reagents on $Z^{+\cdot}$ kinetics are explored.

To My Parents

ACKNOWLEDGEMENTS

I would like to thank the technical staff in the Chemistry Department for their invaluable assistance with this project. I also owe special thanks to my fellow lab members, and most especially Professor Jerry Babcock, for making my years at Michigan State as rewarding and enjoyable as they were.

TABLE OF CONTENTS

Chapter Page

LIST OF TABLES. . . . . .

LIST OF FIGURES. . . . . .

I. INTRODUCTION. 1

A. Models of Photosystem II - Energetics and Kinetics. 1

B. Experimental Approaches to the Oxygen Evolving System. 15

1. Oxygen and proton evolution. 15

2. Prompt Fluorescence. 16

3. Delayed Fluorescence. 18

4. Absorption Changes. 19

5. Magnetic Resonance. 20

a. Manganese Measurements. 20

b. Kinetics. 22

II. MEMBRANE SURFACE CHARGE EFFECTS IN PHOTOSYSTEM II - OXIDATION OF CHARGED ELECTRON DONORS. 23

A. Introduction. 23

B. Materials and Methods. 29

1. Kinetic EPR Instrumentation. 29

2. Spinach and Chloroplast Suspensions. 36

3. Experimental Protocol. 37

C. Results. 38

D. Discussion. 61

Chapter Page

III. SURFACE AND CHARGE ASYMMETRY IN PHOTOSYSTEM II. . .71

A. Introduction. 71

B. Materials and Methods. 72

1. Kinetic EPR Instrumentation and Experimental Protocol. 72

2. Fluorescence Instrumentation and Experimental Protocol. 72

3. Calculation of Membrane Surface Charge Density. 76

C. Results. 81

D. Discussion. 89

IV. CHARACTERIZATION OF AN ENDOGENOUS DONOR TO PHOTOSYSTEM II. 99

A. Introduction. 99

B. Materials and Methods. 101

1. Kinetic EPR Instrumentation. 101

2. Spinach and Chloroplast Suspensions. . . . 107

3. Potential Measurements. 108

C. Results. 108

1. Reducing Conditions. 108

a. Ionic Effects. 108

b. Potential Effects. 139

2. Oxidizing Conditions. 143

D. Discussion. 148

REFERENCES. 154

LIST OF TABLES

Table | Page

1. Rate Constants for the Reductions of Z^{+} by Exogenous Electron Donors. 42

2. Selected Values of Thylakoid Surface Charge Densities. 90

LIST OF FIGURES

Figure — Page

1. The basic elements of the Z-scheme, two light reaction hypothesis for green plant photosynthesis. Vertical arrows refer to changes in relative reducing potential. Abbreviations: Z, the primary donor to PS II; P680 The PS II reaction center; Ph, the primary acceptor of PS II; Q, the primary stable acceptor of PS II; PQ, plastoquinone; cyt f, cytochrome f; PCy, plastocyanin; P700, the PS I reaction center; X, the primary acceptor of PS I; Fd, ferredoxin; Fd-NADP, ferredoxin NADP reductase. 2

2. A representation of the thylakoid membrane showing asymmetry, including membrane surface charge. 8

3 EPR spectra of Tris-washed chloroplasts during (a) and after (b) illumination. Field set = 3365 G, scan range = 100 G, modulation amplitude = 5G, power = 20 mW. 26

4. Circuit diagram for diode opto-isolator. 32

5. Block diagram of kinetic EPR instrumentation. . . . 34

6. The effect of exogenous donors on EPR Signal IIF decay kinetics. All experiments were performed on Tris-washed chloroplasts to which 5×10^{-4} M NADP, 10^{-4} M EDTA and 20 µg ferredoxin/ml suspension had been added. The field setting is 3353 G, the modulation amplitude is 5 G and the power is 20 mW. The scans were run at 6 s intervals. (a) pH = 7.5, time constant = 10 ms, 64 scans averaged. (b) 2×10^{-3} M ascorbate, time constant = 3 ms, 120 scans averaged. (c) 2×10^{-3} M ascorbate, time constant = 3 ms, 120 scans averaged. (d) 10^{-5} M Hydroquinone and 2×10^{-3} M ascorbate, time constant = 3 ms, 200 scans averaged. 39

Figure Page

7. Donor concentration dependence of the Signal IIf pseudo-first order decay constant in Tris-washed chloroplasts at pH = 7.5, except where noted, with a 3 ms time constant and 120 scans averaged. 43

8. pH dependence of the Signal IIf pseudo-first order decay constant in Tris-washed chloroplasts with 2 mM ascorbic acid as the exogenous donor. The experimental conditions are described in Figure 7. 49

9. Correlation between observed (k_{obs}) and calculated (k_{calc}) second order rate constants for models of Z^{+} reduction by ascorbic acid. (a) neutral ascorbic acid, H_2Asc, as the reducing agent; (b) H_2Asc and the mono-anion, $HAsc^{-}$, as the reducing agents; (c) same as (b) but a pH dependent ΔpH across the thylakoid membrane, $\Delta pH = 0.7$ at pH 5.5, $\Delta pH = 2.0$ at pH = 8.5. (d) same as (b) but k_2, associated with the reduction of Z^{+} by $HAsc^{-}$ as a function of pH, ranging from 2.2×10^3 M^{-1} s^{-1} at pH = 5.5 to 8×10^2 M^{-1} s^{-1} at pH = 8.5. 51

10. Salt concentration dependence of Signal IIf second order decay constant, k_2, at pH = 8.0 and 2 mM ascorbate. Chloroplasts were incubated in the salt solution for 5 min prior to initiation of the experiment. Inset: salt incubation time dependence of Signal IIf second order decay constant, k_2. The experimental conditions are described in Figure 7. 55

11. Cationic detergent activity dependence of the Signal IIf second order decay constant, k_2, at pH 8.0 with 2 mM ascorbate. The experimental conditions are described in Figure 7. 59

12. Effect of sonication of the Signal IIf deacy half-time at pH = 8.0 with 2 mM ascorbate. Other conditions are described in Figure 7. . . . 62

13. A plot of the inverse squre root of cation activity versus the natural log of k_2 taken from data in Figure 10. 66

14. Circuit diagram for Xenon flash lamp. 73

Figure Page

15. Sample traces from fluorescence induct ion experiments showing the determination of the three quantities, F_∞, F_0 and F_t. 77

16. Effect of KCl on the reduction of Z^+ by $HAsc^-$ (2 mM) in Tris-washed chloroplasts, pH = 8.0, instrument time constant = 3 ms, 75 scans averaged. 83

17. Plot of equation 3.17 with $Z_i = 1$, (see text) for EPR experiments (left) and fluorescence experiments (right), at pH = 8.0. The salt concentration was adjusted by addition of the monovalent salt, KCl, in both series of experiments. 86

18. A schematic representation of the thylakoid membrane and its associated surface potential (a) in dark adapted chloroplasts ($pH_{in} = pH_{out}$) and (b) after illumination ($pH_{in} < pH_{out}$). 95

19. Circuit diagram of kinetic EPR triggering circuit. 103

20. Light induced cavity transient (a) sample in cavity, (b) empty cavity, (c) phase angle 180° out of phase (d) 200 mW power, (e) 20 mW power, (f) light blocked from cavity but flash lamp firing. Instrument time constant 100 μs, 100 scans averaged, 5 G modulation amplitude, 20 mW power unless otherwise noted. 105

21. Effect of Mg^{2+} (top left) and Ca^{2+} (bottom left) on reduction of Z^+ in Tris-washed chloroplasts, pH = 8.0, 2 mM $HAsc^-$, instrument time constant 1 ms, 150 scans averaged. Effect of Mg^{2+} (top right) and Ca^{2+} (bottom right) on the oxidation of Q^- by $Fe(CN)_6^{3-}$ in Tris-washed chloroplasts, pH = 8.0. 109

22. Effect of $HAsc^-$ (2 mM, pH = 8.0) on (a) Tris-washed chloroplasts alone, (b) with 1 mM EDTA, (c) with 50 mM $CaCl_2$. Instrument time constant = 1 ms, 150 scans averaged. 113

23. Effect of instrument time constant on Signal IIf decay traces. (a) instrument time constant = 2 ms and (b) 10 ms. Power = 20 mW, 100 scans averaged, Tris-washed chloroplasts, 2 mM $HAsc^-$ (pH = 8.0). 115

Figure Page

24. Effect of flash frequency on the decay of Signal IIf (a) 1 flash every second, (b) 1 flash every 10 seconds, 1 ms time constant, 20 mW power, Tris-washed chloroplasts, 2 mM $HAsc^-$ (pH = 8.0). 119

25. Experimental points (open circles) taken from Figure 22 fitted to Eqs. 4.1 and 4.2 as indicated in the figure. 122

26. Effect of Mn^{2+} concentration on the decay kinetics of Signal IIf in Tris-washed chloroplasts, 2 mM $HAsc^-$ (pH = 8.0). (a) addition of 1 mM EDTA, (b) no addition, (c) addition of 10 μM Mn^{2+} and (d) addition of 20 μM Mn^{2+}. Instrument time constant = 200 μs, 250 scans averaged. 124

27. A semi-log plot of Figure 26, showing the biphasic nature of the decay at low Mn^{2+} concentrations and how the decay varies with Mn^{2+} concentrations. 127

28. A plot of the observed decay half-time of Signal IIf versus concentration of Ca^{2+}, at pH = 8.0, 2 mM $HAsc^-$, 400 μM EDTA. 129

29. A re-plotting of the data in Figure 28 as decay half-time versus inverse Ca^{2+} concentration. 132

30. A plot of observed decay half-time versus inverse concentration of CCCP. 135

31. The effects of 50 mM KI on the decay kinetics of Tris-washed chloroplasts (pH = 8.0) (a), with 1 mM EDTA (b), with 50 mM Ca^{2+} (c) and with 2 mM $HAsc^-$ (d) as compared to 2 mM $HAsc^-$ alone (e). Time constant = 1 ms, 150 scans averaged. .137

32. The effect of suspension potential (2 mM $HAsc^-$, pH = 8.0) on the decay kinetics of Signal IIf with (a,b) 50 mM Ca^{2+} and (c,d) 1 mM EDTA. time constant = 1 ms, 150 scans averaged. 140

33. The effect of pH on the decay kinetics of Signal IIf in Tris-washed chloroplasts with 100 μM DCMU, 10 mM $Fe(CN)_6^{3-}$ and (a) 50 mM Ca^{2+}, 50 mM Mg^{2+} and (c) 8 μM CCCP and 50 mM Mg^{2+} (except where otherwise noted). Time constant = 1 ms, 150 scans averaged. 146

I. INTRODUCTION

A. Models of Photosystem II - Energetics and Kinetics

Although photosynthetic oxygen evolution was first described by Priestley over two hundred years ago, the molecular mechanism for the process remains unexplained. The role of oxygen evolution relative to the other light driven reactions in photosynthesis is described in Figure 1, a schematic representation of the overall process of higher plant photosynthesis. This model can be divided into two photochemical systems: Photosystem I (PS I) associated with the reduction of NADP and Photosystem II (PS II) associated with the oxidation of water. Light harvesting components, called antenna pigments, transmit energy via both exciton and Forster transfer [1] to specialized chlorophyll molecules, called reaction centers, which undergo photooxidation. The two forms of chlorophyll, antenna pigments and reaction centers, exist in a ratio of roughly four hundred to one [2]. Light energy absorbed by the light harvesting complex of PS II is trapped at the reaction center, P680, so called because of its absorption maximum at 680 nm. P680 is a specialized chlorophyll molecule. Early EPR

Figure 1 -- The basic elements of the Z-scheme, two light reaction hypothesis for green plant photosynthesis. Vertical arrows refer to changes in relative reducing potential. Abbreviations: Z, the primary donor to PS II; P680, the PS II reaction center; Ph, the primary acceptor of PS II; Q, the primary stable acceptor of PS II; PQ, plastoquinone; cyt f, cytochrome f; PCy, plastocyanin; P700, the PS I reaction center; X, the primary acceptor of PS I; Fd, ferredoxin; Fd-NADP, ferredoxin NADP reductase.

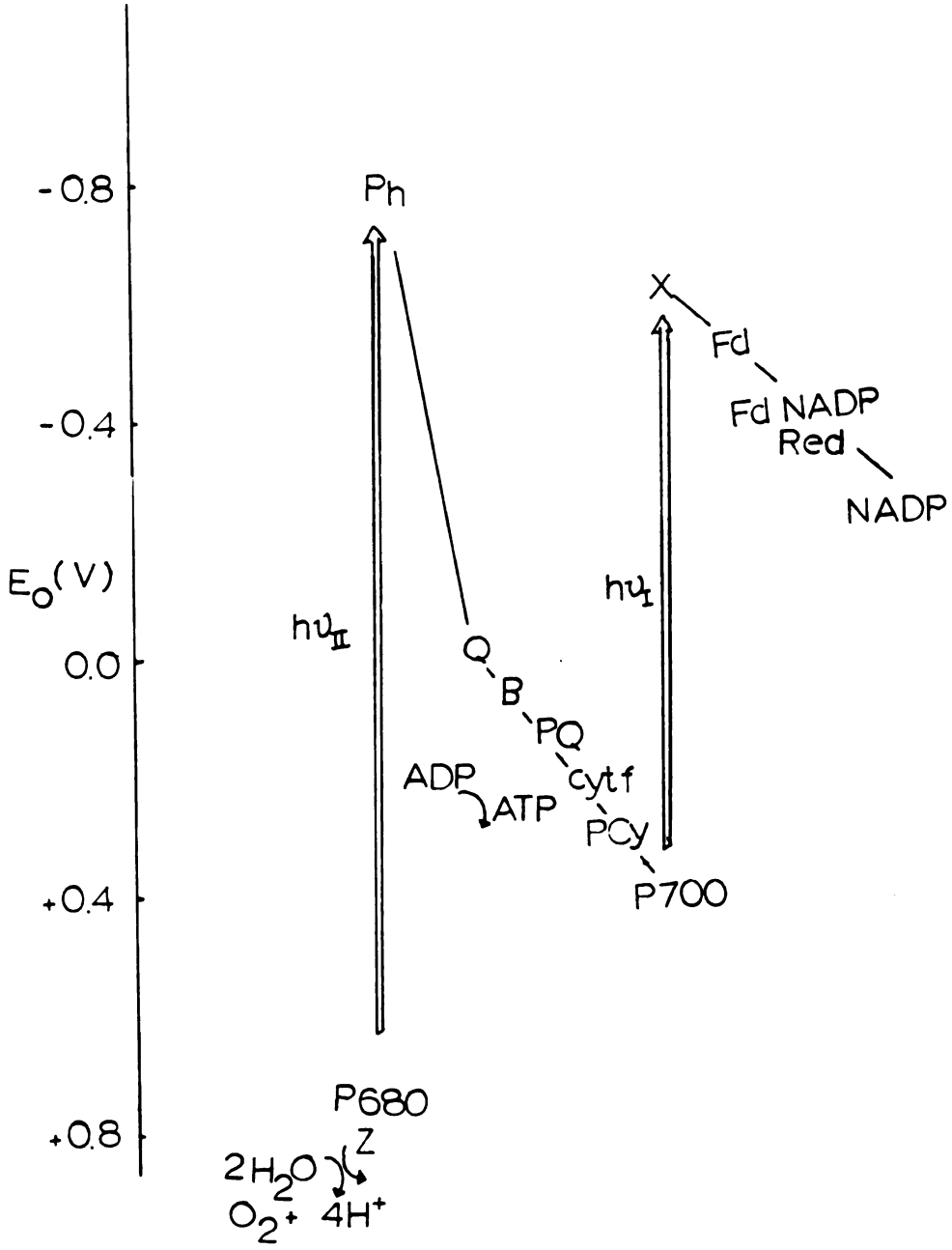
-0.8
-0.4
E_o(V)
0.0
+0.4
+0.8
Ph
X
Fd
Fd NADP
Red
NADP
$h\nu_I$
$h\nu_{II}$
Q
B
PQ
cytf
PCy
P700
ADP
ATP
P680
Z
$2H_2O$
O_2 + $4H^+$

FIGURE 1

studies of a signal attributed to $P680^+$ led to the designation of P680 as a chlorophyll dimer [3] in order to explain the narrow line width observed *in vivo*. Recent work *in vitro* has shown that liganded monomeric chlorophyll can exhibit unusually narrow linewidths [4] and measurement of the zero field splitting parameters of the P680 triplet *in vivo* by Rutherford and coworkers [5] shows that they are very similar to those reported for monomeric chlorophyll, but not conclusively so. Light induced charge separation at this reaction center leads to the oxidation of P680, generating $P680^+$ with a mid-point potential greater than +1.0 V, and to the transient reduction of a pheophytin molecule [6] with a mid-point potential of -0.61 V. The involvement of a pheophytin molecule as the primary electron acceptor of PS II further strengthens the analogy between higher plant PS II and the photosynthetic bacterial reaction center, in which bacteriopheophytin has been shown to be an early electron acceptor [7]. The photooxidation of pheophytin is followed by the reduction of the primary stable electron acceptor, Q, probably a semi-quinone [8] with a potential of about 0.0 V. A second quinone, B [9], a two electron acceptor, connects Q with a pool of plastoquinone molecules. The reduction of $P680^+$ leads to the formation of a strong oxidant $Z^{+\cdot}$ ($E_m' \sim +0.8$ V) which is as yet unidentified chemically, capable of oxidizing

water to molecular oxygen, and which interfaces the reaction center chlorophyll with the enzymatic apparatus actually responsible for oxidizing water.

Similarly, light energy absorbed by the antenna pigments of PS I is trapped at a reaction center containing another photooxidizable chlorophyll molecule, P700, with an absorption maximum around 700 nm. Charge separation at the PS I reaction center leads to the oxidation of P700 to $P700^+$ ($E_m' \geq -4.0$ V) and to the reduction of a primary electron acceptor, X ($E_m' \sim -0.6$ V). The reduced form of Q in PS II and the oxidized form of P700 in PS I are re-oxidized and re-reduced as a result of electron transfer along the electron transport chain connecting the two photosystems. The net result of the photoexcitation of these two photosystems is the transfer of electrons from water to the species X which then mediates the reduction of NADP. This links the oxidation of water to the formation of NADPH, a species used to fuel the enzyme cycles associated with the assimilation of carbon dioxide in the dark, exothermic reactions of photosynthesis.

An important property of the photosynthetic light reactions that is not evident from Figure 1 is their vectorial nature, a factor crucial to the formation of ATP from ADP (phosphorylation), a second high energy product of these reactions. The photosynthetic organelle

of higher plant photosynthesis is the chloroplast. The pigments and enzymes required for the light dependent reactions are localized in the membranes of flattened sacks within the chloroplast called thylakoids. The thylakoid membrane, forming as it does a closed vesicle, separates two chemically different environments, the outside or matrix from the inside or loculus. The distribution of the photosynthetic components within the membrane lipid bi-layer is asymmetric, giving rise to a directionality in the electron flow and proton transport. As required by Mitchell's chemiosmotic model [10], electron and proton carriers alternate in the reaction sequence. The transmembrane electron transport is carried out by the reaction center, P680, and the primary acceptor, pheophytin. The proton carrier on the reducing side of PS II is the plastoquinone pool, non-membrane bound plastoquinone molecules associated with the bound quinones, Q and B. Plastoquinone receives electrons from B, a two electron donor, binds protons from the outer thylakoid volume and, in its fully reduced form, diffuses through the membrane releasing protons to the inner thylakoid volume and donating electrons to PS I. Proton transport on the oxidizing side of PS II results from the release of protons to the inner volume by the S_n complex which mediates the oxidation of water. These asymmetric electron and proton transport reactions result in both charge ($\Delta\psi$) and proton (ΔpH) gradients across the

photosynthetic membrane, which ultimately provide the free energy for ATP synthesis [10,11]. Figure 2 is a representation of the thylakoid membrane which incorporates membrane asymmetry in a schematic manner. The exact placement of the components is an area of active research, making the arrangement shown in Figure 2 tentative. Only the components pertinent to the understanding of PS II have been included. Also represented in the figure is membrane surface charge in the vicinity of PS II; the relevance of the surface charge asymmetry to PS II is the subject of a later section of this work.

Of the two light harvesting, charge separating systems, the understanding of PS II has evolved much more slowly than that of PS I. Although knowledge of the electron transfer pathways and the photochemical reaction remains incomplete, the following model of the PS II reaction sequence has been developed:

$$\text{chl a} + h\nu \longrightarrow \text{chl a}^{*} \qquad (1.1)$$

Light absorption by antenna chlorophyll

$$\text{chl a}^{*} + \text{P680} \longrightarrow \text{chl a} + \text{P680}^{*} \qquad (1.2)$$

Transfer of excitation energy from the antenna chlorophyll to the reaction center

$$\text{P680}^{*} + \text{Ph} \longrightarrow \text{P680}^{+} + \text{Ph}^{-} \qquad (1.3)$$

Charge separation at the reaction center

Figure 2 -- A representation of the thylakoid membrane showing component asymmetry, including membrane surface charge.

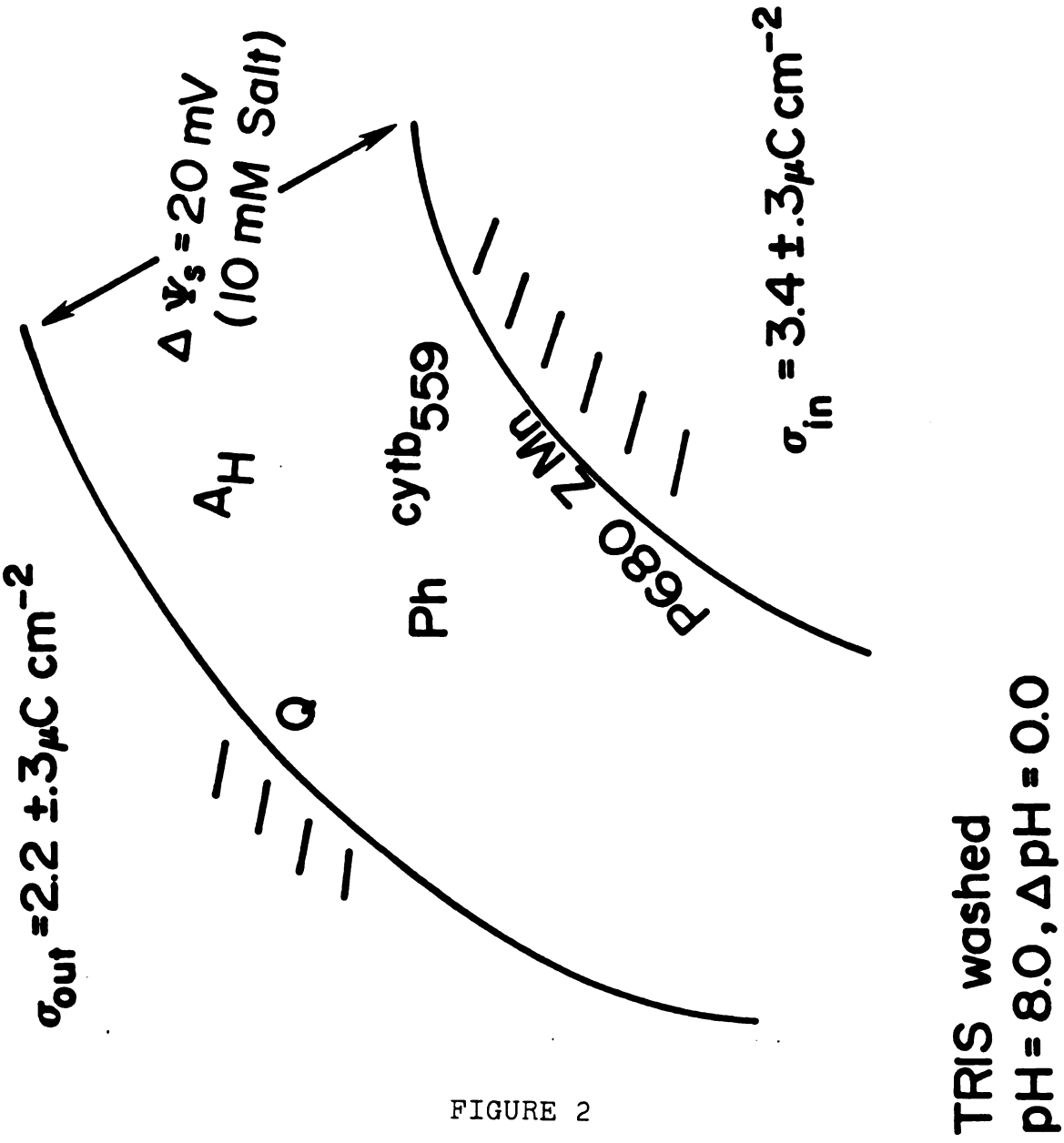
σ_{out} = 2.2 ± .3μC cm^{-2}
Q
A_H
Δ Ψ_s = 20 mV
(10 mM Salt)
Ph
cytb$_{559}$
P680 ZM
σ_{in} = 3.4 ± .3μC cm^{-2}
TRIS washed
pH = 8.0, ΔpH = 0.0

FIGURE 2

$$P680^{+} + Ph^{-} + Q \longrightarrow P680^{+} + Ph + Q^{-} \qquad (1.4)$$

Electron transfer to the stable primary acceptor

$$Z + P680^{+} + Q^{-} \longrightarrow Z^{+}\cdot + P680 + Q^{-} \qquad (1.5)$$

Electron transfer from Z to P680

$$Z^{+}\cdot + Q^{-} + B \longrightarrow Z^{+}\cdot + Q + B^{-} \qquad (1.6)$$

electron transfer to a secondary acceptor, B, linked to the plastoquinone pool

$$S_n + Z^{+}\cdot \longrightarrow S_{n+1} + Z \qquad (1.7)$$

"charge accumulation", n = 0,1,2,3

$$2\ H_2O + S_4 \longrightarrow 4H^{+} + O_2 + S_0 \qquad (1.8)$$

oxygen evolution.

These reactions, except 1.1 and 1.2, although written as bimolecular, are essentially intramolecular. Reactions 1.1, 1.2 and 1.3 occur in picoseconds, 1.4 in less than 20 nanoseconds, 1.5 in less than a microsecond and 1.6 with a half time of about 600 microseconds. A brief description of 1.7 and 1.8 follows.

Measurements by Joliot et al. [12,13] and Kok et al. [14] of oxygen evolution produced by short (duration less than 10 microseconds) saturating flashes show that the amount of oxygen produced by chloroplasts that have been in darkness for 15 minutes (dark adaptation) is

different for each flash. Little or no oxygen is produced by the first two flashes and a maximum is observed after the third flash. A continued series of flashes gives a damped oscillation with a period of four when oxygen yield is plotted against flash number. These results have been interpreted by Kok [14] in the following scheme

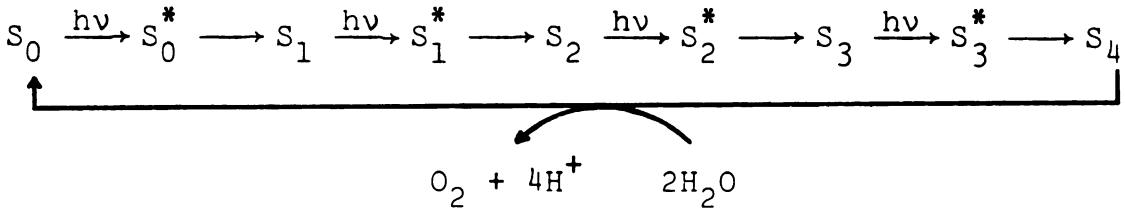

The steps $S_n \longrightarrow S_n^*$ represent photoexcitation of the system and the steps $S_n^* \longrightarrow S_{n+1}$ are the subsequent dark relaxation steps. Rough estimates of the rates of these reactions have been made by Babcock et al. [15] as follows:

$$Z^{+}\cdot + S_0 \longrightarrow Z + S_1 \qquad t_{1/2} \lesssim 100\ \mu s$$

$$Z^{+}\cdot + S_1 \longrightarrow Z + S_2 \qquad t_{1/2} \lesssim 100\ \mu s$$

$$Z^{+}\cdot + S_2 \longrightarrow Z + S_3 \qquad t_{1/2} \approx 400\ \mu s$$

$$Z^{+}\cdot + S_3 \longrightarrow Z + S_4 \qquad t_{1/2} \approx 1\ \mu s$$

$$S_4 + 2H_2O \longrightarrow S_0 + 4H^+ + 4e^- + O_2 \qquad t_{1/2} < 1\ ms$$

Again, these reactions are essentially intramolecular. The

kinetics of these charge transfer reactions are slow compared to the 10 μs flash duration, hence the ability of a single flash to promote a single electron transfer. Oxygen evolution occurs after the accumulation of four oxidizing equivalents. The maximum yield of oxygen after the third flash indicates that most of the reaction centers are in the S_1 state after dark adaptation. To account for this observation quantitatively, Kok et al. postulated that both the S_0 and S_1 states are stable in the dark and exist in a ratio of 1 to 3. The damping of the oscillatory pattern arises from "misses", a percentage of failures to produce charge separation at each reaction center (roughly 10% per flash). The possibility of "double hits", more than one reaction center turn-over per flash, also exists and will be explored in more detail later.

Little is known about the oxygen evolution mechanism itself. It has been shown that membrane bound manganese is involved [16,17] as indicated by Figure 2. It has been hypothesized that the charge accumulation reactions correspond to change in the oxidation state of manganese, although this is a matter of current controversy. There have been reports of manganese valence state changes upon illumination [18-20], however, recent work [21] suggests that the manganese monitored in the previous experiments is not that involved in oxygen evolution. Indeed, it

appears as if the idea of "charge accumulation" should be taken as no more than a formalism. This point is emphasized by studies measuring proton release as a function of flash number. Rather than the synchronous release of four protons with the molecule of oxygen on the third flash, as indicated by the Kok model above, a stoichiometry of proton release for the ($S_0 \rightarrow S_1$), ($S_1 \rightarrow S_2$), ($S_2 \rightarrow S_3$) and ($S_3 \rightarrow S_4$) transitions of 1, 0, 1 and 2 has been observed [22]. Thus, the S states most likely represent different chemical intermediates in the oxidation of water to molecular oxygen rather than different valence states of bound manganese. An example of a scheme incorporating the proton release pattern as well as chemical intermediates is shown below.

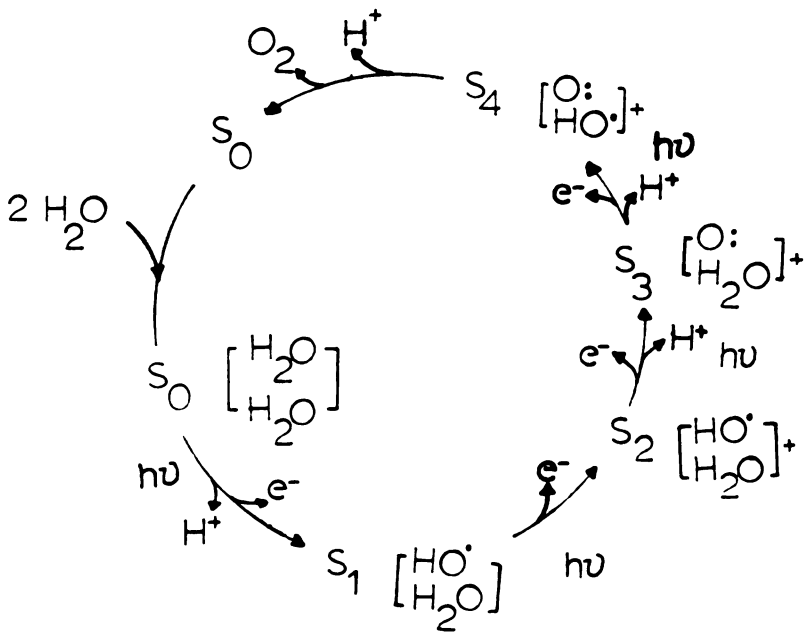

The participation of manganese in water oxidation will be discussed in more detail in a later section.

There remain in Figure 2 two PS II species to be discussed, cytochrome b_{559} and A_H, neither of which has been shown to participate directly in the reactions leading to oxygen evolution under normal experimental conditions. There are two molecules of cytochrome b_{559} per four hundred chlorophyll molecules, one of which has an unusually high mid-point potential ($E_m' \sim +0.38$ V) and is associated with PS II. This mid-point potential can be irreversibly shifted negative by as much as 0.3 V by a number of techniques which also inhibit oxygen evolution. Among these are tris-washing [23], hydroxylamine incubation [24] and addition of chaotropic agents [25]. PS II mediated oxidation of the high potential form of cytochrome b_{559} has been observed at 77 K [26] and a rapid photooxidation and photoreduction have been reported recently in samples containing tetraphenylborate [27]. The ability of a single component to undergo both photooxidation and reduction is a strong indication of cyclic electron flow, in this case, around PS II. This role has been previously suggested for cytochrome b_{559} [28,29] and it is in this context that the cytochrome will be discussed in a later section.

Another component, also implicated in PS II cyclic electron flow, has been described by a number of

researchers [30-36] using a variety of experimental techniques. Each has assigned it a new name so, following the lead of a recent review article [37], it will be referred to here as A_H. It was first seen as an acceptor for PS II, only observable at high potentials (above +0.4 V at pH = 7). The EPR studies by Babcock and Sauer [36] have shown that it can also serve as a donor to PS II, again, at high potentials. Their work has been extended and will be the subject of later sections.

B. Experimental Approaches to the Oxygen Evolving System

The kinetic data and models discussed above are based on results from a variety of experimental techniques. Two useful methods of studying oxygen evolution, because they monitor the actual products of the reaction, are measurements of oxygen and proton release as functions of flash number. The spectroscopic techniques employed include prompt and delayed fluorescence measurements, which provide only indirect detection of membrane component reactions, absorption changes and both nuclear magnetic resonance (NMR) and electron paramagnetic resonance (EPR).

1. Oxygen and proton evolution

The oxygen yield data have been presented as the basis for the Kok model of the S states. One additional oxygen evolution experiment is of particular relevance to the work presented here. Kok and Velthuys [34] measured the effect

of ferricyanide on the yield of oxygen as a function of flash number and interpreted their results as reflecting the presence of a second acceptor (A_H) before the DCMU block. This herbicide, 3-(3,4-dichlorophenyl)-1, 1-dimethylurea, binds to a site on the thylakoid membrane and prevents the reduction of B by Q^-. This effectively stops PS II photochemistry until Q^- is re-oxidized. With the proper redox poise (> +0.4) A_H provides one oxidizing equivalent, in competition with the S states, and can lead to an alteration of the O_2 yield pattern.

The pattern of proton release has been controversial [38,22] but the pattern shown above of 1, 0, 1, 2 is now fairly well accepted and has been supported by pH dependence experiments in which both prompt and delayed fluorescence were used [39].

2. Prompt fluorescence

Fluorescence emission with a quantum yield of about 0.03 is observed in functioning chloroplasts. Duysens and Sweers [40] demonstrated that the reduction and oxidation of Q, the primary stable electron acceptor of PS II, causes a corresponding increase and decrease, respectively, in the fluorescence yield of the antenna chlorophyll. Oxidized Q is associated with low chlorophyll fluorescence, an observation which has led to the assignment of the term "quencher" to the species Q. An additional hypothesis, proposed by Butler et al. [41], on the basis of experiments at 77 K is that not only Q but

also $P680^+$ quenches fluorescence. This postulate explains the low fluorescence yield observed for the P680 Q, $P680^+$ Q^- and $P680^+$ Q states. Immediately after a flash, when the system is in the $P680^+$ Q^- state, the fluorescence yield is low. It will subsequently rise upon re-reduction of $P680^+$ by Z giving Z^+ P680 Q^-, a state with no quenchers. The kinetics of the rise in fluorescence are, therefore, generally interpreted as reflecting the rate of reduction of $P680^+$. Sonneveld et al. [42] have used chlorophyll a fluorescence as a monitor of nanosecond reduction of $P680^+$. They used ruby laser flashes of 15, 30 and 350 ns halftime as both the actinic and measuring beams and found that the $P680^+$ reduction time depends on the flash number. For the first flash in dark adapted chloroplasts, they find a 35 ns reduction time. For the succeeding four flashes, the decay time of $P680^+$ is longer than 35 ns but correlated to the S states. Under steady state conditions, after damping of the period four oscillations, they find a 400 ns reduction time. The chief advantage of this technique is the excellent time resolution. They are, however, problems as well. One must essentially subtract the laser flash profile from the detected radiation and the time range of detection lasts only as long as the flash itself. Additionally, one must take into account the existence of a third fluorescence quencher, C^T, a carotenoid triplet state that is formed by the reaction [39]:

$$P680 + Q^- + C \xrightarrow{h\nu} P680 + Q^- + C^T$$

A variation of this technique includes the use of a continuous low intensity measuring beam, incapable of sustaining photochemistry, in conjunction with a short, intense actinic beam. This allows measurement of fluorescence for times extending beyond the actinic flash duration. For enhanced signal-to-noise, the analytical beam and signal detection can be synchronously modulated, although this imposes a time constant on the system leading to loss of time resolution.

3. Delayed fluorescence

Luminescence or delayed fluorescence, which has a typical quantum yield of 10^{-4} to 10^{-5}, has also been used to study the kinetics of P680 oxidation and reduction. Lavorel [43] has hypothesized that this delayed light arises from the reaction:

$$P680^+ + Q^- \longrightarrow P680^* \; Q \longrightarrow P680 + Q + h\nu$$

The species $P680^*$ is the lowest excited singlet state of P680. Dark regeneration of this state leads to the delayed emission of light. Luminescence intensity is, then, proportional to the concentration of $P680^+ \; Q^-$. Since Q^- is re-oxidized much more slowly than $P680^+$ is re-reduced, the decay rate of the luminescence is proportional to the reduction rate of $P680^+$. One is generally constrained to the microsecond domain in these

experiments because of photomultiplier gating requirements. This does, however, eliminate flash artifacts as well as quenching by C^T which decays in a few microseconds in the dark [44].

An interesting modification to the delayed light experiment is a technique called electrophotoluminescence (EPL) pioneered by Arnold and Azzi [45]. This technique takes advantage of the vectorial nature of the electron transfer reactions. By imposing a laboratory generated electric field after illumination, a dramatic enhancement in the yield of delayed light is observed, presumably because the field has forced recombination of the photoinduced hole and electron. This technique has been used to show that delayed light and EPL are both PS II phenomena, by demonstrating a period of four flash number dependence on the yield [46].

4. Absorption changes

Time resolved optical spectroscopy has been used extensively in photosynthetic research although until recently, no absorption changes attributable to the reaction center of PS II could be observed under physiological conditions. At low temperatures or in the presence of detergents the reduction of photooxidized P680 and re-oxidation of Q^- can be slowed. Floyd et al. [47] observed a bleaching at 680 nm upon illumination with short laser pulses at 77 K. This absorption change decays with a halftime of 4-5 ms after the flash.

Von Gorkom et al. [48] observed the photooxidation of P680 in chloroplasts treated with the detergent deoxycholate and, in the presence of ferricyanide, have found that the reduction of $P680^+$ is slowed to such an extent that an appreciable amount of $P680^+$ can actually be accumulated under conditions of continuous illumination. Recent work done by Van Best and Mathis [49] allows the study of the reduction kinetics of $P680^+$ at physiological temperatures. Their development of a flash absorption photometer with nanosecond time resolution has made this possible. The reaction is monitored not at 680 nm, the absorption maximizing of P680, but at 820 nm, where $P680^+$ absorbs. Following a single flash on dark adapted chloroplasts they have found a fast (30 ns) decay time for $P680^+$, reflecting its reduction by the secondary electron donor, Z. Of all of the optical techniques outlined, this is the only one that directly measures a reaction rate on the oxidizing side of PS II. It is the intent of the work presented here to investigate additional means of collecting data directly from the electron transport system between P680 and the water oxidizing complex.

5. Magnetic resonance

a. Manganese measurements

As discussed in the Model section, photoinduced valence changes in bound manganese have been suggested as a possible mechanism for charge accumulation leading to

water oxidation. Wydryzynski and Sauer [20] have used room temperature EPR to look for such oscillations in manganese valence state. Because the membrane bound manganese is EPR undetectable under their experimental conditions, they have monitored the pattern of manganese released from thylakoid membranes following a rapid temperature shock. They found that the hexaquo Mn^{2+} signal amplitude varied with the number of flashes given the chloroplasts prior to the heat treatment. They interpreted the pattern as indicating that manganese is oxidized by the first two flashes but undergoes a partial reduction on the third. Wydryzynski et al. [18] have used NMR to look for similar oscillations. They have measured the spin lattice relaxation times (T^{-1}) of water protons under a series of experimental conditions and have interpreted the results as arising from photoinduced oxidation state changes of membrane bound manganese. Both the NMR and EPR results have been challenged by Robinson et al. [21,50] who postulate that the changes detected arise from extraneous manganese (i.e., not integral to oxygen evolution) which has been oxidized not by the S_n complex, but by superoxide ion which they have shown to be generated, under aerobic conditions, by acceptors of PS I. Thus, the possibility of photo-induced valence state changes of functional manganese at room temperature remains unresolved.

At cryogenic temperatures, Dismukes and Siderer [51] have reported an EPR signal that they assign to a pair of antiferromagnetically coupled manganese ions in which Mn^{3+} and Mn^{4+} are present. They also report changes in the signal intensity with flash number, again of period four, suggesting a cyclic change in manganese valence state.

b. Kinetics

The observation and characterization of a photo-induced EPR detectable species by Babcock and Sauer [52] and Blankenship et al. [53] provides an excellent tool in studying the complex kinetics of reactions which occur on the oxidizing side of PS II. The EPR active species functions as an intermediate in the electron transport process between P680 and the S states. The signal, called Signal II because of its association with PS II, is observed under a variety of conditions, each exhibiting different kinetic properties. The remainder of the work presented here involves the study and manipulation of Signal II kinetics and the use of these data to make topological and energetic assignments to components associated with the oxidizing side of PS II.

II. MEMBRANE SURFACE CHARGE EFFECTS IN PHOTOSYSTEM II - OXIDATION OF CHARGED ELECTRON DONORS

A. Introduction

At room temperature, two EPR detectable species are generated by illumination of oxygen evolving thylakoid membrane suspensions. The first, Signal I, has rapid rise and decay kinetics and has been established as arising from $P700^+$, the oxidized reaction center of PS I [54,55]. Reports have been made of a transient EPR signal corresponding to $P680^+$ [56,57]. These measurements were necessarily made at low temperatures to bring the P680 reaction rates into the EPR time domain ($\gtrsim$10 μs) and under conditions in which the oxidized PS I reaction center, $P700^+$, is chemically induced and maintained. This allows discrimination between the two, superimposed reaction center signals.

The second room temperature signal, Signal II, is less well characterized. It has line width of about 20G (the difference, in Gauss, between the positive and negative extrema in the derivative spectrum) with partially resolved hyperfine structure. Kohl and coworkers [58-60] have presented evidence, from model compound studies, that

the molecular species giving rise to Signal II may be plastoquinone or a related molecule. Signal II has a fairly slow, light induced rise time ($t_{\frac{1}{2}} \sim 1$ s) and subsequent dark decay time ($t_{\frac{1}{2}} \sim 4$ h). These slow kinetics have led to its designation as Signal IIs [36]. Babcock and Sauer [61] have demonstrated that Signal IIs arises from the oxidation of its precursor by the S_2 or S_3 states. The slow reaction times of IIs take it out of the direct electron transport pathway, leaving its physiological function unresolved.

A much faster component of Signal II has been observed in oxygen evolving chloroplasts by Babcock et al. [15]. It appears to have the same line shape as Signal IIs but very fast kinetics, which has led to designation as Signal IIvf. Its position on the oxidizing side of PS II is shown below:

$$P680 \longleftarrow Z \longleftarrow Sn \quad \left(\begin{matrix} 2H_2O \\ O_2 + 4H^+ \end{matrix} \right.$$

After photooxidation of P680, an intermediate, Z, donates an electron to reduce $P680^+$ and becomes EPR detectable as the $Z^{+\cdot}$ free-radical (Signal IIvf). Thus, the rise time of the EPR signal should correspond to reduction time of $P680^+$ by Z. The decay of the EPR signal corresponds to the reduction of $Z^{+\cdot}$, in this case, by the S_n complex. Z has been proposed as the primary donor to P680, although

its measured rise time of 20 μs ± 10 μs [62] is far too slow to correspond to the measured reduction times of $P680^+$ as discussed in Section I. It has a decay half-time of about 700 μs under steady state conditions. In dark adapted samples, the decay time varies as a function of flash number, as expected if it were reduced by the S_n complex. The decay times were noted in Section I.

Inhibition of oxygen evolution by incubation in alkaline Tris-buffer (Tris-washing) activates a component of Signal II not observed in oxygen evolving chloroplasts, Signal IIf, which exists in a 1:1 ratio with the slower decaying Signal IIs [52]. Figure 3 shows spectra of Tris-washed chloroplasts during [a] and after [b] illumination. Upon darkening, Signal I [I] decays rapidly while the behavior of the Signal II species is noted in the figure. The light induced signal again arises from a component on the water side of PS II. The reaction sequence in inhibited chloroplasts is shown below.

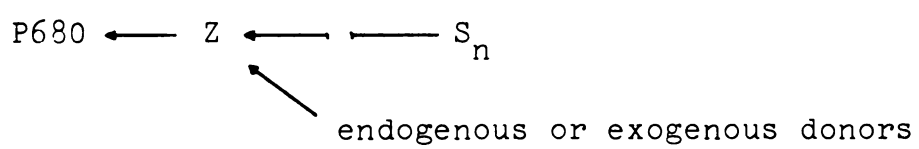

The physiological pathway between Z and S_n can be blocked by a number of inhibitory treatments, among them, tris-washing, heating, aging, incubation in hydroxylamine or addition of chaotropic agents. Under these conditions the ultimate reducing agent for $P680^+$ is not water, but

Figure 3 -- EPR spectra of Tris-washed chloroplasts during (a) and after (b) illumination. Field set = 3365 G, scan range = 100 G, modulation amplitude = 5 G, power = 20 mW.

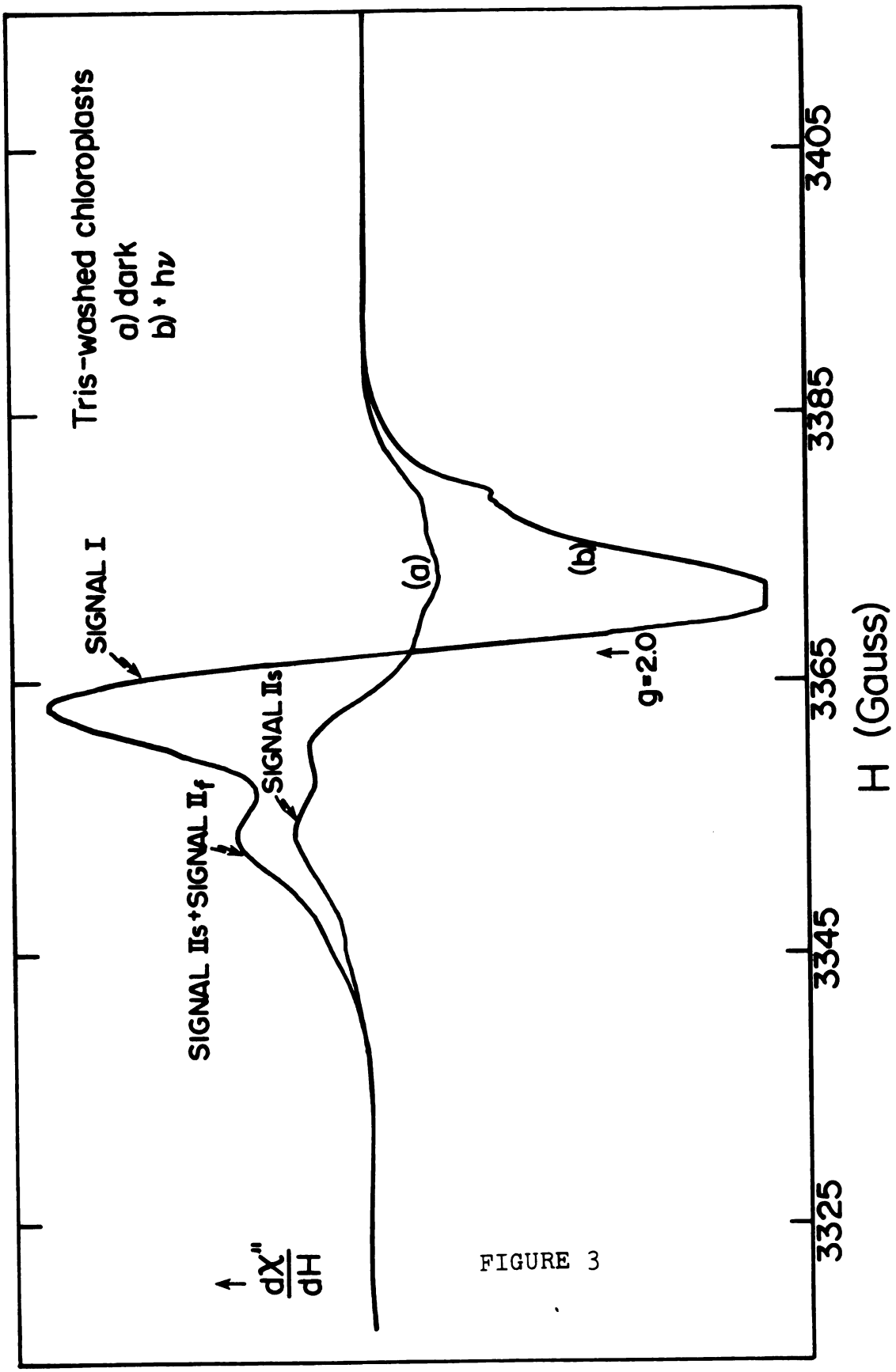
Tris-washed chloroplasts
a) dark
b) + hν
SIGNAL I
SIGNAL IIs+SIGNAL IIf
SIGNAL IIs
(a)
(b)
g-2.0
dX"/dH
3325
3345
3365
3385
3405
H (Gauss)

FIGURE 3

endogenous or exogenous electron donors. Under these conditions, the rise time of IIf is instrument limited at 100 μs [53] and the reduction half time of the $Z^{+\cdot}$ radical in slower than IIvf and typically in the 500 ms range in the absence of exogenous donors.

The decay of Signal IIf follows pseudo-first order kinetics in the presence of several commonly used electron donors, including hydroquinone, phenylenediamine and diphenylcarbazide and indicates that $Z^{+\cdot}$ is the site of their interaction with the oxidizing side of PS II. The kinetic simplicity of this system makes it especially useful because quantitative models of the system can be developed and tested. Additionally, one must consider the intrinsic importance of the reaction. Aside from the recent observation of absorbance changes associated with the photooxidation of P680 [49], the rise and decay of Signal IIf and of its physiological counterpart, Signal IIvf, are the only directly observable reactions occurring in the oxidizing side of PS II.

A detailed study of the kinetics and of those factors which influence the electron transfer rates through the Z species is used here to provide insight into membrane phenomena associated with the water splitting process. Ascorbic acid has been used in this study not only as a reducing agent for $Z^{+\cdot}$ but also as a probe to reactions occurring on the water side of PS II. Ascorbic acid

has two characteristics which make this possible. First, like the donors listed above, it effectively alters the rate of $Z^{+\cdot}$ reduction at relatively low concentrations. However, unlike those donors which are neutral at physiological pH values and, therefore, of little use in studying ionic or membrane surface charge effects, ascorbic acid exists largely as the ascorbate mono-anion in the pH range from 4.5-9.5, thus providing the system with a negatively charged donor. It will be shown that other negatively charged donors, among them I^-, $Fe(CN)_6^{4-}$ and $W(CN)_8^{4-}$, are effective at only extremely high concentrations.

From the results presented here, a kinetic model will be postulated in which both neutral ascorbic acid (H_2Asc) and its mono-anion ($HAsc^-$) serve as donors to $Z^{+\cdot}$. Through this model, it has been possible to situate Z near the inner surface of the thylakoid membrane. Furthermore, the results suggest the existence of a net negative surface charge on the inner surface of the membrane in the vicinity of Z.

B. Materials and Methods

1. Kinetic EPR Instrumentation

These experiments were performed with a Varian model E-4 spectrometer with a TM_{110} mode cavity (Varian E-238) and a Scanlon EPR flat cell (S-814); microwave power of 20 mW and modulation amplitude of 5G were used. Because of the relatively low concentration of the paramagnetic

species obtainable in the chloroplast suspensions (10-20 μM) the time course for the transient rise and decay of Signal IIf were enhanced through signal averaging. Data were collected and stored with a Nicolet model 1074 signal averager with a model SD 72124 analog to digital converter and a model SW-71A time base in the 1074 main frame. The number of scans accumulated is noted in the figure legends. A TTL logic based timing circuit was designed and built by the Michigan State University Chemistry Department Electronics Shop which allows the triggering of up to six different instruments at intervals continuously variable from 1 μs to 100 s. This was used to trigger the averager sweep followed, after collecting a suitable dark baseline, by a laser pulse.

The laser head, containing the main discharge capacitor, flash lamp, pump and dye cell, is a model DL-1100 from Phase-R Corporation. New Durham, New Hampshire. It is rated at 250 mJ output light energy with rhodamine 6-G (λ_{max} = 590 nm) with a pulse duration of 450 nm. The 25 KV power supply was built by the M.S.U. Electronics Shop. The triggering system, based on schematics supplied by Phase-R, was further developed in our laboratory.

The first experiments in which the laser light source was used revealed a large electrical transient generated by the triggering of the laser which obscured the EPR signal. The following shielding scheme evolved

to separate the laser and EPR systems. The laser is in a Faraday cage with r.f. shielding (Instrument Specialties Co., Inc., Little Falls, NJ) at all of the joints. The two systems, laser and EPR, are grounded separately and are interfaced via opto-isolators whose circuit diagrams are shown in Figure 4. These measures have eliminated the electrical transient. The dye used is a solution of cresyl-violet perchlorate and rhodamine 6-G in methanol. This solution emits at 660 nm, a wavelength close to the absorption maximum of P680 (680 nm). The absolute and relative cresyl-violet (4×10^{-5} M) to rhodamine (2.7×10^{-5} M) concentrations in the lasing solution were determined experimentally to give optimum light intensity at moderate (16 KV) voltages. The light intensity was monitored as described by Van Best [63]. It consists of a glass plate mounted between two white surfaces with openings to allow passage of most of the beam. Part of the light is reflected by the glass surface and is then detected and integrated by four photodiodes (Hewlett-Packard) connected in parallel with an 820 pf capacitor. The voltage is read from an oscilloscope (B & K Precision, model 1411 B). This circuit is mounted on a filter holder accomodating neutral density filters which were used to construct a light saturation curve for Signal IIf formation and to show that the illumination was of saturating intensity. A block diagram showing the main components of the kinetic EPR instrumentation is shown in Figure 5.

Figure 4 -- Circuit diagram for diode opto-isolator.

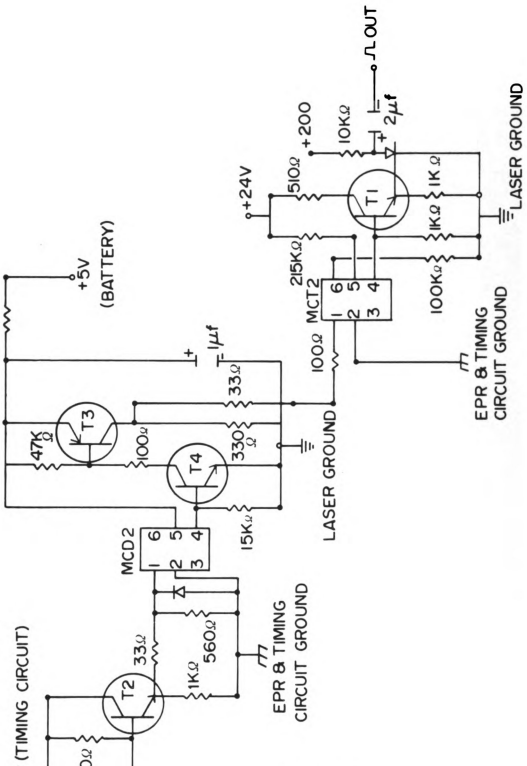
DIODE OPTO-ISOLATOR
56KΩ
+5V
(BATTERY)
+5V (TIMING CIRCUIT)
330Ω
ΠINTO
T2
33Ω
1KΩ
560Ω
MCD2
EPR & TIMING
CIRCUIT GROUND
47KΩ
T3
100Ω
T4
330Ω
33Ω
μf
15KΩ
LASER GROUND
100Ω
MCT2
+24V
510Ω
215KΩ
100KΩ
+200
10KΩ
2μf
T1
1KΩ
1K Ω
ΠOUT
EPR & TIMING
CIRCUIT GROUND
LASER GROUND

FIGURE 4

Figure 5 -- Block diagram of kinetic EPR instrumentation.

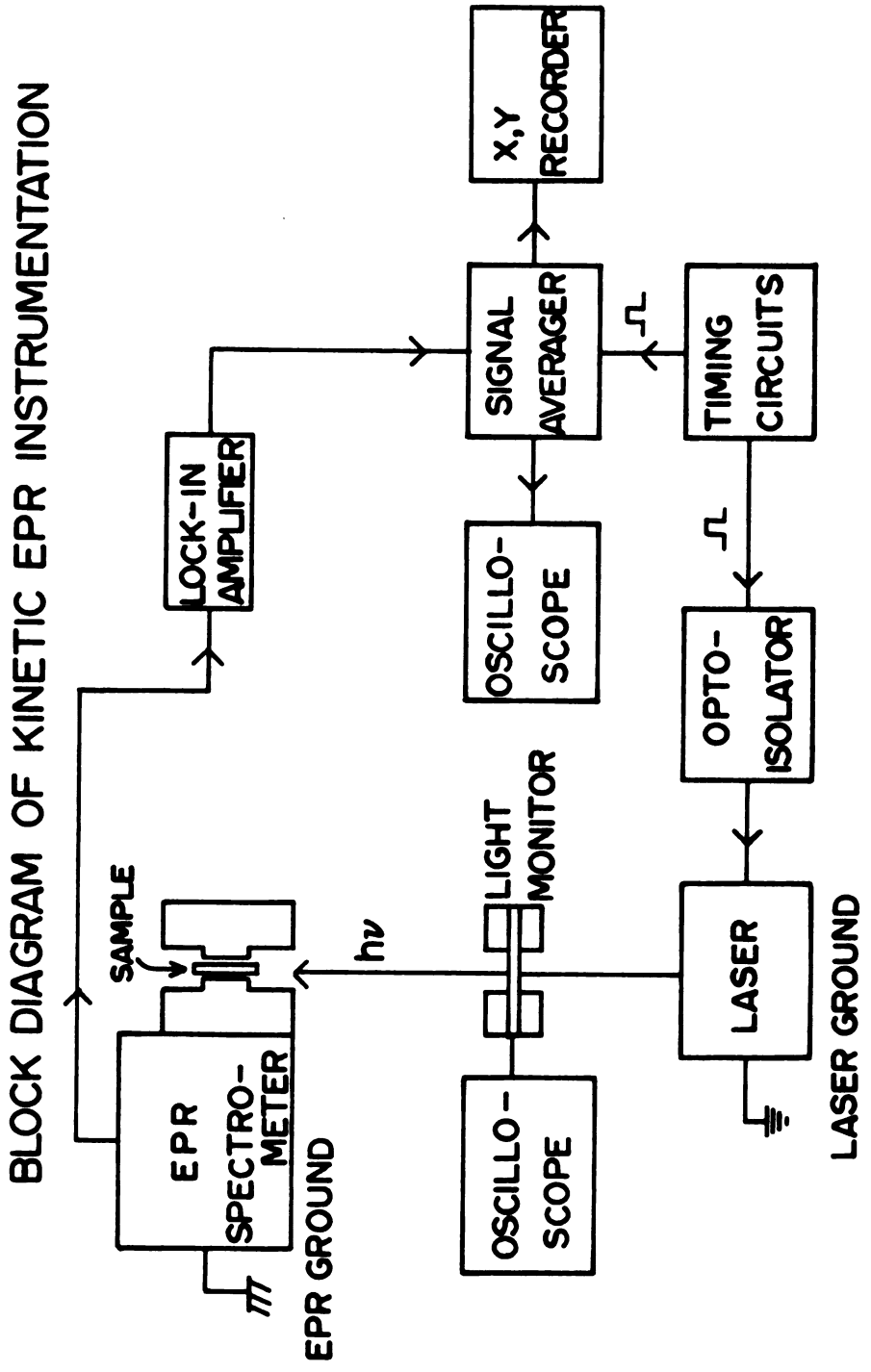
BLOCK DIAGRAM OF KINETIC EPR INSTRUMENTATION
EPR SPECTRO-METER
EPR GROUND
SAMPLE
hν
LOCK-IN AMPLIFIER
LIGHT MONITOR
OSCILLO-SCOPE
OSCILLO-SCOPE
SIGNAL AVERAGER
X,Y RECORDER
TIMING CIRCUITS
OPTO-ISOLATOR
LASER
LASER GROUND

FIGURE 5

Modifications to the lock-in amplifier (Princeton Applied Research, Model 126) were made, bringing the fastest time constant from about 800 μs to 50 μs. Measurements of the Z^{+} kinetics are made by setting the EPR magnetic field at the Signal II maximum, as indicated by the arrows in Figure 3. The change in magnetic susceptibility ($d\chi''$) is measured as a function of magnetic field (dH) via the 5G modulation of the magnetic field about this central field setting. With a 5G modulation amplitude, there is no overlap with the photo-induced Signal I. This has been verified by adding 100 μM DCMU to the suspension mixture. This reagent blocks the re-oxidation of Q^{-}, thus effectively bringing PS II photoactivity to a halt. Under these conditions, no photoinduced signal is observed at the field position at which Signal IIf amplitude is maximal.

2. Spinach and Chloroplast Suspensions

Market spinach was used in these experiments. Leaves were kept dark and cold (4°C) prior to use, then washed in distilled water and deveined under low light conditions. They were broken in a Waring blender (model 700) for 10 s in a standard reaction solution. The solution is 0.4 M sucrose, 10 mM NaCl and 50 mM buffer. MES buffer (pK_a = 6.1) was used in the pH range from 5.5-6.5, HEPES (pK_a = 7.5) for 7.0-7.5 and TRICINE (pK_a = 8.1) for 8.0-8.5. In oxygen evolution experiments these buffers were overlapped at the limits of their pH ranges and no

deleterious buffer effects were observed. The homogenate was then strained through 10 layers of cheesecloth and centrifuged for 4 min (5000 r.p.m., SS-34 Sorvall rotor) at about 4°C. The pellets were resuspended in 0.8 M Tris buffer (pH = 8.0) and incubated under room light, at 4°C, for 20 min. This constitutes Tris washing [64]. The Tris washed samples were re-centrifuged, re-suspended in the proper pH buffering solution (washing), spun down and re-suspended in a minimal volume of the reaction mixture. Chlorophyll concentrations ranged between 3 and 5 mg chlorophyll per ml suspension as determined by the method of Sun and Sauer [65]. 10^{-4} M EDTA was added to all samples to suppress the hexaquo Mn^{2+} EPR signal present in Tris-washed chloroplasts [17]. 20 μg/ml spinach ferredoxin and 5×10^{-4} M NADP, obtained from Sigma, were added to the final chloroplast suspensions as an electron acceptor system. The $K_4W(CN)_8$ was prepared as described previously [52]; all other reagents were purchased from standard commercial sources and used as received except for the DCMU which was recrystallized from methanol.

3. Experimental Protocol

The chloroplast suspensions were kept dark and at 0°C. These suspensions contained the thylakoid membranes (3-5 mg chlorophyll ml^{-1} suspension), the reaction mixture described above, 10^{-4} M EDTA, and an electron acceptor system (5×10^{-4} M NADP and 20 μg ml^{-1} ferredoxin). Prior

to each experiment, an aliquot of this suspension (.45 ml) was mixed with a known concentration of exogenous donors and enough distilled water to bring the final volume to .5 ml. This mixing and the filling of the EPR flat cell was carried out under low light conditions. The EPR sample cell was then centered in the cavity and the detector diode allowed to stabilize. In most cases, 6 s were left between laser flashes for the chloroplasts to relax to the dark equilibrium state. The number of scans averaged was chosen according to the instrument time constant which was, in turn, determined by the rate of decay of the radical. These parameters are noted in the figure legends.

C. Results

Figure 6 is a collection of experimental traces of Signal IIf decay from Tris-washed chloroplasts under different experimental conditions. Figure 6a is the decay transient observed from chloroplasts (pH = 7.5) in the absence of exogenous electron donors. Under these conditions, the decay kinetics are biphasic. Our results, reported elsewhere [66], suggest that the decay halftimes for the two phases exhibit different pH dependencies and that the relative magnitudes of the two signals also vary as a function of pH. These results have since been confirmed by other workers [67] and have been ascribed to a protonation equilibrium of the oxidized species

Figure 6 -- The effect of exogenous donors on EPR Signal IIf decay kinetics. All experiments were performed on Tris-washed chloroplasts to which 5×10^{-4} M NADP, 10^{-4} M EDTA and 20 µg ferredoxin/ml suspension had been added. The field setting is 3353 G, the modulation amplitude is 5 G and the power is 20 mW. The scans were run at 6 s intervals. (a) pH = 7.5, time constant = 10 ms, 64 scans averaged. (b) 2×10^{-3} M ascorbate, time constant = 3 ms, 120 scans averaged. (c) 2×10^{-3} M ascorbate, time constant = 3 ms, 120 scans averaged. (d) 10^{-5} M Hydroquinone and 2×10^{-3} M ascorbate, time constant = 3 ms, 200 scans averaged.

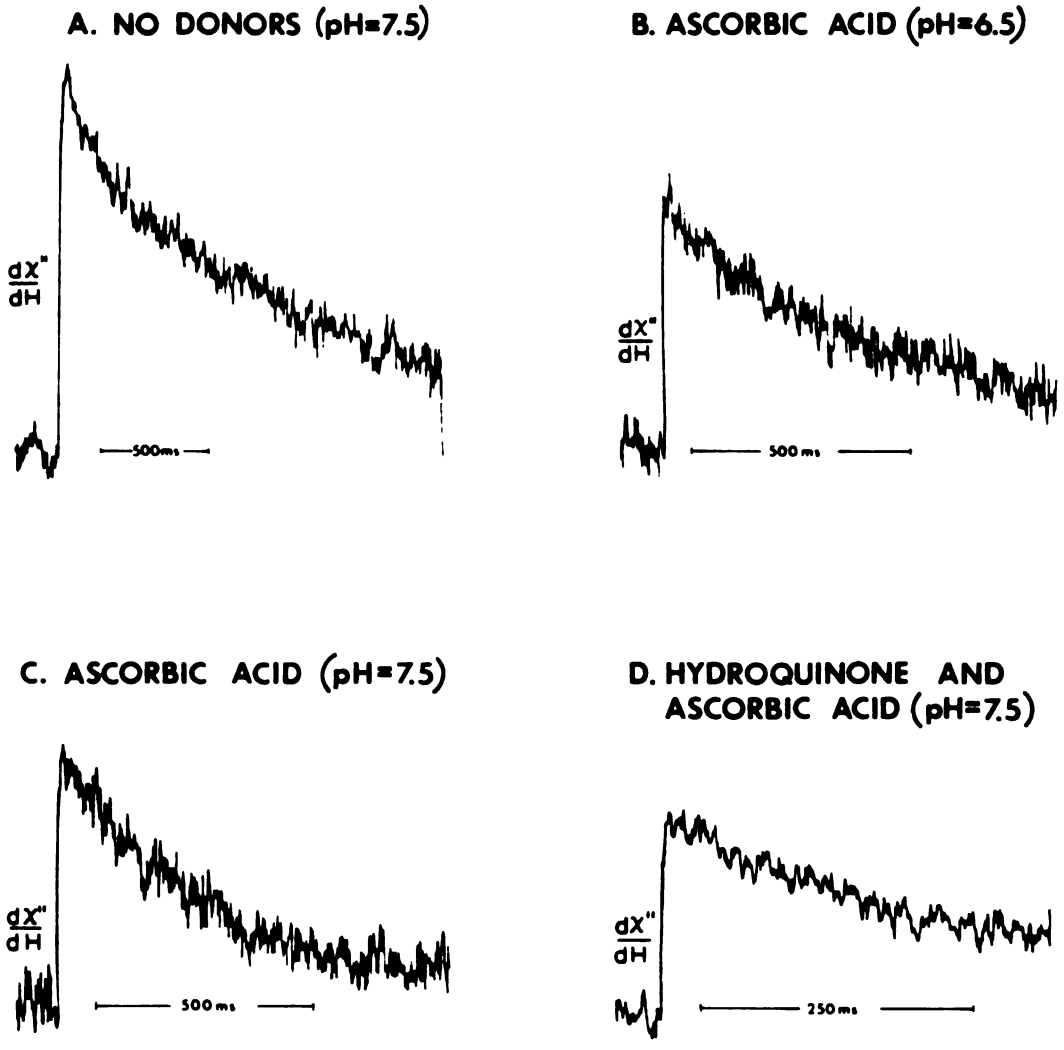
A. NO DONORS (pH=7.5)
B. ASCORBIC ACID (pH=6.5)
C. ASCORBIC ACID (pH=7.5)
D. HYDROQUINONE AND ASCORBIC ACID (pH=7.5)
dX''/dH
500ms
500 ms
500 ms
250 ms

FIGURE 6

giving rise to Signal IIf.

Upon addition of exogenous electron donors, ascorbic acid in Figure 6b and c and hydroquinone in Figure 6d, Signal IIf exhibits exponential decay kinetics. Figure 7 illustrates the variety of donors that have been studied. Hydroquinone and other neutral, lipophilic donors (benzidene, phenylenediamine) increase the decay rate of Signal IIf at low (μM) concentrations [68]. However, their electroneutrality diminishes their usefulness in studying ionic effects. We have investigated the effectiveness of several anionic donors, including iodide (Figure 7), ferrocyanide (Table I) and cyanotungstate (Table I) and have found that these species are effective only at donor concentrations in the 10-100 mM range. Ascorbic acid, with pK_a = 4.10, exists largely as the ascorbate mono-anion in the pH range studied (5.5-8.5) and thus may provide a charged donor to the system. Moreover, the ascorbic acid system is an effective donor to $Z^{+\cdot}$ at low concentrations (Figure 7). These two characteristics combine to make ascorbic acid an ideal probe. Although it has been used as a donor to PS II [69,70], the kinetics of these reactions have not been examined in detail. In particular, it has not been established whether both the mono-anion and the fully protonated neutral acid are effective as donors. As the ascorbic acid data in Figure 7 demonstrate, there is a pseudo-first order reaction between $Z^{+\cdot}$ and ascorbate acid

Table 1 -- Rate Constants for the Reduction of $Z^{+\cdot}$ by Exogenous Electron Donors.*

Donor	$k(M^{-1} s^{-1})$
Benzidine	1.3×10^6
Phenylenediamine	4.6×10^5
Hydroquinone	2.5×10^5
H_2Asc	1.4×10^4
Diphenylcarbazide	8.0×10^3
$HAsc^-$ (infinite salt)	3.6×10^3
I^-	2.4×10^1
$Fe(CN)_6^{4-}$	2.4×10^1
$W(CN)_8^{4-}$	1.8×10^1

*Samples prepared and experimental protocol as described in Materials and Methods.

Figure 7 -- Donor concentration dependence of the Signal IIf pseudo-first order decay constant in Tris-washed chloroplasts at pH = 7.5, except where noted, with a 3 ms time constant and 120 scans averaged.

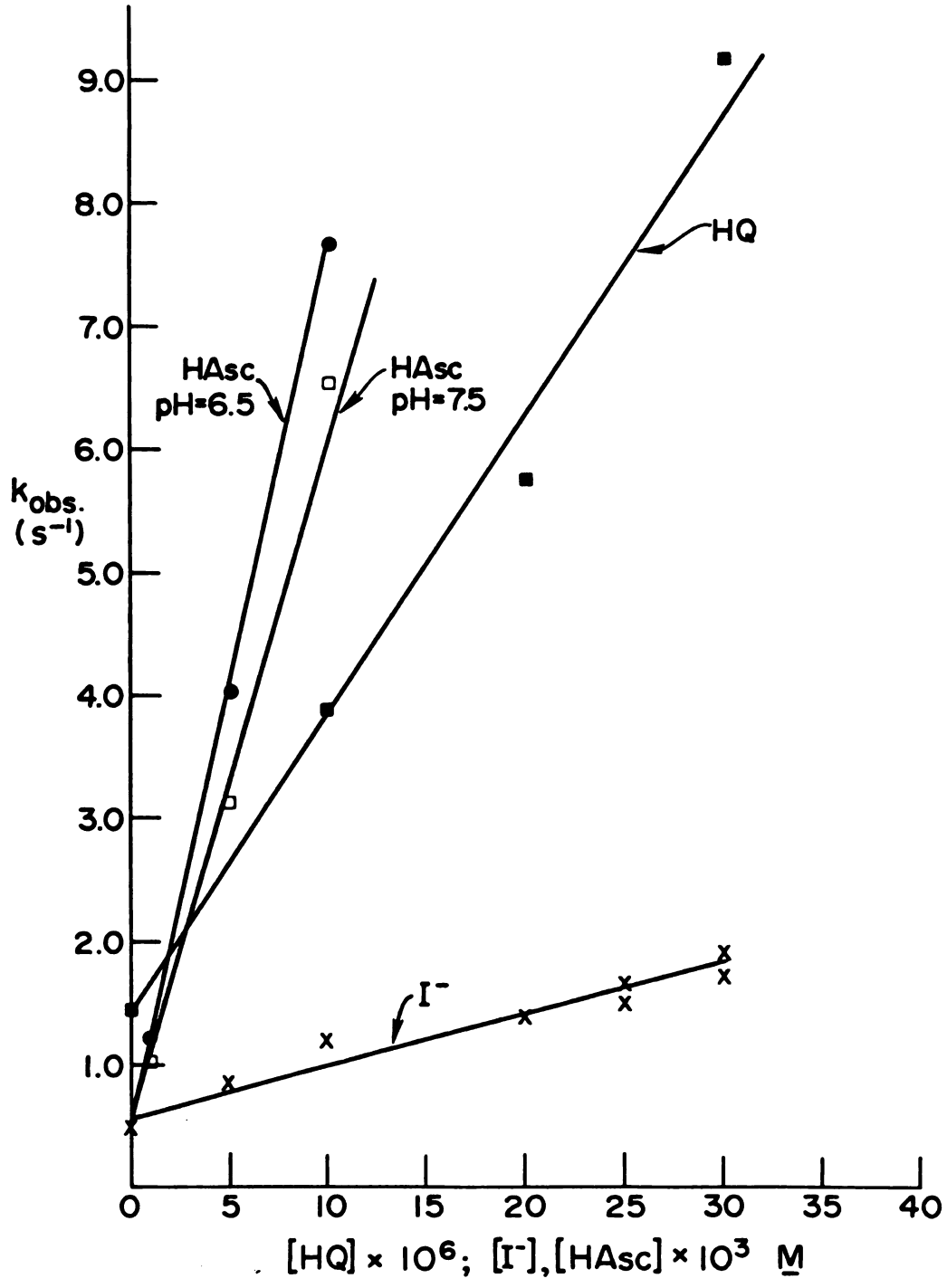
9.0
8.0
7.0
6.0
5.0
4.0
3.0
2.0
1.0
$k_{obs.}$ (s^{-1})
HAsc pH=6.5
HAsc pH=7.5
HQ
I^-
0
5
10
15
20
25
30
35
40
[HQ] × 10^6; [I^-],[HAsc] × 10^3 M

FIGURE 7

and this reaction is pH dependent. Figure 8, a plot of the pseudo-first order rate constants (k_{obs}) versus pH, verifies this pH dependence over the entire experimental pH range. We have examined a number of models to explain this pH dependence and have calculated theoretical rate constants corresponding to each of these models. The calculated rate constants, k_{calc}, can be compared to the observed rates, k_{obs}, obtained from data such as those shown in Figure 7. The correlation of these values is a good indication of the accuracy of the model.

The most simple scheme to explain the pseudo-first order kinetics as well as the pH dependence of the reaction postulates electron donation by the neutral species only and is summarized by the following reactions:

$$Z^{+\bullet} + H_2Asc \xrightarrow{k} Z + H_2Asc^{+\bullet} \qquad (2.1)$$

where the decay of Signal IIf is given by

$$-\frac{d[Z^{+\bullet}]}{dt} = k[Z^{+\bullet}][H_2Asc] \qquad (2.2)$$

and the pH dependence is explained by the equilibrium reaction:

$$H^+ + HAsc^- \overset{K_e}{\rightleftharpoons} H_2Asc \qquad (2.3)$$

The correlation between the second order rate constant calculated for this reaction mechanism and the observed rate is shown in curve a of Figure 9. The fit to the experimental data based on this model is clearly

unsatisfactory. We have also found that a model which postulates only the ascorbate mono-anion as a reductant is unable to explain the observed pH dependence.

In a third model, both the neutral acid and its mono-anion are postulated as reducing agents as follows:

$$Z^{+}\cdot + H_2Asc \xrightarrow{k_1} Z + H_2Asc^{+}\cdot \qquad (2.4)$$

$$Z^{+}\cdot + HAsc^{-} \xrightarrow{k_2} Z + HAsc \qquad (2.5)$$

$$H^{+} + HAsc^{-} \overset{K_e}{\rightleftharpoons} H_2Asc \qquad (2.6)$$

The decay Signal IIf is now given by

$$\frac{-d[Z^{+}\cdot]}{dt} = [Z^{+}\cdot][HAsc^{-}]\left(\frac{k_1[H^{+}]}{k_e} + k_2\right) \qquad (2.7)$$

In this model, the observed second-order rate constant is associated with the quantity $[(k_1[H^+]/K_e) + k_2]$. Using the data of Figure 7, we calculate k_1 to be 1.4×10^4 M^{-1} s^{-1} and k_2 to be 6.6×10^2 M^{-1} s^{-1} and with these values we find that the ratio k_{obs}/k_{calc} is close to unity for all pH values between 5.5 and 8.5, (Figure 9b). Thus the model summarized in Eqns. (2.4)-(2.6) provides a reasonable, first order explanation for the experimental data. The non-zero slope in Figure 9b indicates, however, a residual pH dependence in the experimental rate constant not explained by this model.

Two additional postulates to the basic model of Eqns. (2.4)-(2.6) have been tested to resolve this pH

dependence (Figures 9b and c). In the first, a variable pH gradient across the thylakoid membrane is postulated to account for the non-zero slope. In the second, k_2, the rate constant associated with the reduction of Z^+ by the ascorbate mono-anion is assumed to be pH dependent and to decrease as the pH increases from 5.5 to 8.5.

The first model assumes that the Z species is located near the inner surface of the thylakoid membrane. This situation of Z has been postulated [68] and implies that the relevant $[H^+]$ in Eqns. (2.6) and (2.7) is that inside the thylakoid membrane ($[H^+]_{in}$), not that of the suspending medium ($[H^+]_{out}$). By assuming a ΔpH across the membrane ($[H^+]_{in} \neq [H^+]_{out}$) and by allowing it to vary from about 0.6 pH units at pH_{out} = 5.5 to about 1.7 pH units at pH_{out} = 8.5, the observed and calculated rates are brought into excellent agreement (Figure 9c). The existence of a pH gradient across the membrane under these experimental conditions is not unreasonable. Yamashita and Butler [64] have shown that upon addition of electron donors, Tris-washed chloroplasts continue to phosphorylate, an indication that a pH gradient develops even after inhibition of oxygen evolution. To test this model, experiments have been carried out in which the uncoupler, gramicidin, which should collapse any pH gradient, independent of the suspension pH [71] was used. The model predicts that the decay rate at high pH values should be most susceptible to uncoupler action as the ΔpH is largest at those pH

values, and that the rate should decrease as the ΔpH approaches zero. We observed, however, that gramicidin addition produces only a slight increase in the rate at pH = 8.0. We conclude, therefore, that in Tris-washed chloroplasts under the intermittent flash conditions of our experiments (one flash every 6 s) there is no appreciable buildup of a membrane pH gradient.

The physical basis for the alternative postulate (Figure 9d) is suggested by the 20-fold difference in magnitude between k_1, the rate constant associated with neutral ascorbic acid, and k_2 associated with the mono-anion in Eqn. (2.7). This difference indicates that Z^+ may be more accessible to the neutral form of the reducing agent than to its anion. An explanation for this behavior may be the existence of a negative charge on the surface of the thylakoid membrane. Nakatani and coworkers [72] have conducted electrophoretic experiments which demonstrate the presence of a net negative charge on the exterior of the thylakoid at physiological pH values. They attribute this charge to protein carboxyl groups which are found to have an effective pK_a of about 4.3. If the inner membrane surface were to carry a similar charge in the vicinity of Z, this could explain the efficiency of neutral ascorbic acid relative to the mono-anion in reducing Z^+. According to Gouy-Chapman diffuse double layer model, the concentration of a neutral species in the vicinity of a charged surface

Figure 8 -- pH dependence of the Signal IIf pseudo-first order decay constant in Tris-washed chloroplasts with 2 mM ascorbic acid as the exogenous donor. The experimental conditions are described in Figure 7.

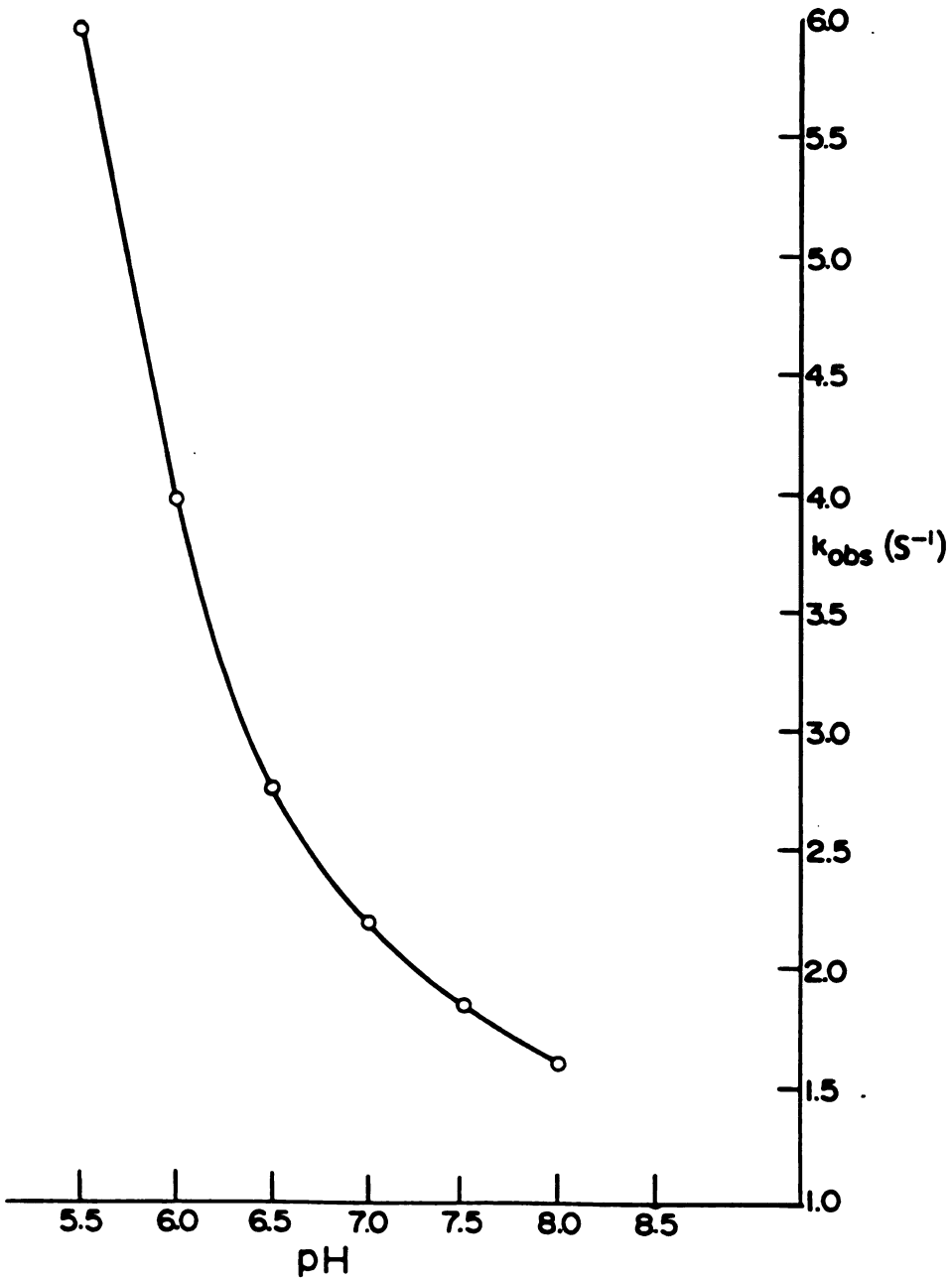

FIGURE 8

Figure 9 -- Correlation between observed (k_{obs}) and calculated (k_{calc}) second order rate constants for models of $Z^{+\cdot}$ reduction by ascorbic acid. (a) neutral ascorbic acid, H_2Asc, as the reducing agent; (b) H_2Asc and the mono-anion, $HAsc^-$, as the reducing agents; (c) same as (b) but a pH dependent ΔpH across the thylakoid membrane, $\Delta pH = 0.7$ at pH = 5.5, $\Delta pH = 2.0$ at pH = 8.5. (d) same as (b) but k_2, associated with the reduction of $Z^{+\cdot}$ by $HAsc^-$ as a function of pH, ranging from 2.2×10^3 M^{-1} s^{-1} at pH = 5.5 to 8×10^2 M^{-1} s^{-1} at pH = 8.5.

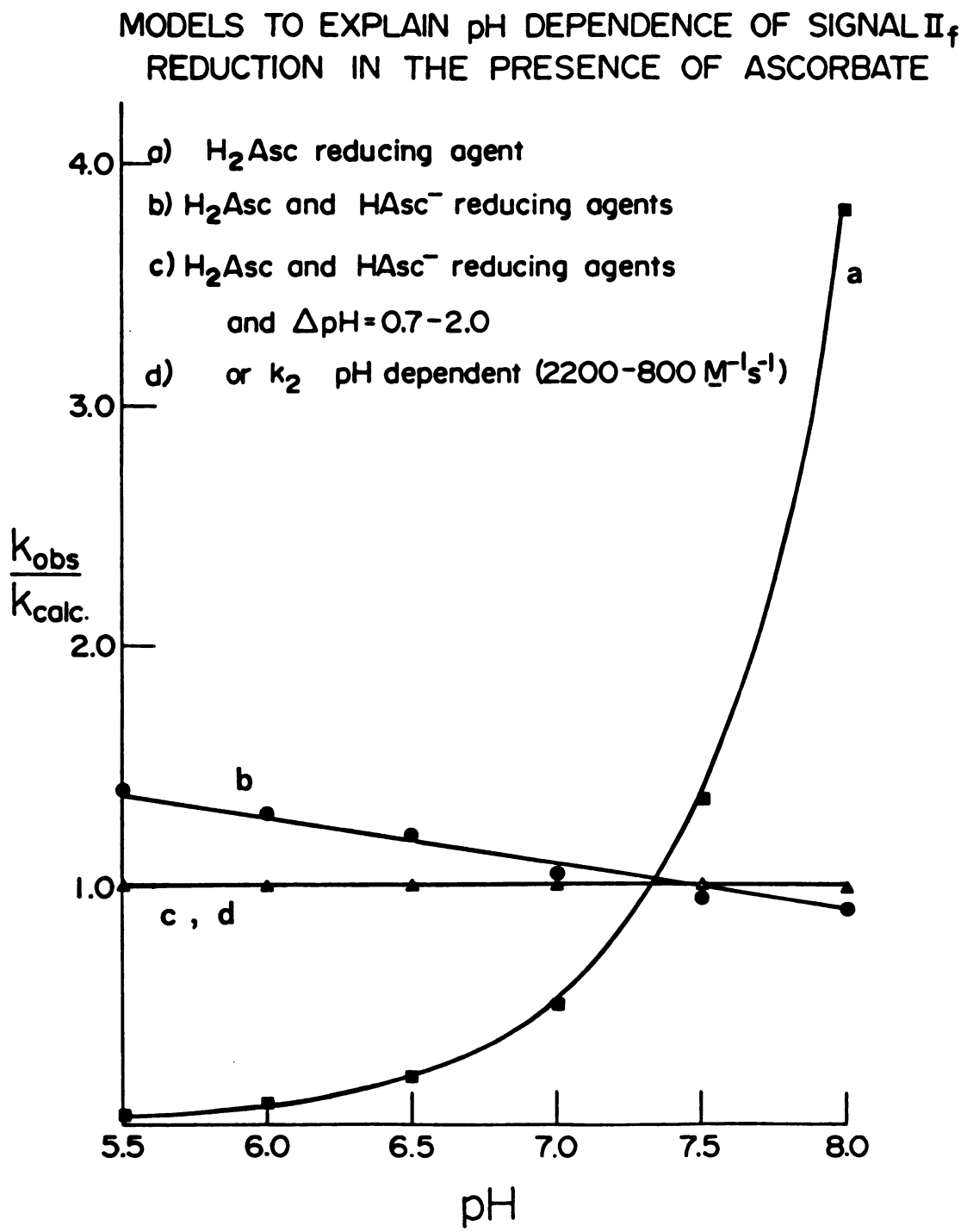
MODELS TO EXPLAIN pH DEPENDENCE OF SIGNAL II$_f$ REDUCTION IN THE PRESENCE OF ASCORBATE
a) H_2Asc reducing agent
b) H_2Asc and $HAsc^-$ reducing agents
c) H_2Asc and $HAsc^-$ reducing agents and $\Delta pH = 0.7-2.0$
d) or k_2 pH dependent (2200-800 $M^{-1}s^{-1}$)
$\frac{k_{obs}}{k_{calc.}}$
4.0
3.0
2.0
1.0
a
b
c , d
5.5
6.0
6.5
7.0
7.5
8.0
pH

FIGURE 9

should be unaffected by the surface potential whereas the local concentration of ionic species such as the ascorbate mono-anion will be determined by the magnitude and sign of the surface charge density and its associated surface potential. This would explain the rapid k_1 kinetics as the neutral acid concentration in the vicinity of Z would be unaffected by surface charges and would be the same as the concentration in the bulk phase. The k_2 kinetics would, instead, reflect the mono-anion concentration in the double layer.

At high pH values, the membrane bound groups giving rise to the surface charge would be largely deprotonated, resulting in a large, negative surface potential, a lower concentration of the ascorbate anion near the membrane surface and, thus, to a lower value of k_2. As the pH is decreased, these groups would protonate, decreasing the surface charge density, and the value of k_2 would show a corresponding rise. This trend in k_2 is in agreement with that demonstrated above: the k_2 is pH dependent and that it increases as the pH decreases.

To test this model, we have made use of the inverse relationship between the surface potential and the square root of the solution salt concentration [73]. This relationship arises from the Gouy-Chapman equations. Its applicability to biological membrane membrane surface and the approximations necessitated by this application will be discussed in detail in the next section when this model will be used to actually measure membrane surface

charge density. Qualitatively, the model predicts that as the salt concentration of the solution is raised, an increase in the signal decay rate should be observed if the residual pH dependence (Figure 9b) is a surface charge phenomenon. The experiments were performed at pH = 8.0 because under these conditions over 99% of the Z^{+} is reduced by the mono-anion [Eqn. (2.7)]. We have used KCl, primarily, in these experiments since previous work suggested that Signal II is localized near the inner surface of the thylakoid membrane [68] and both K^{+} and Cl^{-} diffuse fairly readily through the thylakoid membranes [74]. Figure 10 shows the result of a series of salt concentration experiments. As the concentration of K^{+} is increased, the reaction rate increases as predicted. To insure that the diffusion time of K^{+} is not rate limiting, chloroplasts were incubated in a 400 mM salt solution and the Signal IIf decay rate in the presence of 2 mM ascorbic acid was determined at various times. During the course of the incubation, no time dependence is observed in the decay rate of Signal IIf as seen in the inset to Figure 10. A divalent cation, Mg^{2+}, was also examined and its effect on the decay kinetics of Signal IIf is summarized in Figure 10. It is effective at lower concentrations than K^{+}, as predicted by the Gouy-Chapman model, which further substantiates the mediation of a surface charge effect in Z^{+} reduction kinetics.

Figure 10 -- Salt concentration dependence of the Signal IIf second order decay constant, k_2, at pH = 8.0 and 2 mM ascorbate. Chloroplasts were incubated in the salt solution for 5 min prior to initiation of the experiment. Inset: salt incubation time dependence of Signal IIf second order decay constant, k_2. The experimental conditions are described in Figure 7.

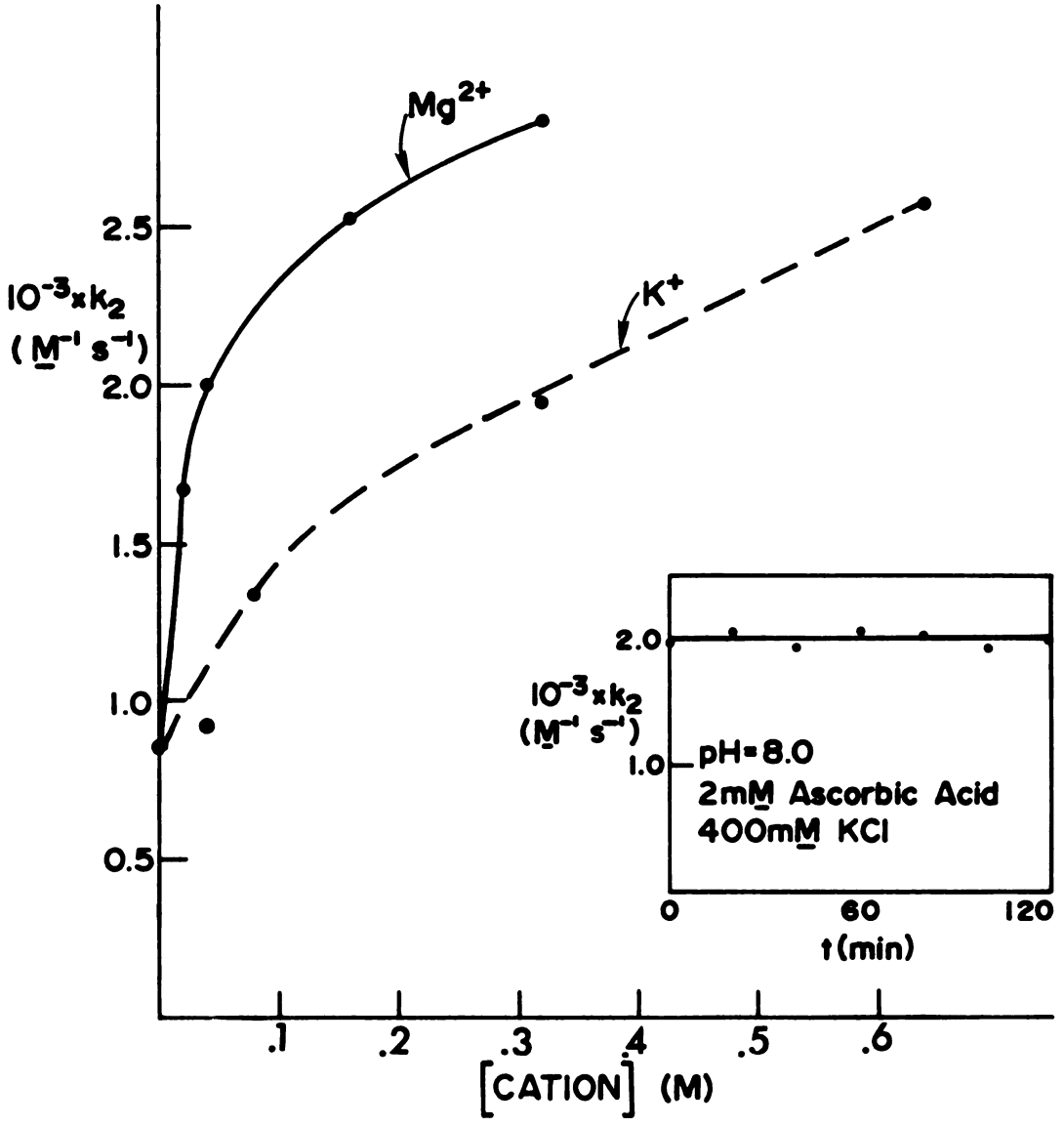
Mg2+
K+
2.5
2.0
1.5
1.0
0.5
10-3xk2
(M-1 s-1)
.1
.2
.3
.4
.5
.6
[CATION] (M)
2.0
1.0
10-3xk2
(M-1 s-1)
pH=8.0
2mM Ascorbic Acid
400mM KCl
0
60
120
t(min)

FIGURE 10

Additional work has been carried out to determine if the mediating surface charge exists on the inner or outer thylakoid surface. This involves the use of cationic detergents. Itoh and coworkers [75,73] have shown that the addition of low concentrations of cetyltrimethylammonium chloride to chloroplasts suspensions effectively lowers the outer surface potential of thylakoid membranes. The hydrocarbon tail is adsorbed to the outer membrane surface, preventing the diffusion of the molecule through the membrane, while the positively charged head group lowers the negative surface charge density. In this way, one may selectively mask the surface charge on the outer membrane. In our experiments, however, the choice of detergent is severely limited. In the experiments in which cetyltrimethylammonium chloride was used [75], the chlorophyll concentration was around 50 μg ml^{-1} suspension. The detergent concentration ranged from about 30 to 90 μM. In the EPR experiments, much higher chlorophyll concentrations are required (3-6 chlorophyll ml^{-1}). To maintain the same detergent to chlorophyll ratio, detergent concentrations in the range of 3-9 mM would be required. This is above the critical micellar concentration of cetyltrimethylammonium chloride (9×10^{-4} M) [76], and we have found that at these detergent concentrations there is a complete loss of Signal IIf, most likely due to the solubilization of the membrane. One detergent meeting our requirements is nonyltrimethylammonium bromide with a

critical micellar concentration of 1.4×10^{-1} M [76]. Its structure and the results of these experiments are shown in Figure 11. Addition of this cationic detergent up to its critical micellar concentration has no appreciable effect on the rate of $Z^{+\cdot}$ reduction by ascorbate, while in the same concentration range K^+ concentration effects are readily discerned (Figure 11). Above the critical micellar concentration there is, again, a complete loss of Signal IIf.

In the work of Itoh [75] the detergent/chlorophyll ratios that we have used were sufficient to alter the outer membrane surface potential substantially, leading to a ten fold enhancement in the rate of the reaction that was being monitored. In our experiments, virtually no effect is seen due to the shielding of the outer membrane surface charge of the cationic detergent. We conclude, therefore, that the surface charge density which determines the rate of reduction of $Z^{+\cdot}$ by the ascorbate anion is that of the inner membrane surface in the vicinity of $Z^{+\cdot}$.

During the course of this study, we have observed a variation in the absolute reaction rates among chloroplast suspensions, which we suspected was a result of having used market spinach in these experiments and thus, of having had very little control over its age and the conditions of the membranes. We have investigated, therefore, the effect that membrane integrity plays in the decay kinetics of Signal IIf. A chloroplast suspension

Figure 11 -- Cationic detergent activity dependence of the Signal IIf second order decay constant, k_2, at pH 8.0 with 2 mM ascorbate. The experimental conditions are described in Figure 7.

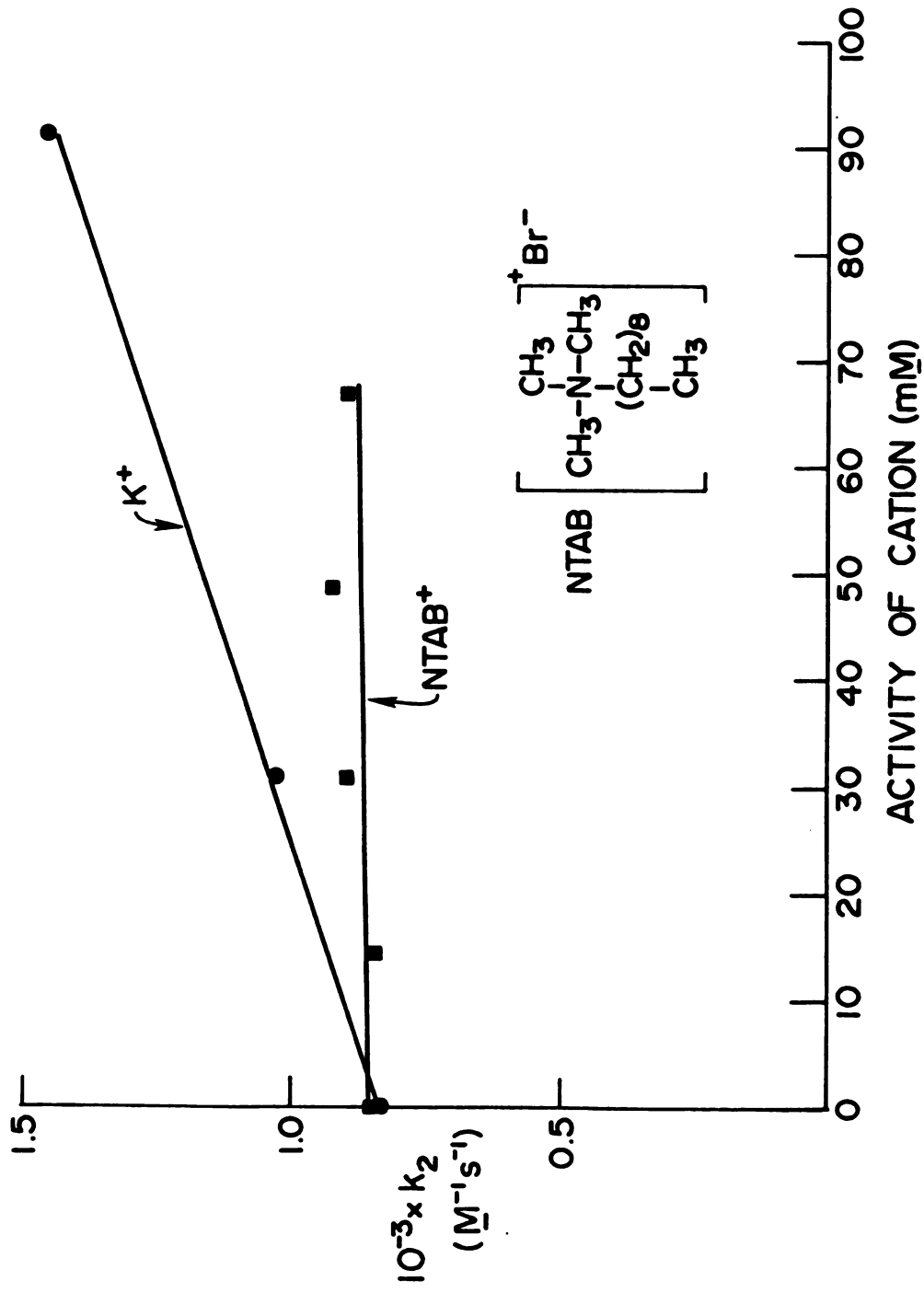
1.5
1.0
0.5
0
10
20
30
40
50
60
70
80
90
100
ACTIVITY OF CATION (mM)
$10^{-3} \times k_2$ ($M^{-1}s^{-1}$)
K^+
$NTAB^+$
NTAB
CH_3
CH_3-N-CH_3
$(CH_2)_8$
CH_3
$^+Br^-$

FIGURE 11

was sonicated and these treated samples examined for changes in the decay rates. The results are shown in Figure 12. Upon mild sonication, there is a gradual increase in the reaction rates. The condition of the thylakoid membrane does appear to contribute to the observed rate of reduction of $Z^{+\cdot}$ by ascorbatic acid and is the most likely explanation for the variation in quantitative rate constants among chloroplast suspensions.

D. Discussion

The origin of Signal IIf, a photoinduced, EPR detectable radical observed in nonoxygen evolving chloroplast suspensions, has been attributed to an as yet unidentified quinone derivative, $Z^{+\cdot}$, which lies along the electron transport chain between the PS II reaction center, P680, and the site of water oxidation. In inhibited chloroplasts, $Z^{+\cdot}$ is the principal site of PS II mediated exogenous electron donation [68]. In this study, we have investigated the Signal IIf decay rate enhancement induced by several charged donors and have focused, in particular, on the mode of ascorbic acid donation. From the observed pH dependence of the reduction of $Z^{+\cdot}$ by ascorbic acid, the kinetic scheme summarized in Equations (2.4)-(2.6) have been hypothesized. The overall rate of Signal IIf decay is given by Eq. (2.7). Values of $k_1 = 1.4 \times 10^4\ M^{-1}\ s^{-1}$ and $k_2 = 6.6 \times 10^2\ M^{-1}\ s^{-1}$ (pH = 7.0) have been calculated from a set of experiments (Fig. 7) in which the decay

Figure 12 -- Effect of sonication of the Signal IIf decay half-time at pH = 8.0 with 2 mM ascorbate. Other conditions are described in Figure 7.

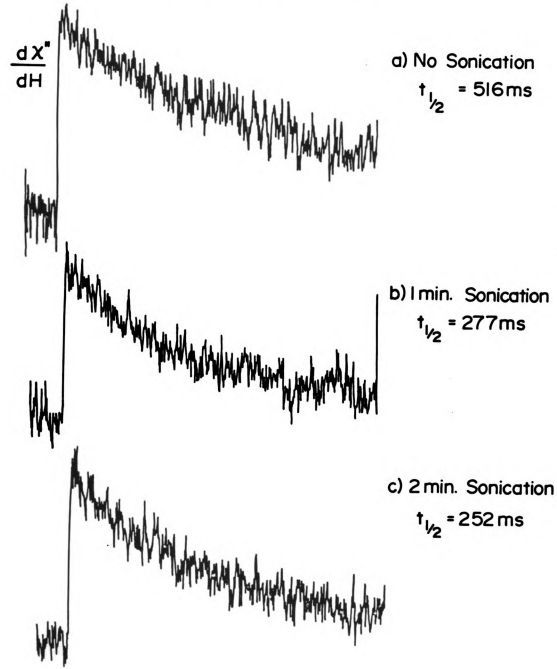
EFFECT OF SONICATION ON
SIGNAL II_f DECAY HALF TIMES
(2mM Ascorbate, pH = 8.0)
$\frac{dX''}{dH}$
a) No Sonication
$t_{1/2}$ = 516ms
b) 1 min. Sonication
$t_{1/2}$ = 277ms
c) 2 min. Sonication
$t_{1/2}$ = 252 ms

FIGURE 12

rate was examined as a function of both pH and the ascorbate acid concentration. As noted above, we have found the quantitative values of k_1 and k_2 for different chloroplast preparations to be somewhat variable. For example, in a second set of experiments, identical to those described in Figure 7, values of k_1 and k_2 were found to be 4×10^4 M^{-1} s^{-1} and 8×10^2 M^{-1} s^{-1} (pH = 7.0), respectively. One cause for this variation appears to arise from differences in the integrity of the chloroplast membrane as detailed in the sonication experiments of Figure 12. In addition, the greater variability in the value of k_1, the constant associated with the neutral acid, can probably be explained by the extreme sensitivity of this species to variation in pH, arising from the low first pK_a value of ascorbic acid (4.1). In going from pH 6.0 to 6.5, for example, the concentration of neutral ascorbic acid decreases by 70%, whereas the concentration of the mono-anion, associated with k_2, varies less than 5% over the entire pH range (5.5-8.5). Thus, small pH errors can be magnified in the calculated values of k_1.

These calculated rate constants provide a first order explanation for the pH dependence of the reduction kinetics of $Z^{+\cdot}$ by ascorbic acid but do not explain the residual pH dependence shown in Fig. 9b. The primary cause of this residual pH dependence appears to arise from surface charge effects which have been incorporated into a reaction mechanism, described by Eqs. (2.4)-(2.6), by

allowing k_2, the rate constant associated with the ascorbate mono-anion, to become a function of the suspension pH. This relationship between membrane surface charge effects, pH and the value of k_2 has been explained in terms of the Gouy-Chapman diffuse double layer theory. In this way, calculated and observed decay rates are brought into excellent agreement (Fig. 9d). The double layer model predicts that the rate of reaction between $Z^{+\cdot}$ and $HAsc^-$ should vary not only as a function of pH, which would involve a change in the membrane surface charge density and, hence, the surface potential, but also with the salt concentration which would alter only the surface potential. Fig. 10 illustrates that this is true when either KCl or $MgCl_2$ is added to the chloroplast suspension. These data have been used to construct a plot of the inverse square root of the salt concentration versus the natural log of k_2 as shown in Fig. 13. A linear relationship is observed for both salts, as predicted by the diffuse double layer mode. Moreover, the difference in the slopes of the K^+ and Mg^{2+} data in Fig. 13 indicates that the divalent cation effectively masks the surface charge at lower activities than the monovalent cation, again as predicted by the double layer model. For either salt, the extrapolated rate at infinite salt concentration should reflect the intrinsic ability of $HAsc^-$ to reduce $Z^{+\cdot}$, when the membrane surface charge has been completely masked. The data of Fig. 13 show that this rate is, as it

Figure 13 -- A plot of the inverse square root of cation activity versus the natural log of k_2 taken from data in Figure 10.

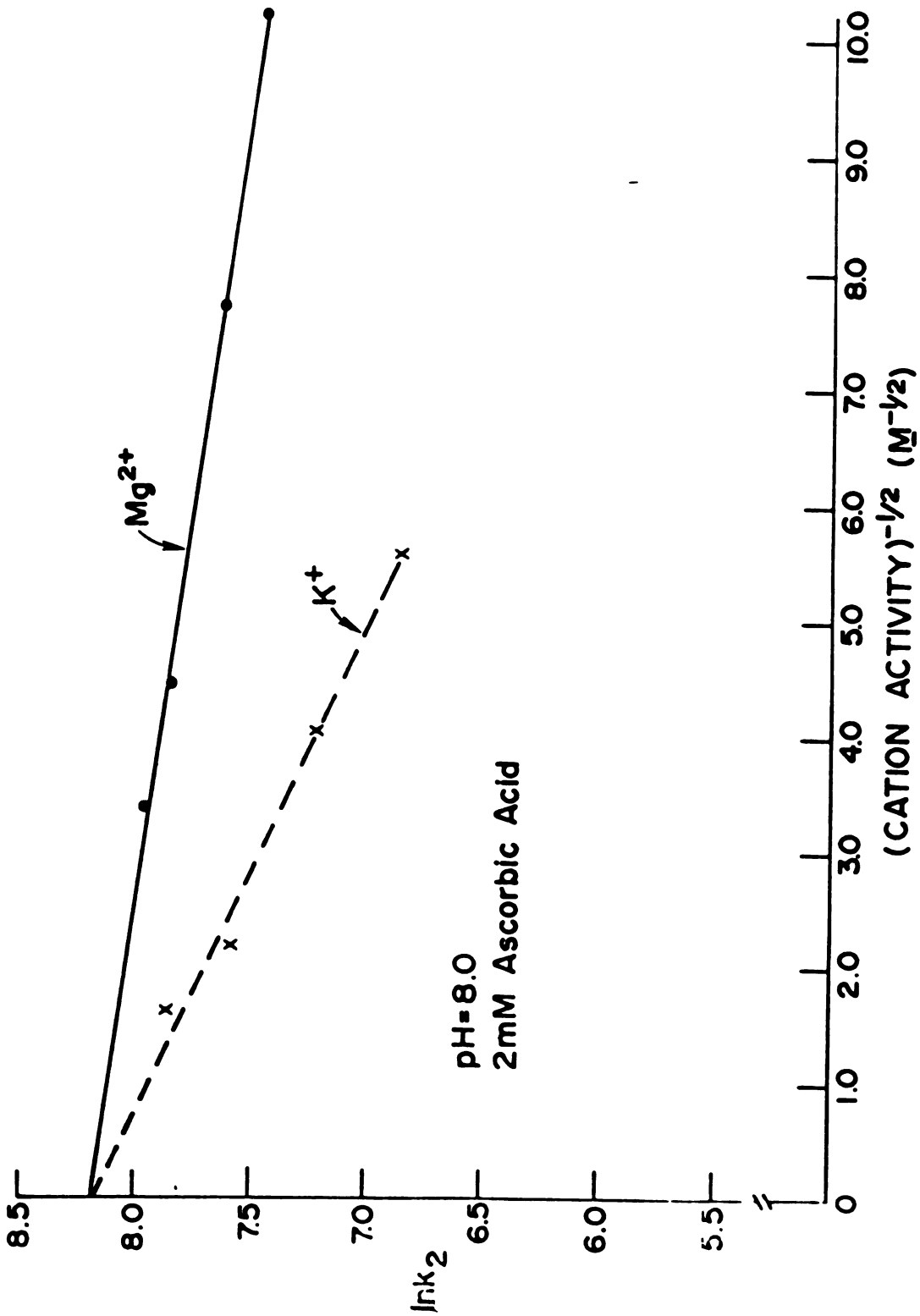
Mg2+
K+
pH=8.0
2mM Ascorbic Acid
lnk2
8.5
8.0
7.5
7.0
6.5
6.0
5.5
0
1.0
2.0
3.0
4.0
5.0
6.0
7.0
8.0
9.0
10.0
(CATION ACTIVITY)-1/2 (M-1/2)

FIGURE 13

should be, independent of both the charge and chemical identity of the masking cation. From the data of Fig. 13, we assign k_2^{∞} the value 3.6×10^3 M^{-1} s^{-1}. A comparison of the value of k_2 in the absence of added salt with k_2^{∞} shows that a four-fold enhancement in k_2 can be achieved through salt addition. Although k_2 values vary somewhat from chloroplast preparation to preparation, as discussed above, this same degree of enhancement is observed, independent of the chloroplast sample.

As Saha et al. have done for exogenous acceptors to PS II [77] one can characterize the donors studied here and in an earlier report [68] according to their lipophilicity as shown in Table 1 (p. 36). The progression from benzidene, which exhibits the most rapid reduction of $Z^{+\cdot}$, through diphenylcarbazide roughly parallels the increasing polarity of the donors as reflected by their solubility properties [78,79]. These data support the placement of Z in a lipophilic environment (within the thylakoid membrane) as the lipophilicity of the donor appear to define the efficiency with which it reduces $Z^{+\cdot}$. At the other end of Table 1, I^- through $W(CN)_8^{4-}$, the reaction rates are slow. The negative charge on the outer membrane surface [72] should lead to low local concentrations of these species. This, as well as the low dielectric constant of the membrane double layer, should severely hinder the passage of these anions to Z

and render good reductants ineffective. The ascorbate mono-anion occupies an anomolous position in Table 1. It exhibits a very high reaction rate ($k_2^{\infty} = 3.6 \times 10^3\ M^{-1}\ s^{-1}$) yet carries a negative charge. Even the value in the absence of salt, $k_2 = 6.6 \times 10^2\ M^{-1}\ s^{-1}$, is an order of magnitude greater than the rate constants of the other anionic donors ($k \approx 2 \times 10^1\ M^{-1}\ s^{-1}$). This may be resolved by postulating that it is the neutral form of the acid which diffuses across the membrane and subsequently dissociates to give the mono-anion in the inner thylakoid volume. The extent of this diffusion is controlled by the pH of the suspension and a similar mechanism involving the diffusion of neutral amines, with their subsequent protonation in the inner thylakoid volume, has already been established [80]. In this model, the pool of $HAsc^-$ used in the reduction of $Z^{+\cdot}$ need not be sensitive to the outer membrane surface charge as it is the neutral form, H_2Asc, which diffuses across the membrane. The $HAsc^-$ reducing $Z^{+\cdot}$ would presumably be that found in the inner thylakoid volume as Z has been situated toward the inner membrane surface [68]. The observed surface charge mediation (Fig. 10) of the reaction between $HAsc^-$ and $Z^{+\cdot}$ must, therefore, arise from a charge on the inner thylakoid membrane. This conclusion is strengthened by the results of the detergent experiments (Fig. 11). In these, a cationic detergent, nonyltrimethylammonium bromide, was added to the chloroplast suspension at

concentrations below its critical micellar concentration and its effect on the reduction kinetics of Z^{+} by $HAsc^{-}$ examined. Previous experiments, reported by Itoh [73, 75] demonstrated that the addition of a cationic detergent, cetyltrimetylammonium chloride, in the same detergent to chlorophyll ratio as we have used, dramatically alters the surface charge density, and hence the surface potential, of the outer chloroplast membrane surface. As our data in Fig. 11 show, the addition of nonyltrimethylammonium bromide up to its critical micellar concentration, has an effect in the reduction kinetics of Z^{+} by $HAsc^{-}$ while addition of similar concentrations of K^{+}, which freely diffuses across the membrane, significantly alters the rate of reaction. We conclude that the species Z, which gives rise to Signal IIf in Tris-washed chloroplast membranes, lies near the inner surface of the thylakoid membrane, most probably in a lipophilic site. We have shown as well that the reduction of Z^{+} by a charged donor, the ascorbate mono-anion, is mediated by membrane surface charge effects and that the mediating surface potential arises from the inner membranes surface, in the vicinity of Z. The magnitude of this inner surface charge should now be accessible by using data such as those shown in Fig. 13.

III. SURFACE CHARGE ASYMMETRY IN PHOTOSYSTEM II

A. Introduction

In the previous section, an extensive analysis of the decay kinetics of EPR Signal IIf, arising from the photooxidation of an intermediate, Z, allowed us to postulate the existence of a net negative membrane surface charge in the vicinity of Z. The analysis allowed us to localize Z toward the inner membrane surface and to suggest that the membrane potential mediating the reaction between Z^{+} and the ascorbate mono-anion arises from the inner thylakoid membrane surface. Both experimental results and theoretical treatments [81-83] have appeared in the literature recently which suggest that the charge on the thylakoid inner membrane surface may be different from that of the outer surface. Recently reported techniques for measuring the outer surface charge density in the vicinity of PS II [73,75,84] enable us to compare directly the surface charge densities on either side of the membrane in the vincinity of PS II. To avoid ambiguities caused by comparison of quantitative results between different laboratories, both EPR and fluorescence

induction experiments have been carried out and reveal that a surface charge asymmetry does, indeed, exist in the vicinity of PS II.

B. Materials and Methods

1. Kinetic EPR Instrumentation and Experimental Protocol

Only the light source differs from the experimental instrumentation described in the previous section. The protocol remains the same. The light source was a xenon flash lamp (ILC, Sunnyvale, CA) fired by a discharge circuit designed in the laboratory (Fig. 14). The pulse duration was 14 μs (full width at 1/3 maximum); the electrical discharge energy was typically 20 J. The flashes were of saturating intensity as determined by a saturation curve for Signal IIf formation. The flash lamp is housed in a r.f. shielded aluminum box at one focus of an elliptical reflector. The other focus is occupied by one end of a two foot long, tapered lucite light pipe and a plano-convex lens which serve to focus the light onto the grating of the TM_{110} model EPR cavity.

The high voltage power source is from Del Electronics, Mount Vernon, New York. Again, through opto-isolation and careful shielding, no electrical transient is detected by the EPR spectrometer when the lamp is fired.

2. Fluorescence Instrumentation and Experimental Protocol

Fluorescence experiments were performed with either sucrose-washed or Tris-washed chloroplasts as noted.

Figure 14 -- Circuit diagram for Xenon flash lamp.

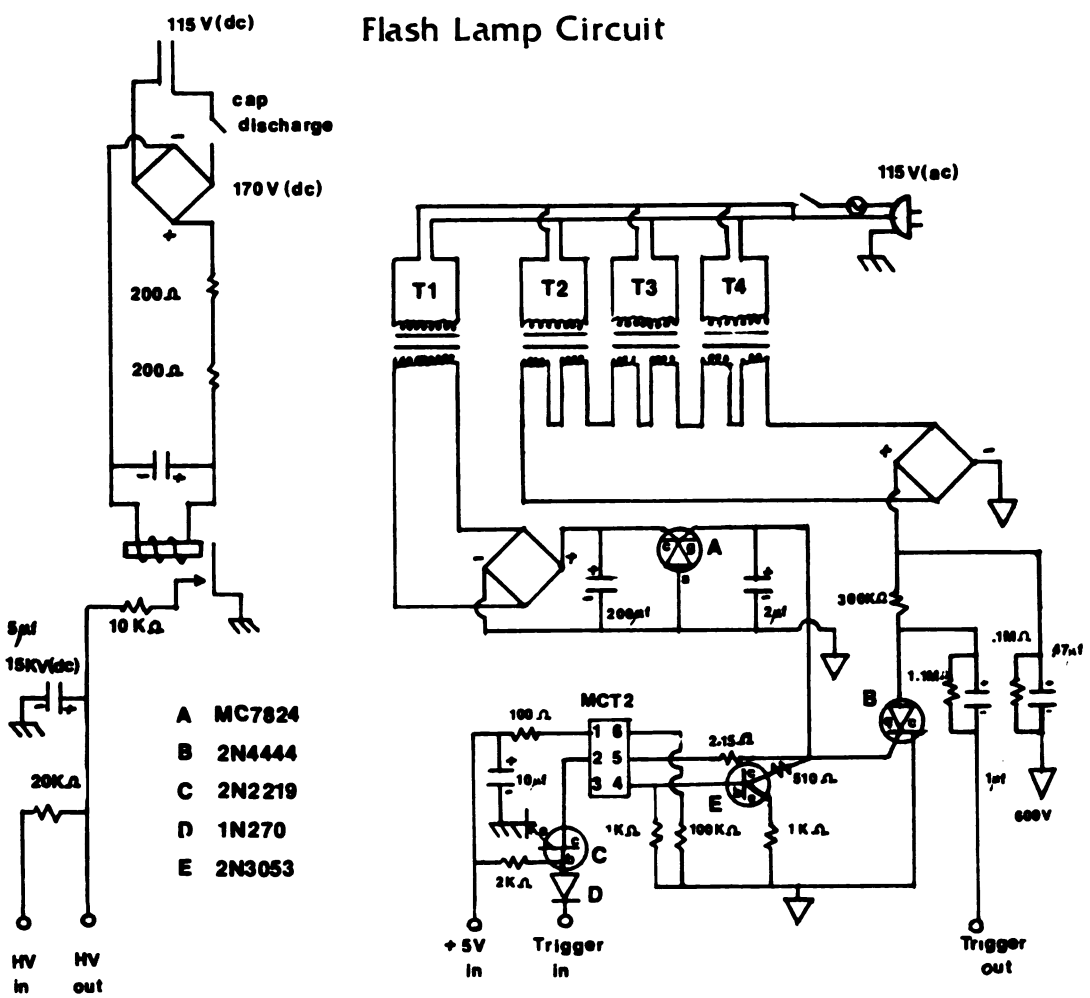
Flash Lamp Circuit
115 V(dc)
cap
discharge
170 V (dc)
200Ω
200Ω
10 KΩ
5μf
15KV(dc)
20KΩ
HV
in
HV
out
A MC7824
B 2N4444
C 2N2219
D 1N270
E 2N3053
115 V(ac)
T1
T2
T3
T4
A
200μf
2μf
300KΩ
.188Ω
B
MCT2
100Ω
10μf
2.15Ω
510Ω
E
1KΩ
100KΩ
1 KΩ
C
2KΩ
D
+5V
in
Trigger
in
Trigger
out
1μf
600V

FIGURE 14

The chloroplasts were suspended (25 to 40 µg chlorophyll per ml suspension) in 0.4 M sucrose, 10 mM NaCl and 50 mM Tricine (pH = 8.0) containing 1 µM 3-(3,4-dichlorophenyl)-1,1-dimethylurea (DCMU). $K_3Fe(CN)_6$ (0.5 mM) was added as noted. The light source was a 200 W tungsten lamp (General Electric Model EJL) operated at 5 V (d.c.) whose output was passed through two filters (Corning CS4-96) and a short pass filter (Baird-Atomic, 600 nm) in order to select blue exciting light. The excitation intensity was 5×10^3 erg cm^{-2} s^{-1}. The fluorescence, measured at a right angle to the excitation beam, was detected by a photomultiplier (EMI 9558QB) protected by two red filters (Corning CS2-58). A camera shutter was used to begin and end the illumination of the sample. The signal from the photomultiplier was recorded on a strip chart recorder. All measurements were made at room temperature.

Aliquots of the dark adapted chloroplast suspensions were added to the reaction solution, including DCMU and $Fe(CN)_6^{3-}$ and allowed to incubate for 1 min in the dark. The sample was illuminated for 90 s to insure complete formation of Q^-. The shutter was then closed. After a variable (5 s - 80 s) dark delay time, the sample was re-illuminated and the state of Q calculated from the equation [82]:

$$\frac{[Q^-]}{[Q_{tot}]} = \frac{F_t - F_o}{F_\infty - F_o} \qquad (3.1)$$

where F_o is the initial "dead fluorescence" level when the dark sample is first illuminated, F_t is the initial fluorescence level upon re-illumination after the dark period (5 s - 80 s), F_∞ is the fluorescence level, measured in the presence of DCMU but absence of $Fe(CN)_6^{3-}$, at the end of a 90 s illumination period. Determination of these fluorescence levels from experimental traces is shown in Fig. 15.

3. Calculation of Membrane Surface Charge Density

The effects of membrane surface potential on reactions involving surface bound reactants can be quantified by using the Gouy-Chapman diffuse double layer model and by making suitable approximations [85-87]. A brief derivation follows. The coulombic interaction between charges in an aqueous system is given by the Poisson equation:

$$\nabla^2\psi = -\frac{4\pi\rho}{\varepsilon} \tag{3.2}$$

where ψ is the potential, ε is the permittivity of water [78.4 ε_o] and ρ is the charge density. The distribution of ions in the solution will be described by a Boltzmann equation:

$$n_i = n_{ib} \exp(-Z_i e\psi/kT) \tag{3.3}$$

where n_i is the concentration of the ith species where the potential is given by ψ, n_{ib} is the concentration at $\psi = 0$ in the bulk solution and Z_i is the ionic charge.

Figure 15 -- Sample traces from fluorescence induct ion experiments showing the determination of the three quantities, F_∞, F_0 and F_t.

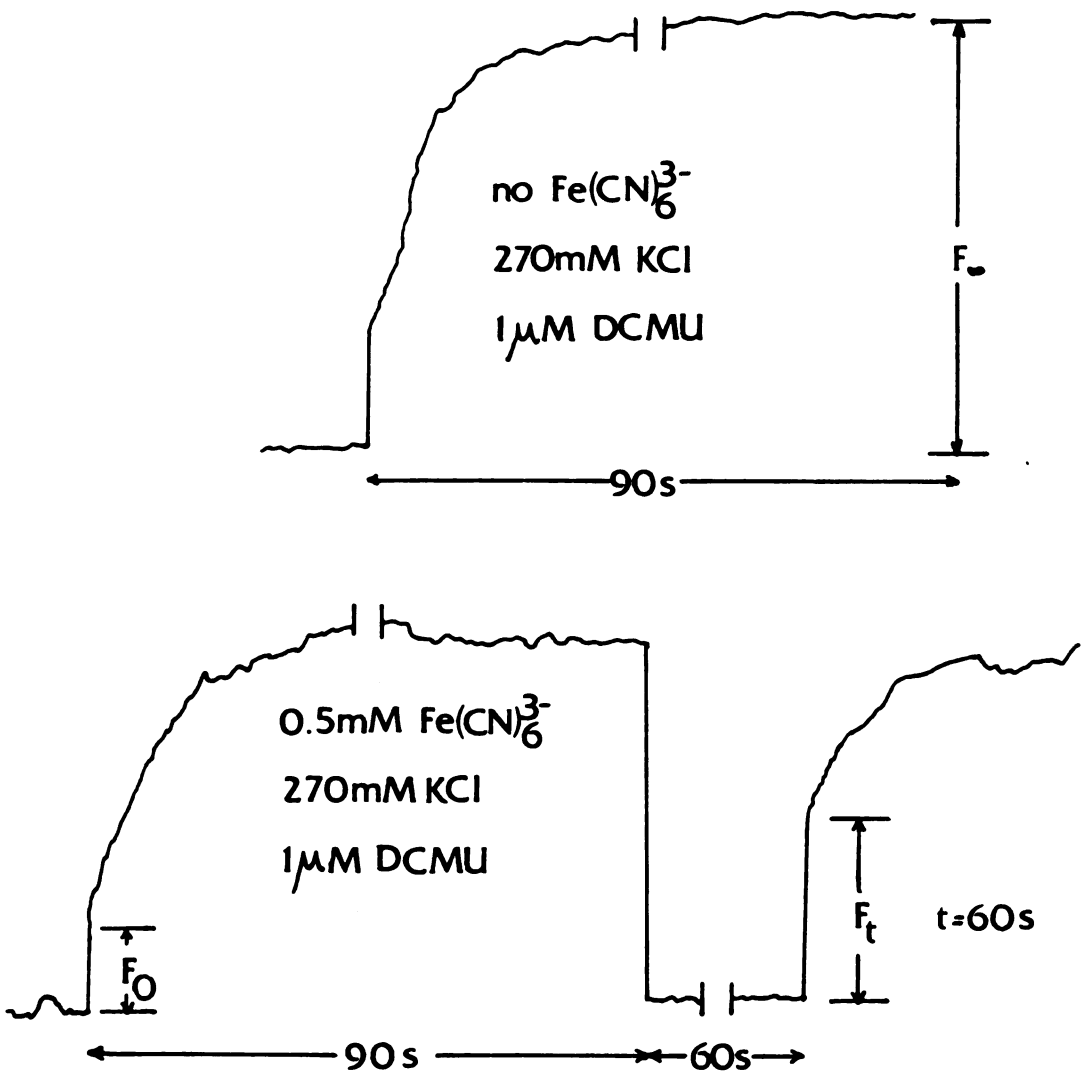
no $Fe(CN)_6^{3-}$
270mM KCl
1μM DCMU
F_∞
90s
0.5mM $Fe(CN)_6^{3-}$
270mM KCl
1μM DCMU
F_0
F_t
t=60s
90s
60s

FIGURE 15

All other terms assume their standard values. The space charge density, ρ, or the sum of ionic charges per unit volume is given by:

$$\rho = \sum_i Z_i e n_i \tag{3.4}$$

By combining Eqs. (3.2), (3.3) and (3.4) one arrives at the expression:

$$\nabla^2\psi = - \frac{4\pi}{\varepsilon} \sum_i Z_i e n_{ib} \exp(-Z_i e\psi/kT) \tag{3.5}$$

The LaPlace operator, ∇^2 is next simplified to d^2/dx^2 by making the assumption that the membrane surface approximates an infinitely large planar interface with the solution. The radius of a single thylakoid is approximately 2500 Å while the electrical double layer exerts an influence on ions at distances no greater than about 100-200 Å from the surface making this approximation reasonable. Equation (3.5) may then be integrated, after some manipulation, to give:

$$(\frac{d\psi}{dx})^2 = \frac{8\pi kT}{\varepsilon} \sum_i n_{ib}[\exp(-Z_i e\psi/kT)-1] \tag{3.6}$$

The condition of electroneutrality requires:

$$\sigma = - \int_o^\infty \rho dx \tag{3.7}$$

where σ is the surface charge density which is equal and opposite to the solution space charge density. Using Poisson's relation, this integrates to give:

$$\sigma = \frac{-\varepsilon}{4\pi} \left(\frac{d\psi}{dx}\right)_{x=0} , \qquad \psi_{x=0} \equiv \psi_s \tag{3.8}$$

where ψ_s is the surface potential. Combining Eqs. (3.6) and (3.8) gives:

$$\sigma = \pm \left| \frac{\varepsilon kT}{2\pi} \sum_i n_{ib}[\exp(-Z_i e\psi_s/kT)-1] \right|^{\frac{1}{2}} \tag{3.9}$$

For $\psi_s < 50$ mV/Z and a Z:Z symmetrical salt:

$$\psi_s = \left(\frac{2\pi kT}{e^2 \varepsilon n_{ib}}\right)^{\frac{1}{2}} \sigma/Z_i \tag{3.10}$$

Again, ψ_s is the membrane surface potential, n_{ib} the concentration of charge on the ith species and σ is the membrane surface charge density. This equation allows the calculation of surface charge density from apparent rate constants as follows [87]. Consider an electron transfer reaction between a redox agent, D, and a membrane bound species, A. The subscripts b and s denote molecules in the bulk phase and at the surface. The rate of reduction of A^+ is described by:

$$- \frac{d[A^+]}{dt} = k^\circ \alpha_{Ds} [A^+] \tag{3.11}$$

where α_{Ds} represents the activity of the redox reagent D near the membrane surface, which is related to the bulk activity of D by the Boltzmann distribution:

$$\alpha_{Ds} = \alpha_{Db} \exp\left(\frac{-Z_D e\psi_s}{kT}\right) \tag{3.12}$$

The apparent rate of reaction is given by:

$$\frac{-d[A^+]}{dt} = k[D_b][A^+] \tag{3.13}$$

By equating (3.11) and (3.13) one arrives at:

$$k^\circ \alpha_{Ds} = k[D_b] \tag{3.14}$$

which, upon substitution of (3.12) becomes:

$$k_o \alpha_{Db} \exp(\frac{-Z_D e\psi_s}{kT}) = k[D_b] \tag{3.15}$$

By defining $\alpha_{Db} = \gamma_{Db}[D_b]$, where γ_{Db} is the activity coefficient as calculated by the extended Debye-Hückel equation, this simplifies to:

$$k = k^\circ \gamma_{Db} \exp(\frac{-Z_D e\psi_s}{kT}) \tag{3.16}$$

By taking the natural log of this equation and substituting equation (3.10) one gets:

$$\ln \frac{k}{\gamma_{Db}} = \ln k^\circ - \frac{Z_D}{Z_i} (\frac{2\pi}{kT\varepsilon})^{\frac{1}{2}} n_{ib}^{-\frac{1}{2}} \sigma \tag{3.17}$$

the final form which relates the apparent rate constant, k, to the bulk salt concentrates, n_{ib}, as well as the surface charge density, σ.

C. Results

The relation between membrane surface charge density (σ) and the rate constant of an electron transfer reaction between a membrane bound component (Z,Q) and a charged redox reagent in the suspension medium ($HAsc^-$, $Fe(CN)_6^{3-}$) has been described by the linearized form of the Gouy-

Chapman equation (3.17) which is valid for monovalent (Z_i = 1) symmetrical salts. For this reason, only the KCl concentration dependence has been used in calculating surface charge density values from the data presented below. The terms γ and Z refer to the activity coefficient and charge of the redox reagent, $HAsc^-$ for the EPR experiments and $Fe(CN)_6^{3-}$ for the fluorescence experiments. The extended Debye-Hückel equation [88] was used to calculate γ; the ion size parameters were taken from Kielland [88] and the value for $HAsc^-$ estimated to be a=6. Because relatively high ionic strengths were used, γ was also calculated by using the Hückel modification to the extended equation which is valid at high (a few molar) ionic strengths [88]. The difference in the calculated values of γ by these two methods leads to a difference in σ, the net surface charge density, which falls within the range of experimental error (± 0.3 μC cm^{-2}). The use of relatively high ionic strengths is dictated by equation (3.17) which is only valid if the surface potential is less than about 50 mV [87]. The terms Z_i and n_i refer to the charge and bulk concentration of the salt in the medium. All other terms assume their standard values.

The salt concentration dependence of EPR Signal IIf is apparent in Figure 16, a series of experimental traces which demonstrate the salt induced enhancement of the decay kinetics. The apparent rate constants were

Figure 16 -- Effect of KCl on the reduction of Z^{+} by $HAsc^{-}$ (2 mM) in Tris-washed chloroplasts, pH = 8.0, instrument time constant = 3 ms, 75 scans averaged.

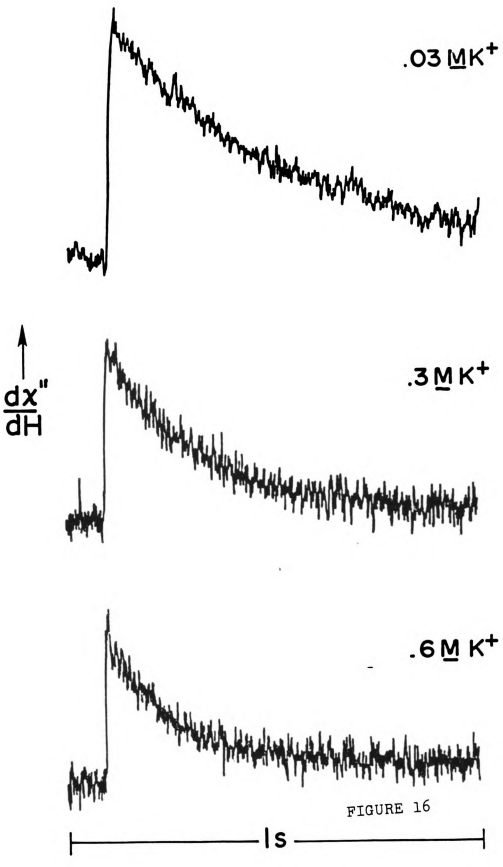

FIGURE 16

calculated from these data and have been plotted in Figure 17 (left) as $(Z_1/Z)\ln(k/\gamma)$ versus $[K^+]^{-\frac{1}{2}}$. As indicated by Eq. (3.17) the slope is proportional to the surface charge density. The EPR data yield a value for σ of -3.4 ± 0.3 $\mu C \cdot cm^{-2}$ for the inner surface of the thylakoid membrane in the vicinity of Z at pH = 8.0. Figure 17 (right) is a similar plot of the results of fluorescence induction experiments on Tris-washed chloroplasts. The fluorescence data show an outer surface charge density near Q of -2.2 ± 0.3 $\mu C \cdot cm^{-2}$, also at pH = 8.0. Analogous fluorescence experiments have been carried out with sucrose-washed, oxygen evolving chloroplasts as a control. The surface charge density near Q calculated from these experiments is -2.1 ± 0.3 $\mu C \cdot cm^{-2}$. Therefore, under dark adapted conditions, a surface charge asymmetry exists across the thylakoid membrane in the vicinity of PS II.

Attempts to measure $\Delta\sigma$ at lower pH values have been complicated by the mechanism of electron donation to $Z^{+\cdot}$ by ascorbic acid. At pH values below 8.0, reduction by the neutral acid, H_2Asc ($pK_a = 4.1$) becomes increasingly important and the surface charge effect is lost [89].

Secondary salt effects on the concentration of $HAsc^-$ and $Fe(CN)_6^{3-}$ were calculated and found to be negligible over the KCl concentration range studied.

To verify that the charge densities we have measured by EPR and fluorescence techniques do correspond to those

Figure 17 -- Plot of equation 3.17 with $Z_i = 1$, (see text) for EPR experiments (left) and fluorescence experiments (right), at pH = 8.0. The salt concentration was adjusted by addition of the monovalent salt, KCl, in both series of experiments.

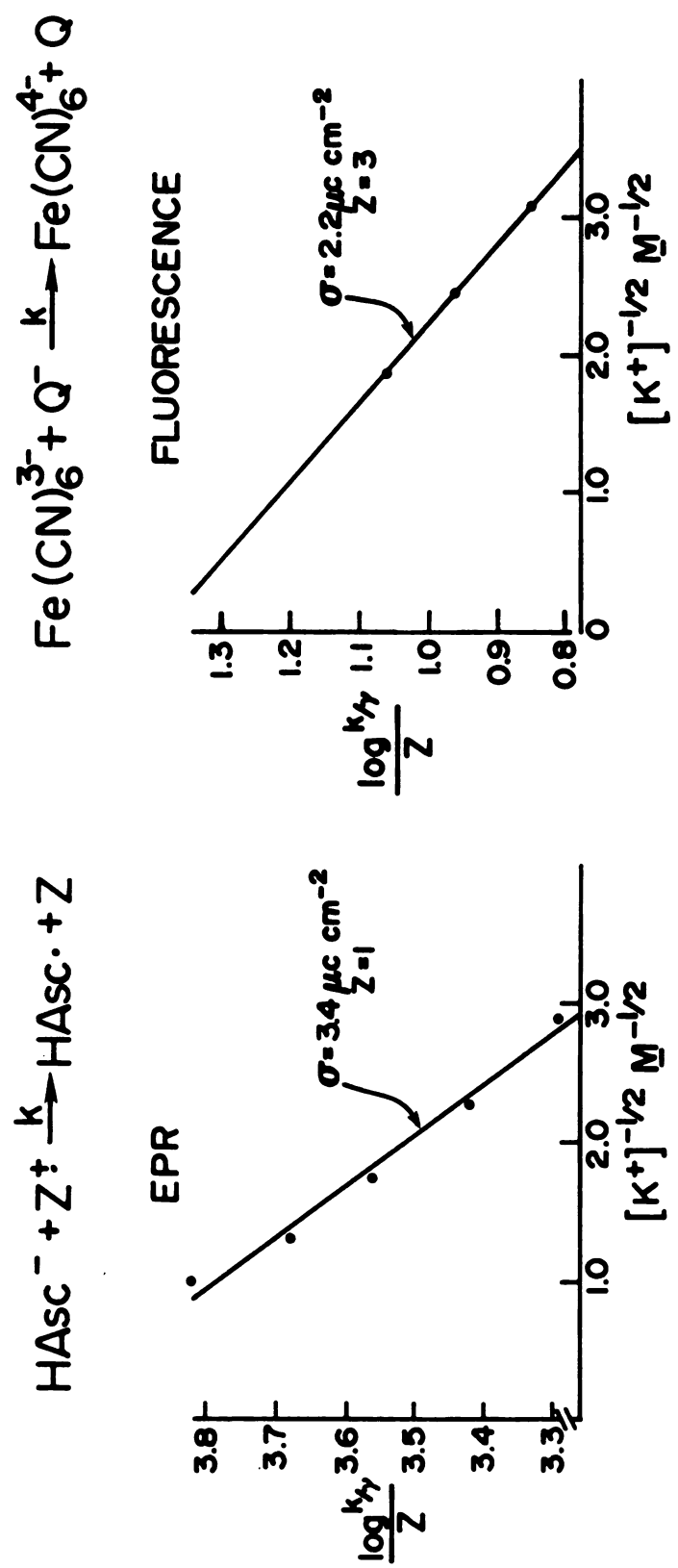
Fe(CN)6 3- + Q- → Fe(CN)6 4- + Q
FLUORESCENCE
σ = 2.2 μc cm-2
Z = 3
log kγ/Z
[K+]-1/2 M-1/2
HAsc- + Z+· → HAsc· + Z
EPR
σ = 3.4 μc cm-2
Z = 1
log kγ/Z
[K+]-1/2 M-1/2

FIGURE 17

at the inner and outer membrane surfaces, respectively, the effects of cationic detergents on the rates of the two reactions have been studied. Detergents modify the surface potential not through a double layer effect, but through specific adsorption. Itoh [73,75] has postulated that the hydrocarbon tails adsorb to the membrane and serve to anchor the positively charged head groups to the surface. He has demonstrated that the resulting decrease in surface potential leads to faster rates of Q^- oxidation by $Fe(CN)_6^{3-}$ in chloroplasts inhibited with DCMU, when cetyltrimethylammonium chloride is used as the detergent. We have reported [89], in contrast to this outer surface behavior, that the addition of a cationic detergent, nonyltrimethylammonium bromide, up to its critical micellar concentration (1.4×10^{-1} M at T = 30°C) shows no effect on the reduction kinetics of $Z^{+\cdot}$ by $HAsc^-$. We have concluded, therefore, that this reaction is mediated by the inner membrane surface potential which remains unaffected, at least at short times, by the addition of cationic detergents. The effect of nonyltrimethylammonium bromide on the kinetics of Q^- oxidation by $Fe(CN)_6^{3-}$ in tris-wash chloroplasts has also been examined. In agreement with the results of Itoh on sucrose-washed chloroplasts in the presence of cetyltrimethylammonium chloride, we have seen an enhancement in the rate of reaction at detergent concentrations below those required to perturb the double layer

through non-specific cationic effects. Thus, only one of the two surface charge densities that we have measured is susceptible to alteration by detergent adsorption, consistent with the hypothesis that one reflects outer, and the other inner, surface effects.

D. Discussion

Two techniques, the decay of EPR Signal IIf and fluorescence induction in tris-washed chloroplasts, have been used to determine net surface charge densities for the inner and outer thylakoid membrane surfaces in the vicinity of PS II. The values obtained are -3.4 ± 0.3 $\mu C \cdot cm^{-2}$ for the inner surface and -2.2 ± 0.3 $\mu C \cdot cm^{-2}$ for the outer surface, corresponding to one electronic charge per 500 $Å^2$ on the inner surface and to one charge per 750 $Å^2$ on the outer surface near PS II. The use of two different ionic species in these experiments does not appear to be a serious limitation judging by the similarity in values for surface charge near P700 obtained by using either ascorbate or ferrocyanide as the charged species (Table 2). As shown previously [89] no pH gradient is built up during the course of an experiment under our conditions. These calculated surface charge densities are, therefore, valid at pH = 8.0, the pH of the suspension medium. It must also be noted that the $\Delta\sigma$ measured in these experiments is specific to the membrane near PS II. Surface potentials

Table 2 -- Selected Values of Thylakoid Surface Charge Densities.

Conditions	Method	Membrane location, surface charge (σ)	Source
Tris-wash H_2Asc pH=8.0	EPR	inside, PS II $-3.4 \pm 0.3\ \mu C \cdot cm^{-2}$	This work
Tris-wash $K_3Fe(CN)_6$ DCMU pH=8.0	Fluorescence induction	outside, PS II $-2.2 \pm 0.3\ \mu C \cdot cm^{-2}$	This work
Sucrose wash $K_3Fe(CN)_6$ DCMU pH=8.0	Fluorescence induction	outside, PS II $-2.1 \pm 0.3\ \mu C \cdot cm^{-2}$	This work
Sucrose wash DCMU pH=7.4-8.0	Fluorescence changes	outside, PS II $-2.5\ \mu C \cdot cm^{-2}$	[86]
Sucrose wash $K_3Fe(CN)_6$ DCMU pH=7.6	Fluorescence induction	outside, PS II $-1.3\ \mu C \cdot cm^{-2}$	[73]
Sucrose wash phenazine-methosulfate DCMU pH=7.6	Fluorescence induction	outside, PS II $-1.47\ \mu C \cdot cm^{-2}$	[73]

Table 2 Continues.

Table 2 Continued.

Conditions	Method	Membrane location, surface charge (σ)	Source
Sucrose wash, sonicated H_2Asc pH=7.8	Absorption	inside, PS I $-0.86\ \mu C \cdot cm^{-2}$	[87]
Sucrose wash, sonicated $K_4Fe(CN)_6$ pH=7.8	Absorption	inside, PS I $-0.84\ \mu C \cdot cm^{-2}$	[87]
Chloroplasts pH=7.0	Electrophoretic mobility	outside, total $-1.1\ \mu C \cdot cm^{-2}$	[72]
Chloroplasts pH=7.2	Electrophoretic mobility	outside, total dark $-0.46\ \mu C \cdot cm^{-2}$ light $-0.95\ \mu C \cdot cm^{-2}$	[127]
Chloroplasts 9-aminoacridine pH=7.5	Fluorescence quenching	outside, total -1.4 to $-3.6\ \mu C \cdot cm^{-2}$	[128]

can be calculated from these charge densities at various salt concentrations by using the equation:

$$\sigma = 7.33 \times 10^{-3} n^{\frac{1}{2}} \sinh\left(\frac{Z\psi_s}{50.9}\right) \qquad (3.18)$$

valid at 25°C and following from Eqs. (3.2)-(3.17). If the chloroplast suspension is 10 mM in monovalent salts, this leads to a $\Delta\psi_s$ of 20 mV across the membrane or a field of 4×10^4 $V \cdot cm^{-1}$ for a membrane thickness of 50 Å. This dark, static field is an order of magnitude smaller [90] and in the opposite direction to the photo-induced field, arising from the photo-oxidation of P680 and photo-reduction of Q across the thylakoid membrane, that being positive toward the inner surface and negative toward the outer surface. This photo-induced field has been shown to cause a red shift in an absorption band, around 515 nm, of an indicator pigment, [91-93], an example of the Stark effect, which predicts that the extent of the band shift is a function of both the dipole moment of the absorbing species and of the magnitude of the electrical field. The change in the molar absorption coefficient, ε, is given approximately by [94]

$$\Delta\varepsilon = \frac{\Delta\mu\cos\Theta}{hc} F \frac{\partial\varepsilon}{\partial\tilde{\nu}} + \frac{1}{2hc} \Delta\alpha F^2 \frac{\partial\varepsilon}{\partial\tilde{\nu}} + \frac{(\Delta\mu)^2\cos^2\Theta}{2h^2c^2} F^2 \frac{\partial^2\varepsilon}{\partial\tilde{\nu}^2} \qquad (3.19)$$

where $\Delta\mu$ is the permanent dipole moment difference between

the ground and excited states of the absorbing molecule, Θ is the angle between $\Delta\bar{\mu}$ and $\bar{F}$, $\tilde{\nu}$ the wavenumber and $\Delta\alpha$ is the polarizability difference between the ground and excited states. The other terms assume their usual values. Electrochromic shifts in chlorophyll b absorbance, *in vivo* and *in vitro*, have been measured and are linear with respect to the field. As chlorophyll b has a permanent dipole moment, this approximately linear response to the field strength is expected from the first term of Eq. (3.19). The extent of the 515 nm absorbance shift has also been shown to be linearly proportional to the light induced membrane field [95-97]. However, since the absorbing species is a carotenoid, probably β-carotene, which has no permanent dipole moment, a quadratic field dependence would be predicted instead. One explanation for this discrepancy has been the assumption that the carotenoids are exposed to a permanent electrical field, F_p, perpendicular to the membrane, which is much stronger that the light induced field F_L [98]. The effective field would then be the sum of the light induced field, F_L, and the permanent field, F_p. Under these conditions, the absorption change, ΔA, would be proportional to $(F_p+F_L)^2$. If F_p were much larger than F_L, the pseudo-linear term, $2F_pF_L$, would predominate over the quadratic term, F_L^2, giving a ΔA proportional to F_L, as is observed experimentally. This "linearizing field", F_p, has been attributed to surface

potential asymmetry in the vicinity of PS II and, to meet the requirements of the argument above, must be not only much larger, but also in the same direction as the light induced field, F_L. As our results indicate, this is most unlikely. We have found a surface charge density asymmetry, leading to a transmembrane field. This field is, however, smaller than the light induced field (4×10^4 V cm^{-1} versus 2×10^5 V cm^{-1}) and in the opposite direction (negative inside). Thus, we concur with Reich and Sewe [99,100] that the permanent, polarizing force felt by the carotenoids is local in nature, and not a transmembrane field arising from membrane surface potential asymmetry.

Our experimental measurements do concur, however, with a model presented by Duniec and Thorne [101] in which they propose a mechanism of proton uptake by chloroplast membranes in terms of asymmetry of membrane surface charges. The model is presented schematically in Figure 18. The dark adapted case is shown in Figure 18a. Under these dark equilibrium conditions, the enclosed volume and the outside solution have the same electric potential and same concentration of ions, except for the diffuse charge layer adjacent to the membrane. This is a result of the surface potential asymmetry ($\psi_{s,in} \neq \psi_{s,out}$), a consequence of the transmembrane surface charge asymmetry ($\sigma_{in} \neq \sigma_{out}$). In equilibrium, this difference creates an internal electric field in

Figure 18 -- A schematic representation of the thylakoid membrane and its associated surface potential (a) in dark adapted chloroplasts ($pH_{in} = pH_{out}$) and (b) after illumination ($pH_{in} < pH_{out}$).

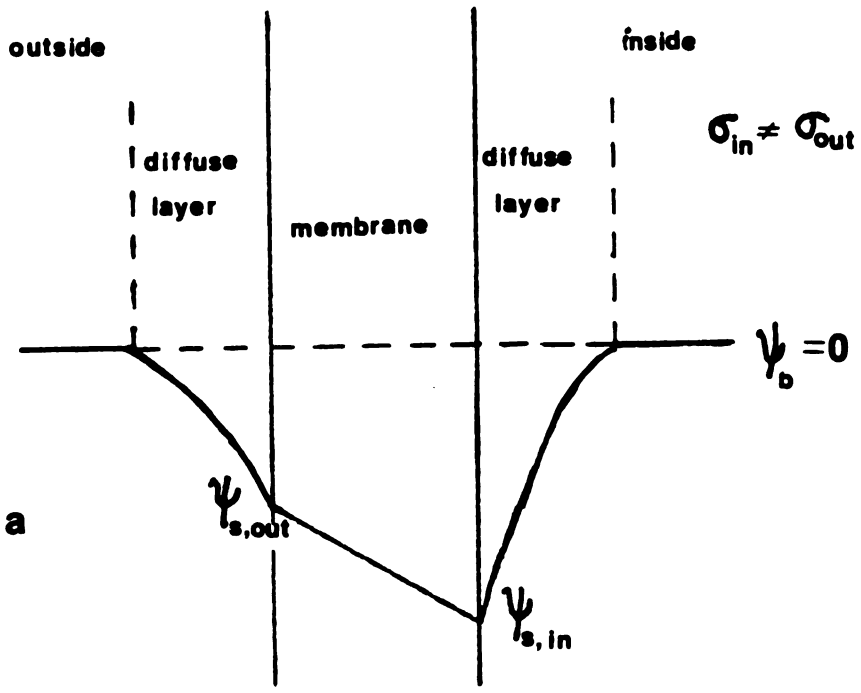
outside
inside
diffuse layer
membrane
diffuse layer
$\sigma_{in} \neq \sigma_{out}$
$\psi_b = 0$
$\psi_{s,out}$
$\psi_{s,in}$
a

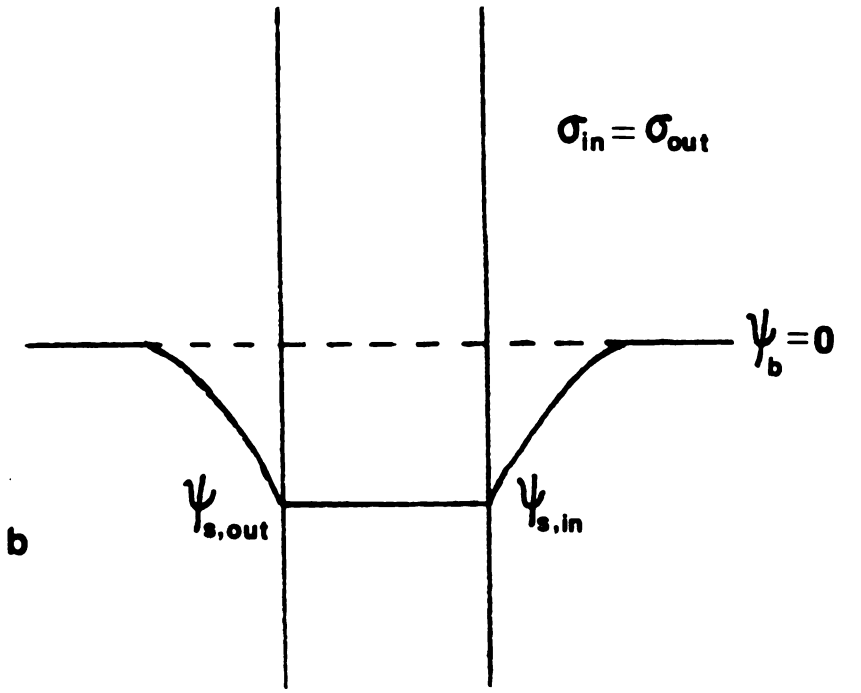
$\sigma_{in} = \sigma_{out}$
$\psi_b = 0$
$\psi_{s,out}$
$\psi_{s,in}$
b

FIGURE 18

the membrane. This field is dissipated, however, after illumination. Figure 18b illustrates the system under steady state conditions. Upon illumination, chloroplasts take up protons via the plastoquinone pool and the proton release from water oxidation. As the inner pH drops, the surface bound groups giving rise to the negative surface charge will protonate and decrease the surface charge density. In Figure 18b, the surface charge densities are shown as being equal, leading to a loss of the membrane field. However, the magnitude and even the orientation of the steady state field are difficult to predict, as we have been unable to measure the effective pK_a of the inner surface with the system we have studied, i.e., by using ascorbic acid as the donor. Average values for the inner (pK_a = 4.1) and outer (pK_a = 4.4) surfaces have been estimated [82] and indicate a charge asymmetry across the membrane, although these are average values for the two surfaces, not localized charge densities as we believe we have measured.

The orientation of the field, negative toward the inside, is such that it could be expected to stabilize the charge separation at the PS II reaction center. For example, <u>in vitro</u>, the rate of the back reaction between bacteriopheophytin and methylviologen, a donor-acceptor pair with a free energy difference comparable to that between bacteriochlorophyll and bacteriopheophytin, is of the order of 2×10^{12} s^{-1} [101]. This is about 10^4

times faster than the *in vivo* reaction between BChl and BPh [102], which has been attributed, to some extent, to stabilization through interaction with other charged components of the reaction center. Assuming that the full 20 mV is experienced by the photogenerated electron and hole, we calculate that the field arising from surface charge asymmetry should slow the deleterious charge recombination by a factor of two [103], an effect that should be lost after light driven acidification of the inner thylakoid volume (Figure 18).

IV. CHARACTERIZATION OF AN ENDOGENOUS DONOR TO PHOTOSYSTEM II

A. Introduction

In both the EPR and fluorescence experiments described in the previous section, we used a variety of mono-(K^+, Na^+) and divalent (Mg^{2+}, Ca^{2+}, Mn^{2+}) cations to probe the surface charge properties of the thylakoid membrane. In general, these species behave in a manner consistent with the Gouy-Chapman model in that we observe increased decay rates, through a double layer effect, as the ionic strength of the medium is increased. We have observed, however, anomalous, non-double layer effects with both Ca^{2+} and Mn^{2+} salts as well as with the anion of carbonylcyanide m-chlorophenylhydrazone, $CCCP^-$. In each case, we see a dramatic enhancement in the decay rate of Signal IIf at salt concentrations far below those required to perturb the membrane surface potential significantly. We have developed a model in which an endogenous donor to Z becomes kinetically competitive with exogenous donors upon addition of low concentrations of Mn^{2+} or $CCCP^-$ (10 μM) or moderate concentrations of Ca^{2+} (10 mM). A second postulate of this model is that the endogenous

donor, which we observe under reducing conditions in Tris-washed chloroplasts, is the membrane component that mediates cyclic electron flow around PS II in DCMU blocked, Tris-washed chloroplasts, under oxidizing conditions.

Other groups have reported general Ca^{2+} effects in the electron transfer reactions of PS II [104-106] but our data localize an effect on the oxidizing side of PS II, between the reaction center and the water oxidizing complex. Piccioni and Mauzerall [107,108] have reported a Ca^{2+} sensitive, high potential component, acting as both an electron donor and acceptor for PS II, which they imply may be cytochrome b_{559}.

Mn^{2+} has also been implicated in the photo reactions of cytochrome b_{559} [109-111] although firm experimental evidence is notably lacking. EPR work has been done, however, which suggests that Mn^{2+} serves as a direct electron donor to $P680^{+}$, as evidenced by a loss of Signal IIf amplitude with increasing Mn^{2+} concentration in Tris-washed chloroplasts [68]. Upon closer investigation, we find that the Mn^{2+} effect on Signal IIf is, phenomenologically, very similar to that of Ca^{2+}, a non-redox active species. This has led us to reinterpret these earlier data in terms of the endogenous donor model.

The third reagent that leads to the enhanced decay rate of Signal IIf, $CCCP^{-}$, is one of a class of ADRY (Acceleration of the Deactivation Reactions of the water

splitting enzyme, Y) reagents. These are lipophilic anions which act to modify the stability of redox equivalents stored in the S-states by decreasing the lifetimes of S_2 and S_3 [112]. The mechanism of destabilization is unknown. The other effects of this class of reagents are worth noting. They lead to the rapid dark decay of EPR Signal IIs [61] which is formed by the S_2 and S_3 states, and they lead to the photooxidation of cytochrome b_{559} [113-115].

Thus, although it is difficult to reconcile the fact that hydrophilic cations (Ca^{2+} and Mn^{2+}) and a lipophilic anion ($CCCP^-$) appear to induce the same changes in the decay rate of EPR Signal IIf, all three species have been previously implicated in a common process, the photooxidation of cytochrome b_{559}, although the mechanism of their involvement has not been well defined. Here, we shall attempt to give a more quantitative description of their effects and to integrate them into a model based on the existence of an endogenous donor to PS II.

B. Materials and Methods

1. Kinetic EPR Instrumentation

These experiments were performed with a Bruker model ER-200D EPR spectrometer. A Varian TM_{110} mode cavity (model E238) was fitted to the microwave bridge by using appropriately modified waveguide and impedence matching circuitry. The sample cell was a Scanlon EPR flat cell

(S-814). The microwave power was 20 mW and an effective modulation amplitude of 5G, as determined by the method of Poole [116], was used in all experiments. The light source was a Xenon flash lamp as described in the preceeding section. Data were collected and stored with a Nicolet model 1180 data system.

A new timing circuit, shown in Fig. 19, was designed by M. Rabb and built in the laboratory. This allows the triggering of the flash lamp after triggering the EPR trace. The delay time is variable for 2 to 20 ms. The repetition rate of this sequence is variable from 2 flashes per second to one every 20 seconds. The novel feature of this circuit is that the triggering is based on a 100 KHz signal from the EPR instrument. This feature is included to help minimize a light induced cavity transient. This transient is seen both with and without sample in the cavity (Fig. 20a,b), is independent of the detector phase angle (Fig. 20c), is dependent on the microwave power (Fig. 20d,e) and is strictly a light induced, i.e. not an electrical, transient (Fig. 20f). The transient apparently arises from light induced change in the Q of the cavity ($Q = \nu_r/\Delta\nu$, where ν_r = resonance frequency and $\Delta\nu$ = difference of frequency values at the half power points or, alternatively, $Q = 2\pi$ maximum microwave energy stored in cavity/energy dissipated per cycle). This gives rise to the positive going spike in Fig. 20 which is followed by a negative going signal during

Figure 19 -- Circuit diagram of kinetic EPR triggering circuit.

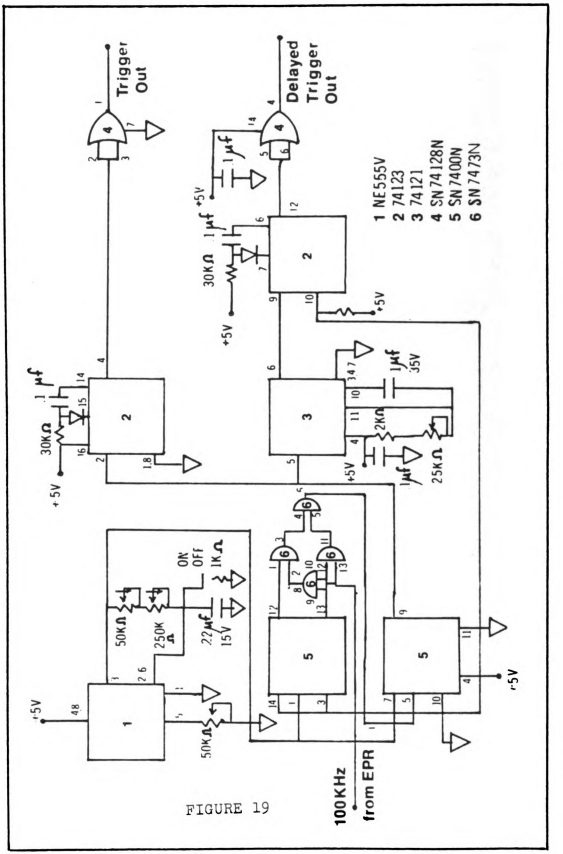
Trigger Out
Delayed Trigger Out
100KHz from EPR
1 NE555V
2 74123
3 74121
4 SN74128N
5 SN7400N
6 SN7473N

FIGURE 19

Figure 20 -- Light induced cavity transient (a) sample in cavity, (b) empty cavity, (c) phase angle 180° out of phase (d) 200 mW power, (e) 20 mW power, (f) light blocked from cavity but flash lamp firing. Instrument time constant 100 μs, 100 scans averaged, 5 G modulation amplitude, 20 mW power unless otherwise noted.

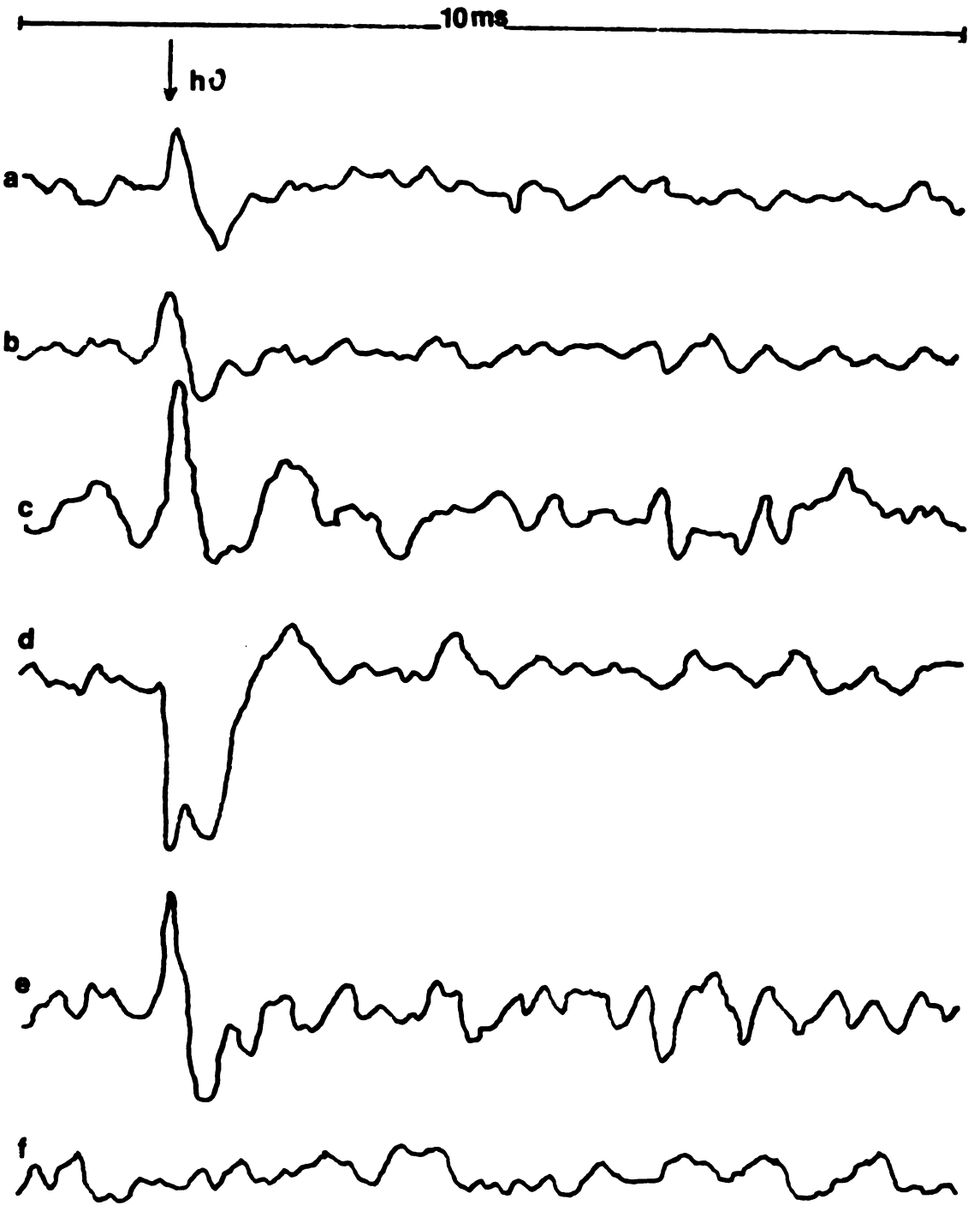

FIGURE 20

a recovery period. These relatively long lived signals may be due to the lock-in amplifier as Fourier components of the Q change will exist and will be amplified. We have attempted to correct this by triggering alternatively on the positive and negative edges of the 100 KHz modulation frequency of the EPR instrument. We have also placed a passive filter (50 KHz low pass) between the microwave detector and signal amplifer and, so, have shortened the duration of the transient. The remaining cavity signal, however, precludes the measurement of signal rise times faster than about 1 ms and subtracts from the EPR signal during the lifetime of the cavity transient, leading to an apparently lower signal height. This has prevented us from seriously pursuing the kinetics of Signal IIvf, whose decay-halftime corresponds roughly to the duration of the cavity transient. This transient has caused difficulty in detecting the newly observed fast phase of Signal IIf, as well.

2. Spinach and Chloroplast Suspensions

Chloroplast suspensions were prepared as described in previous sections, with a few exceptions. Where noted (Tris/EDTA wash) 1 mM EDTA was added to the grinding medium to remove non-essential manganese from the suspension. In some suspensions (EDTA rinse), 1 mM EDTA was also added after the 20 min. light incubation in Tris buffer, before the suspension was centrifuged. This removes Mn^{2+} released during Tris-washing.

3. Potential Measurements

A small volume (5 ml) of Tris-washed chloroplast suspension (3-5 mg Chlorophyll/ml suspension) was used as a sample reservoir in the redox titrations described below. These chloroplasts were kept dark and at room temperature during the course of the experiment (3 hours). The potential of the sample was maintained with a 10 mM $Fe(CN)_6^{3-}/Fe(CN)_6^{4-}$ couple, titrated with a 0.1 M solution of ascorbic acid (pH = 8.0) in STN. A saturated calomel electrode (Radiometer, K 401), which served as the reference electrode, a short length of Pt wire and a model 701-A potentiometer (Orion Research) were used to measure the suspension potential which was recorded before and after each experiment. The reported potentials are an average of these two readings, which usually varied by no more than 5 mV. The system was calibrated using the quinhydrone couple.

C. Results

1. Reducing conditions

a. Ionic Effects

As noted in the introduction, we have found anomalous effects of Ca^{2+} on the decay kinetics of Signal IIf, as shown in Fig. 21. These are experimental traces (2 mM $HAsc^-$, pH = 8.0) which show the relative effect of 50 mM Ca^{2+} (bottom) and 50 mM Mg^{2+} (top). Addition of Ca^{2+} obviously leads to faster decay of the $Z^{+\cdot}$ radical.

Figure 21 -- Effect of Mg^{2+} (top left) and Ca^{2+} (bottom left) on reduction of $Z^{+\cdot}$ in Tris-washed chloroplasts, pH = 8.0, 2 mM $HAsc^-$, instrument time constant 1 ms, 150 scans averaged. Effect of Mg^{2+} (top right) and Ca^{2+} (bottom right) on the oxidation of Q^- by $Fe(CN)_6^{3-}$ in Tris-washed chloroplasts, pH = 8.0.

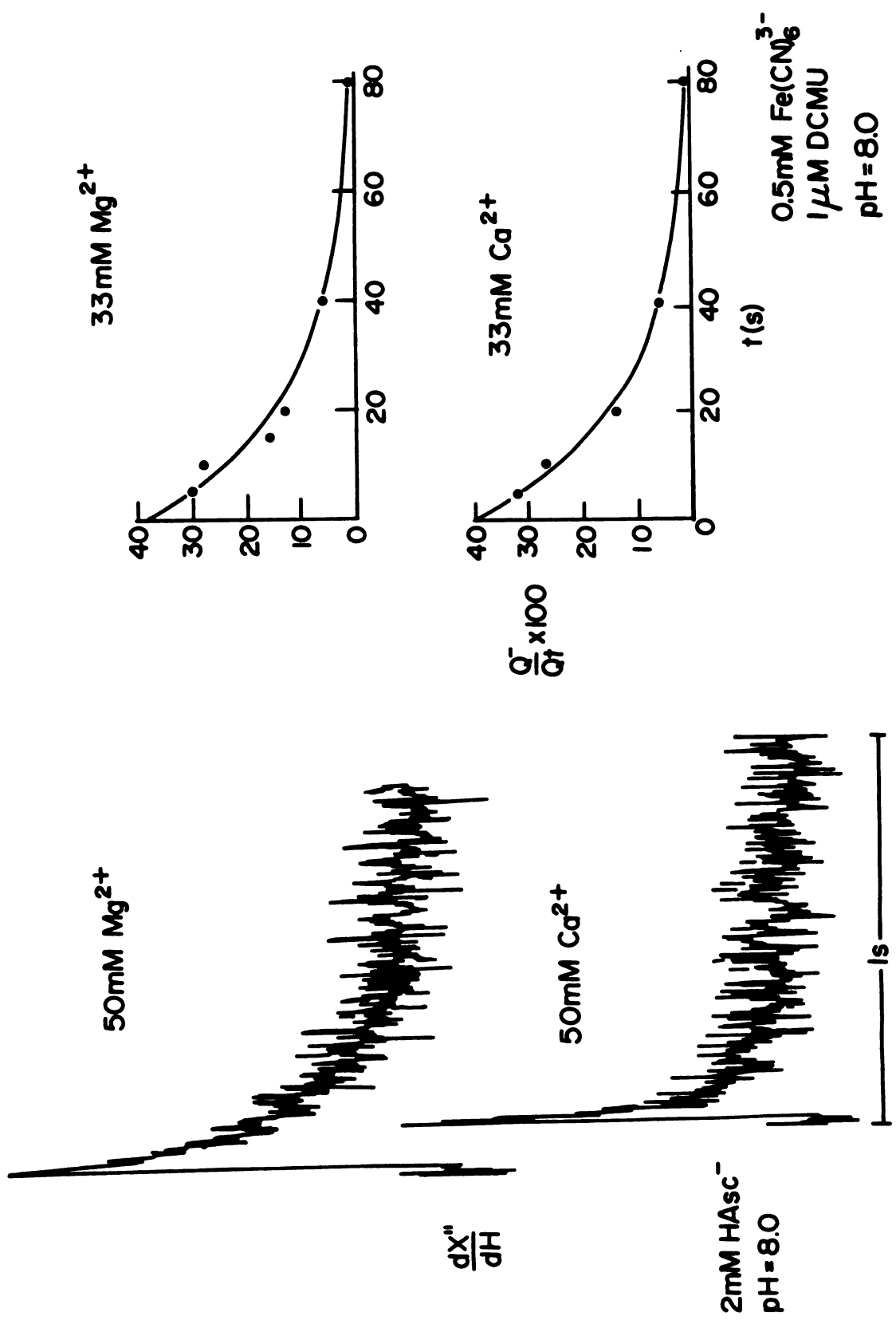
33mM Mg2+
33mM Ca2+
0.5mM Fe(CN)6 3-
1μM DCMU
pH=8.0
t(s)
Q⁻/Qt x100
50mM Mg2+
50mM Ca2+
dX"/dH
2mM HAsc⁻
pH=8.0
1s

FIGURE 21

A trivial explanation for the Ca^{2+} specific enhancement (complex formation between $HAsc^-$ and Ca^{2+}) can be ruled out based on the binding constant for this reaction [117]. The Ca^{2+} effect seems to be specific to the oxidizing side of PS II as demonstrated by the right hand portion of Fig. 21, a plot of the time course of fluorescence induction data for Tris-washed Chloroplasts (pH = 8.0) with 0.5 mM $K_3Fe(CN)_6$, 1 μM DCMU and 33 mM Ca^{2+} (bottom) or Mg^{2+} (top). In these experiments, Ca^{2+} and Mg^{2+} behave simply as divalent cations. Similar fluorescence results were noted by Itoh [75] in experiments on non-Tris-washed chloroplasts.

To test the involvement of Ca^{2+} in non-surface charge effects on the water side of PS II, we have studied the effect of Ca^{2+} and Mg^{2+} on the decay kinetics of Signal IIf under conditions in which diphenylcarbazide, a neutral donor to PS II [89], was used as the reductant. Addition of Mg^{2+} in concentrations ranging from 10 to 50 mM with 0.4 mM diphenylcarbazide had no effect on the rate of Signal IIf decay. Similar concentrations of Ca^{2+}, however, led to a 2.5 fold enhancement in the decay rate. In neither case was any variation in rate detected with increased salt concentration, exactly as would be predicted for a non-charged donor. In attempting to explain this Ca^{2+} effect, we have decreased the EPR instrument time constant to 1 ms or less and, by doing so, have resolved a previouly undetected decay component ($t_{\frac{1}{2}} \sim 20$ ms) of

Signal IIf. What follows is the initial characterization of an endogenous donor to PS II which provides a fast decay pathway for the photo-induced Z^{+} free radical in Tris-washed chloroplasts.

Figure 22 is a series of experimental traces showing the effects of $HAsc^{-}$ (a), EDTA (b), and Ca^{2+} (c) on Signal IIf decay. In the absence of exogenous donors, the decay of Signal IIf corresponds to that reported earlier [66]. Upon addition of 2 mM ascorbic acid (pH = 8.0) (Fig. 22a) there is a dramatic change in the decay rate of Tris-washed chloroplasts. In this trace, taken with an instrument time constant of 1 ms, the decay is clearly bi-phasic, in contrast to the previously reported effects of exogenous donors on IIf decay kinetics [68]. In those experiments, the signal decay was shown to be exponential with a half time dependent on the donor concentration. We have verified this in Section II. However, in all previous experiments a marked decrease in signal amplitude, upon addition of donors, was also reported. This apparent signal loss can be explained in terms of the instrument time constant as demonstrated by Fig. 23, a comparison of the same EPR transient accumulated with a) a 2 ms and b) a 10 ms time constant. The fast decay phase is not resolved in trace b) and is manifest as a decrease in total signal amplitude.

The fast decay phase can be eliminated without loss in signal amplitude (Fig. 22b) by addition of 1 mM EDTA

Figure 22 -- Effect of $HAsc^-$ (2 mM, pH = 8.0) on (a) Tris-washed chloroplasts alone, (b) with 1 mM EDTA, (c) with 50 mM $CaCl_2$. Instrument time constant = 1 ms, 150 scans averaged.

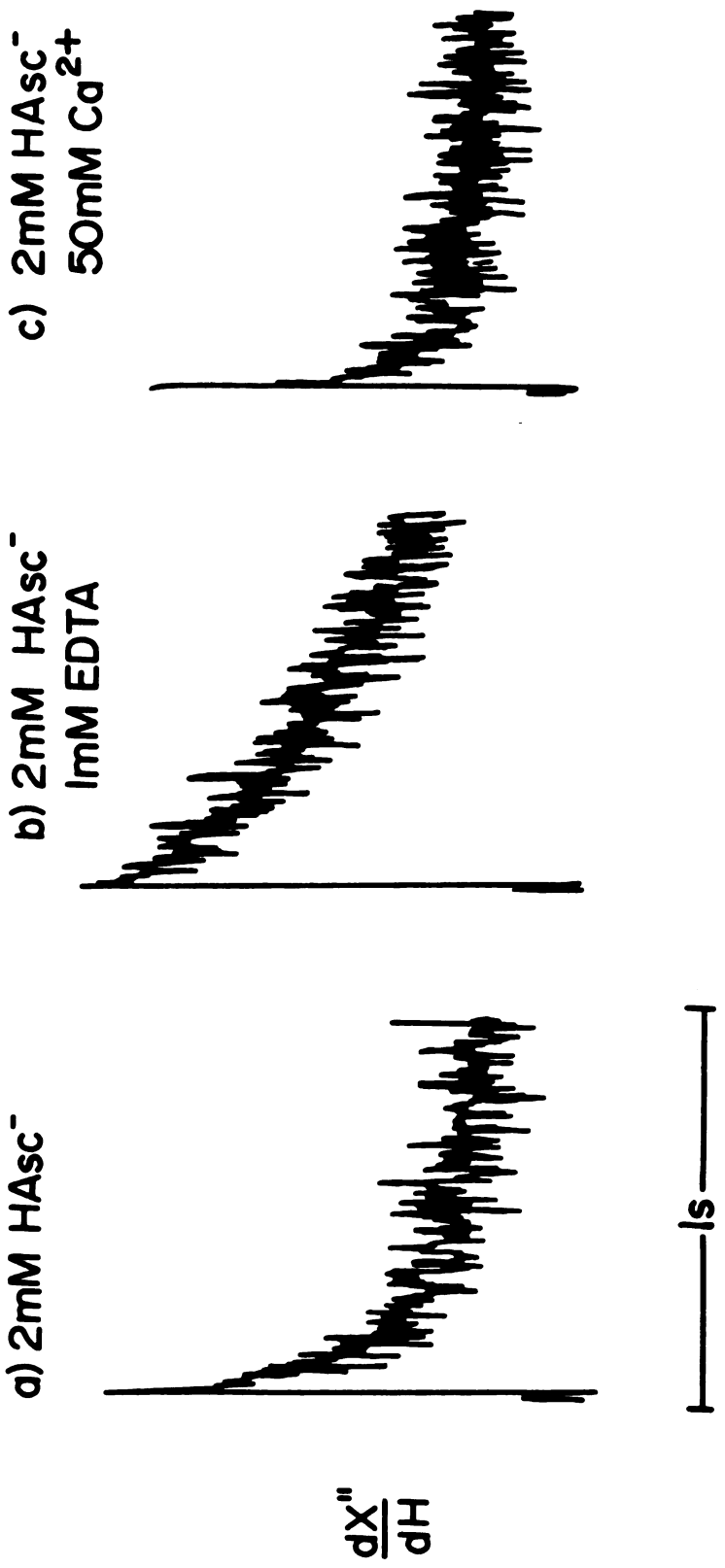

FIGURE 22

Figure 23 -- Effect of instrument time constant on Signal IIf decay traces. (a) instrument time constant = 2 ms and (b) 10 ms. Power = 20 mW, 100 scans averaged, Tris-washed chloroplasts, 2 mM $HAsc^-$ (pH = 8.0).

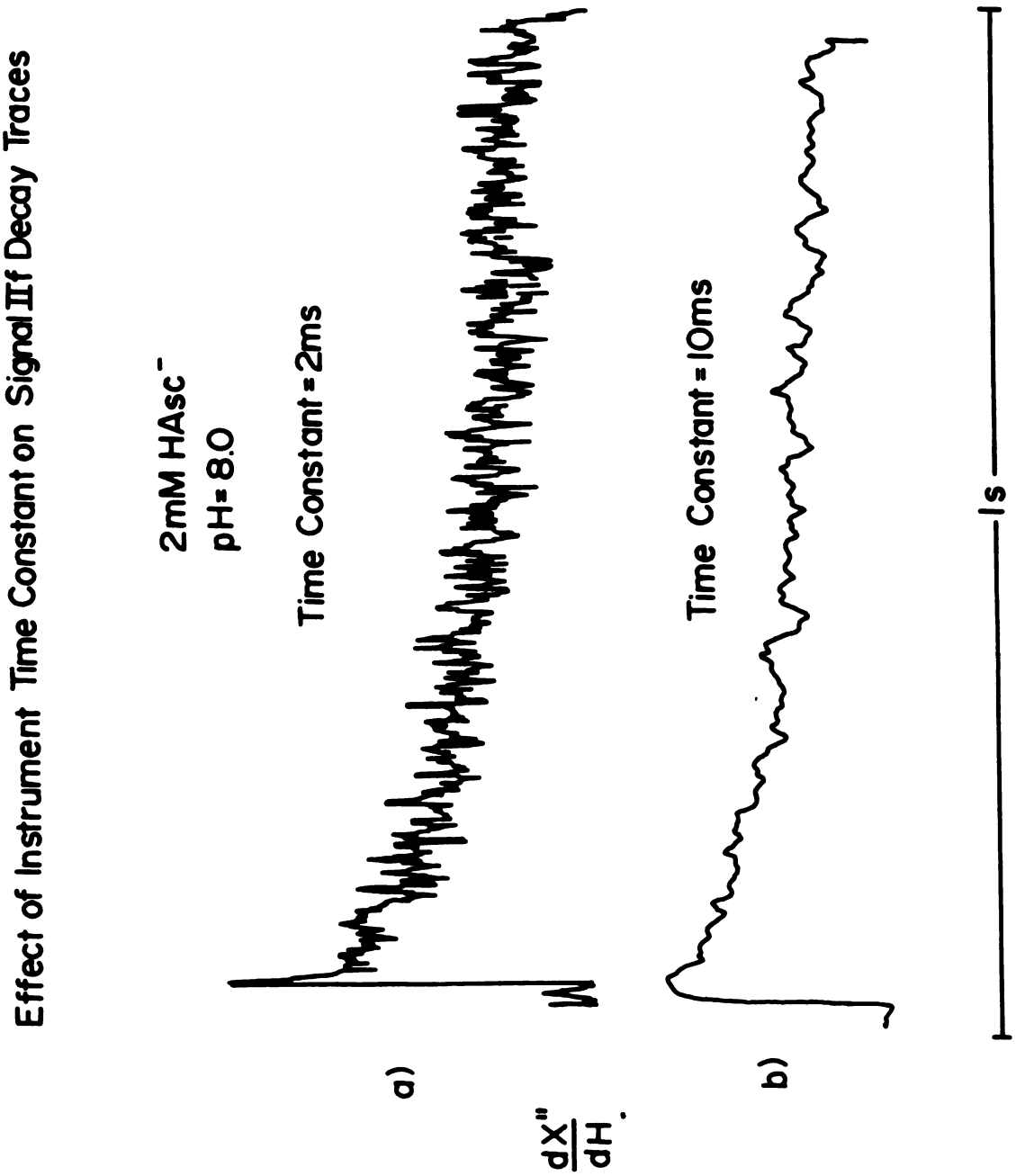
Effect of Instrument Time Constant on Signal IIf Decay Traces
2mM HAsc⁻
pH=8.0
Time Constant=2ms
Time Constant=10ms
a)
b)
dX"/dH
1s

FIGURE 23

after Tris-washing. This treatment removes Mn^{2+} which is only loosely bound to the membrane after Tris-washing. Addition of Ca^{2+} also removes this loosely bound Mn^{2+}, as we have reported elsewhere [118]. In the model which we developed there, four manganese are associated with each reaction center. One of these four is released from the membrane upon treatment with Tris, and a second manganese may be removed by addition of either EDTA (1 mM) or Ca^{2+} (50 mM). As Fig. 22 demonstrates, however, the effect on the decay kinetics of Signal IIf is quite different with these two treatments. Addition of EDTA gives slow, donor concentration dependent decay kinetics (Fig. 22b). Addition of Ca^{2+}, however, leads to a much faster decay rate (Fig. 22c). We propose, therefore, that a rapid decay pathway for $Z^{+\cdot}$ exists when either Ca^{2+} or Mn^{2+} are associated with Z. A simple kinetic scheme can be used to describe the traces in Fig. 22 as follows:

$$A_H\, Z^{+\cdot} + D \xrightarrow{k_1} A_H\, Z + D^+ \qquad k_1\ (2\ \text{mM}\ HAsc^-, pH = 8.0) = 1.4\ s^{-1} \tag{4.1}$$

$$A_H{}^- Z^{+\cdot}\ M \xrightarrow{k_2} A_H\, Z\ M \qquad k_2 \sim 35\ s^{-1} \tag{4.2}$$

$$A_H\, Z\ M + D \xrightarrow{k_3} A_H{}^- Z\ M + D^+ \qquad k_3 > k_4 \tag{4.3}$$

$$A_H\, Z + D \xrightarrow{k_4} A_H{}^- Z + D^+ \qquad k_4 \sim 7 \times 10^{-2}\ s^{-1} \tag{4.4}$$

$$A_H{}^- Z^{+\cdot} \xrightarrow{k_5} A_H Z \qquad k_5 \sim 1\ s^{-1} \tag{4.5}$$

In addition to Z, an endogenous donor, A_H, has been included in this scheme. D represents an exogenous donor and M is either Ca^{2+} or Mn^{2+}. Reaction 4.1 describes the kinetics shown in Fig. 22b. Here, $Z^{+}\cdot$ is reduced by the exogenous donor. Calculations of the rate constant, k_1, for a wide variety of donors is possible by using the data of Table 1. For 2 mM $HAsc^-$ at pH = 8.0, $k_1 = 1.4\ s^{-1}$ when double layer effects are corrected for. Reaction 4.2 describes the decay shown in Fig. 22c, in which $Z^{+}\cdot$ oxidizes the reduced endogenous donor, A_H^-; we estimate $k_2 \sim 35\ s^{-1}$, which gives a decay half time of 20 ms. Reactions 4.3 and 4.4 describe the rate of dark reduction of A_H by the exogenous donor, D. This is necessary to account for the result in Fig. 22a, a convolution of the kinetics in 4.1 and 4.2. This occurs when not all of the endogenous donor is reduced between flashes. This effect has been shown experimentally in Fig. 24, in which Tris-washed chloroplasts (2 mM $HAsc^-$, no EDTA, pH = 8.0) were illuminated at a rate of 1 Hz (left) and 0.1 Hz (right). At high repetition rates, (left) the decay trace is strongly bi-phasic, as in Fig. 22a. At slower repetition rates, (0.1 Hz, right), however, the decay time is shorter and approaches the k_2 half time of 20 ms. Thus, it appears that k_4 is relatively slow and we assign it an approximate half time of 10 s ($k_4 \sim 7 \times 10^{-2}\ s^{-1}$). However, k_3 appears to be faster as we see very little slow phase in Fig. 22c. This could be

Figure 24 -- Effect of flash frequency on the decay of Signal IIf (a) 1 flash every second, (b) 1 flash every 10 seconds, 1 ms time constant, 20 mW power, Tris-washed chloroplasts, 2 mM $HAsc^-$ (pH = 8.0).

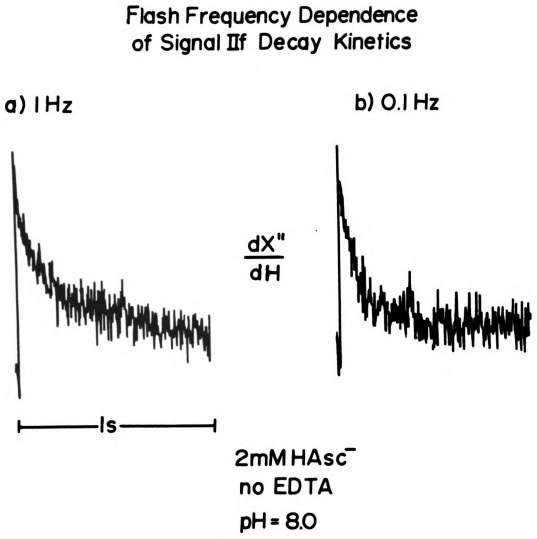
Flash Frequency Dependence
of Signal IIf Decay Kinetics
a) 1 Hz
b) 0.1 Hz
dX"
dH
1s
2mM HAsc⁻
no EDTA
pH = 8.0

FIGURE 24

a simple double layer effect of Ca^{2+} on the rate of A_H re-reduction by the negatively charged donor, $HAsc^-$ (Section II). For the $HAsc^-$ (2 mM, pH = 8.0) case, $k_5 < k_1$ but, as we show below, if $k_5 \sim 1\ s^{-1}$, as additional data suggest, then $k_5 > k_1$ for slower donors to Z^+ (Table 1).

Figure 25 shows experimental points (open circles) taken from the data in Fig. 22, fitted to calculated decay curves (dashed lines) using the k_1 and k_2 values given above. Figure 25a shows all k_1 kinetics, corresponding to Tris-EDTA chloroplasts. Figure 25b shows a mixture of 50% k_1 and 50% k_2, to account for the slow re-reduction time of A_H by the charged donor, $HAsc^-$, in the absence of Ca^{2+} (k_4), presumably a surface charge effect. Figure 25c shows 90% k_2 and 10% k_1 as the reduction of A_H appears to proceed much more rapidly under these conditions (k_3).

We next examined the nature of the association between Ca^{2+} and Mn^{2+} and the A_H Z complex. Figure 26 is a series of traces demonstrating the effect of Mn^{2+} on Signal IIf decay kinetics. These signals were collected with a 200 μs instrument time constant and show only the first 180 ms of the signal decay following a flash. Figure 26a shows the effect of 1 mM EDTA in Tris-washed chloroplasts. Removal of the loosely bound manganese leads to slow ($t_{½} \sim 500$ ms) decay kinetics as described by 4.1, above. In the subsequent three traces (Fig. 26b,c,d) the effect

Figure 25 -- Experimental points (open circles) taken from Figure 22 fitted to equations 4.1 and 4.2 as indicated in the figure.

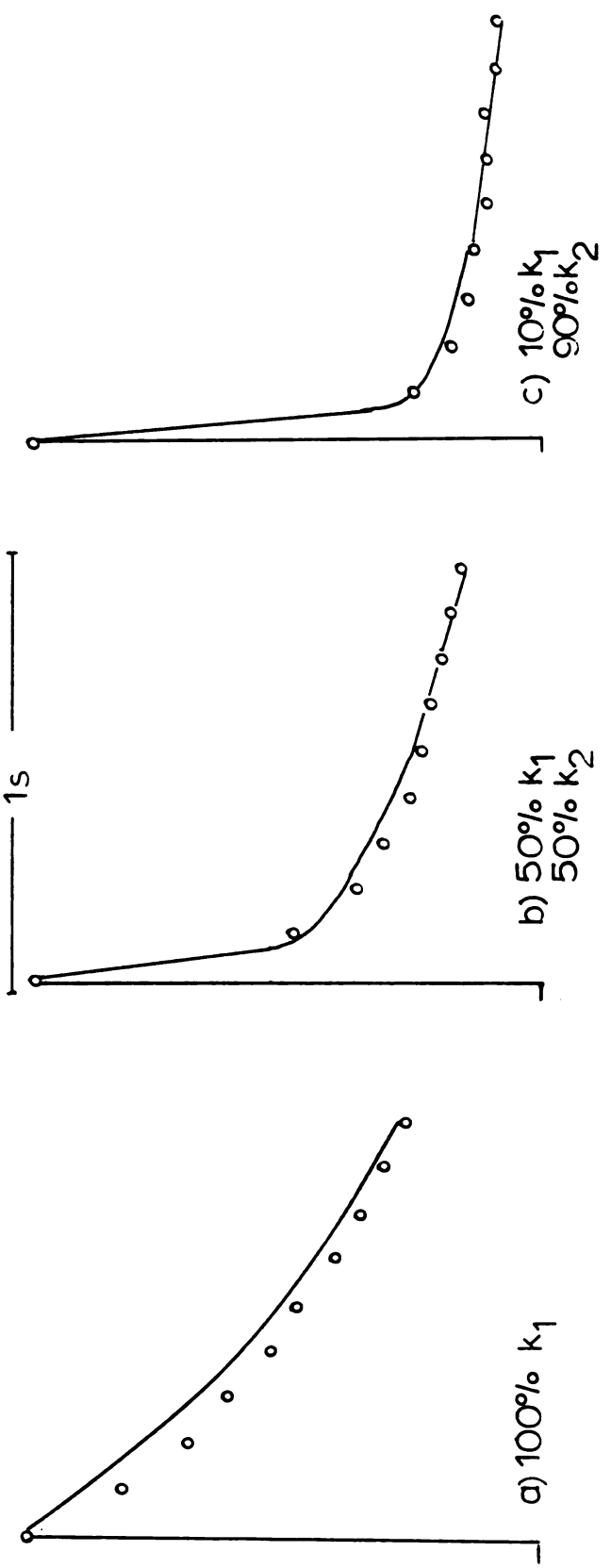

FIGURE 25

Figure 26 -- Effect of Mn^{2+} concentration on the decay kinetics of Signal IIf in Tris-washed chloroplasts, 2 mM $HAsc^-$ (pH = 8.0). (a) addition of 1 mM EDTA, (b) no addition, (c) addition of 10 μM Mn^{2+} and (d) addition of 20 μM Mn^{2+}. Instrument time constant = 200 μs, 250 scans averaged.

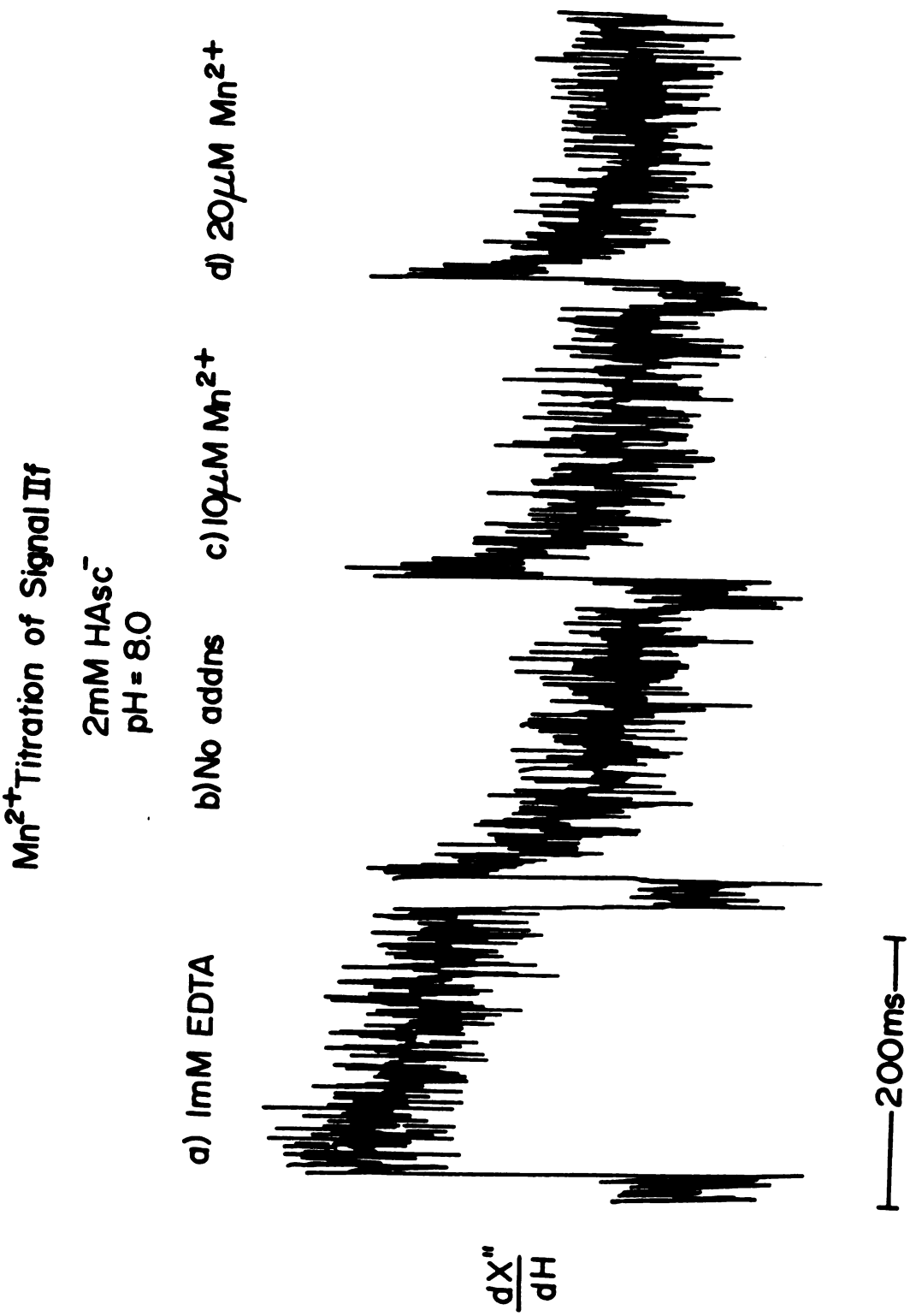
Mn^{2+} Titration of Signal IIf
2mM $HAsc^-$
pH = 8.0
a) 1mM EDTA
b) No addns
c) 10μM Mn^{2+}
d) 20μM Mn^{2+}
200ms
$\frac{dX''}{dH}$

FIGURE 26

of membrane associated manganese (EDTA/Ca^{2+} labile Mn^{2+}, Fig. 26b) and added Mn^{2+} (10 μM in Fig. 26c and 20 μM in 26d) on Signal IIf amplitude and decay kinetics is demonstrated. These have been plotted as ln(signal height) versus time after flash in Fig. 27. This treatment of the data shows that the decay of IIf is bi-phasic and that the effect of Mn^{2+} addition is to increase the proportion of the signal decaying via the k_2 kinetics. It is difficult to carry the titration farther as Signal IIf is coincident with the hexaaquo Mn^{2+} signal. Fairly high instrument gain is necessary to detect Signal IIf. This becomes impossible at higher Mn^{2+} concentrations as the detector diode is saturated by the Mn^{2+}: $6H_2O$ signal.

The Signal IIf amplitude in Figure 26 can be compared to the measured Signal IIs amplitude for the same sample (data not shown). As stated earlier, Signal IIs and Signal IIf should exist in a 1:1 ratio. We calculate that these photoinduced signals represent over 80% of the amplitude of Signal IIs and, thus, we see no appreciable signal loss, implying that Mn^{2+} is not donating directly to $P680^+$ as has been contended previously [68,119,120]; at least not under these experimental conditions.

The titration of the fast phase is more accessible with Ca^{2+} than with Mn^{2+} as there is no interfering Mn^{2+}: $6H_2O$ signal. Figure 28 is a plot of [Ca^{2+}] versus decay half-time (2 mM $HAsc^-$, 400 μM EDTA, pH = 8.0). The limiting half-time at high Ca^{2+} concentrations appears to

Figure 27 -- A semi-log plot of Figure 26, showing the biphasic nature of the decay at low Mn^{2+} concentrations and how the decay varies with Mn^{2+} concentration.

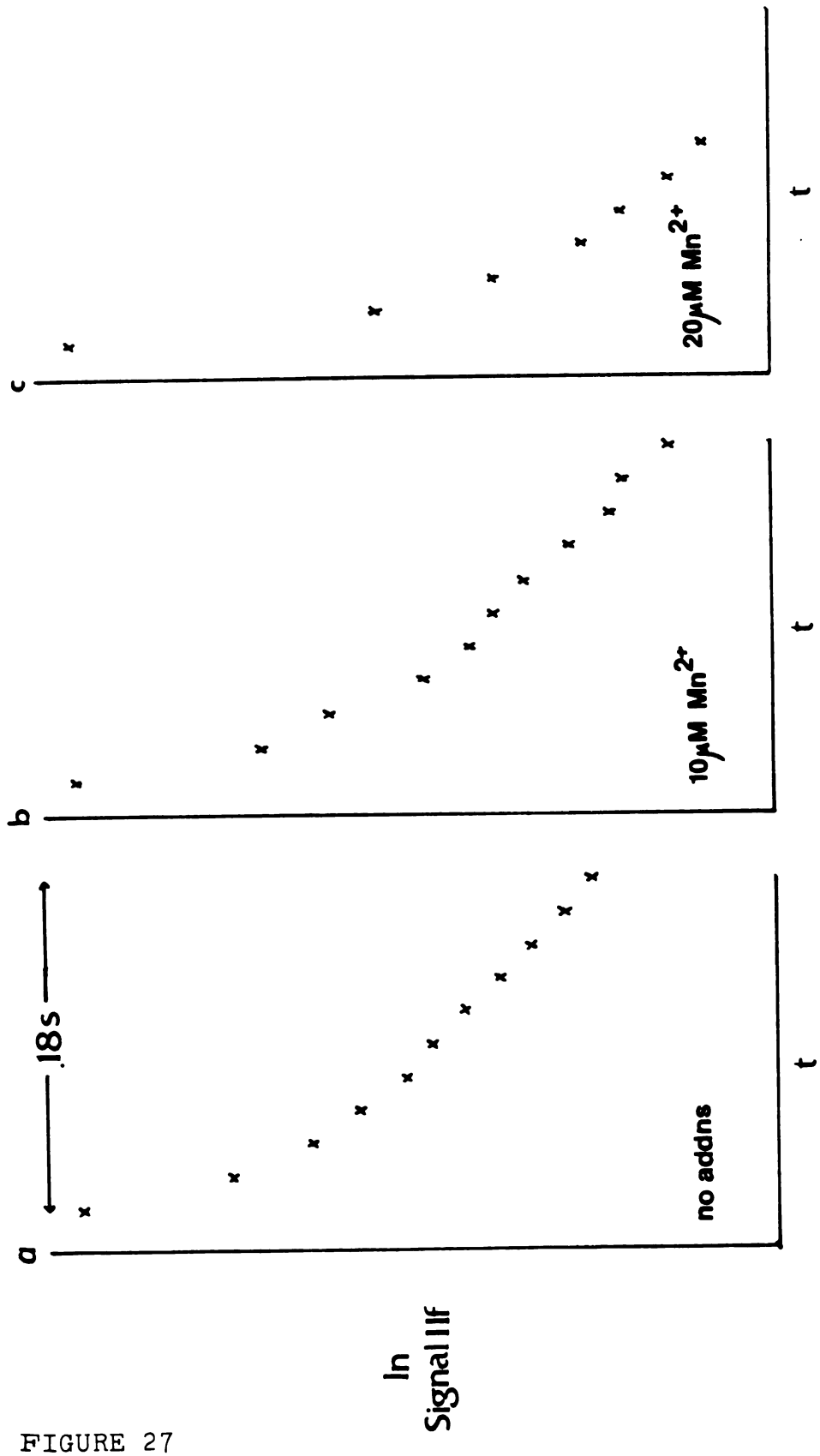

FIGURE 27

Figure 28 -- A plot of the observed decay half-time of Signal IIf versus concentration of Ca^{2+}, at pH = 8.0, 2 mM $HAsc^{-}$, 400 μM EDTA.

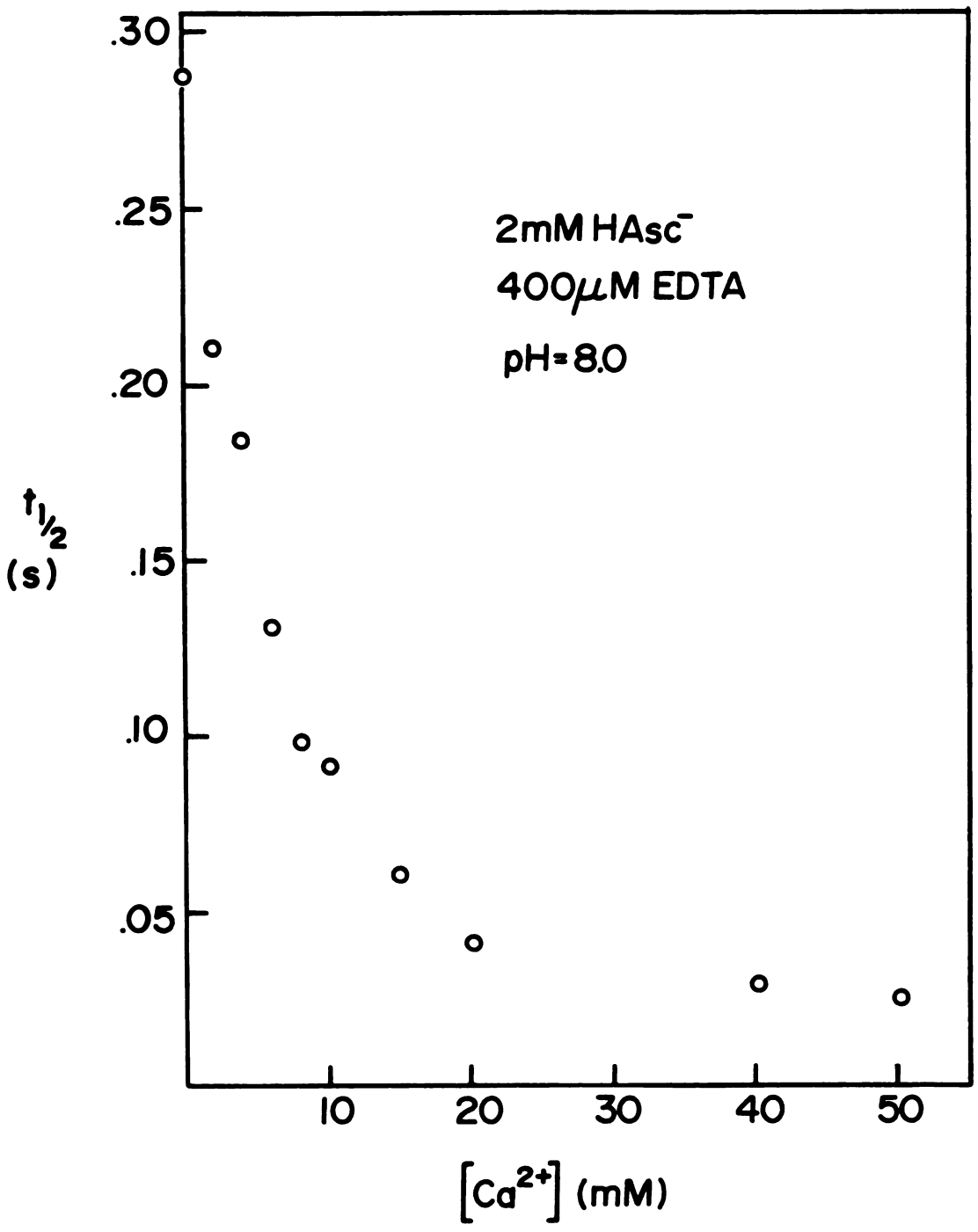
.30
.25
.20
.15
.10
.05
$t_{1/2}$ (s)
2mM HAsc⁻
400μM EDTA
pH=8.0
10
20
30
40
50
[Ca²⁺] (mM)

FIGURE 28

be 20 ms. These data can be re-plotted as $t_{\frac{1}{2}}$ versus $[Ca^{2+}]^{-1}$, as shown in Fig. 29, and a reaction mechanism can be developed to explain these kinetics. Additional assumptions about the association between Ca^{2+} (Mn^{2+}) and the A_H Z complex are necessary and are shown below.

$$A_H^- Z^+ + M \underset{k_{-6}}{\overset{k_6}{\rightleftharpoons}} A_H^- Z^+ \cdot M \qquad (4.6)$$

and

$$K_M = \frac{k_6}{k_{-6}} = \frac{[A_H^- Z^+ \cdot M]}{[A_H^- Z^+][M]} \qquad (4.7)$$

Because we have assumed that $k_2 >> k_1$, the decay of $A_H^- Z^+$ is then given by:

$$\frac{-d[A_H^- Z^+]}{dt} = k_2[A_H^- Z^+ M] = k_2 K_M [A_H^- Z^+][M] \qquad (4.8)$$

Ca^{2+} (and Mn^{2+}) is not consumed in the reduction reaction and if one assumes that the equilibrium given in 4.7 is rapid, 4.8 can be rearranged to give:

$$\frac{-d[A_H^- Z^+]}{dt} \sim k'[A_H^- Z^+] \quad \text{where} \quad k' = k_2 K_M [M] \qquad (4.9)$$

The decay half time is then given by

$$t_{\frac{1}{2}} = \frac{\ln 2}{k'} = \frac{\ln 2}{k_2 K_M [M]} \qquad (4.10)$$

The slope of the plot in Fig. 28 gives a $K_{Ca^{2+}} = 50\ M^{-1}$. There is one point in Fig. 29, corresponding to 2 mM Ca^{2+}, which is obviously not described by this mechanism. A

Figure 29 -- A re-plotting of the data in Figure 28 as decay half-time versus inverse Ca^{2+} concentration.

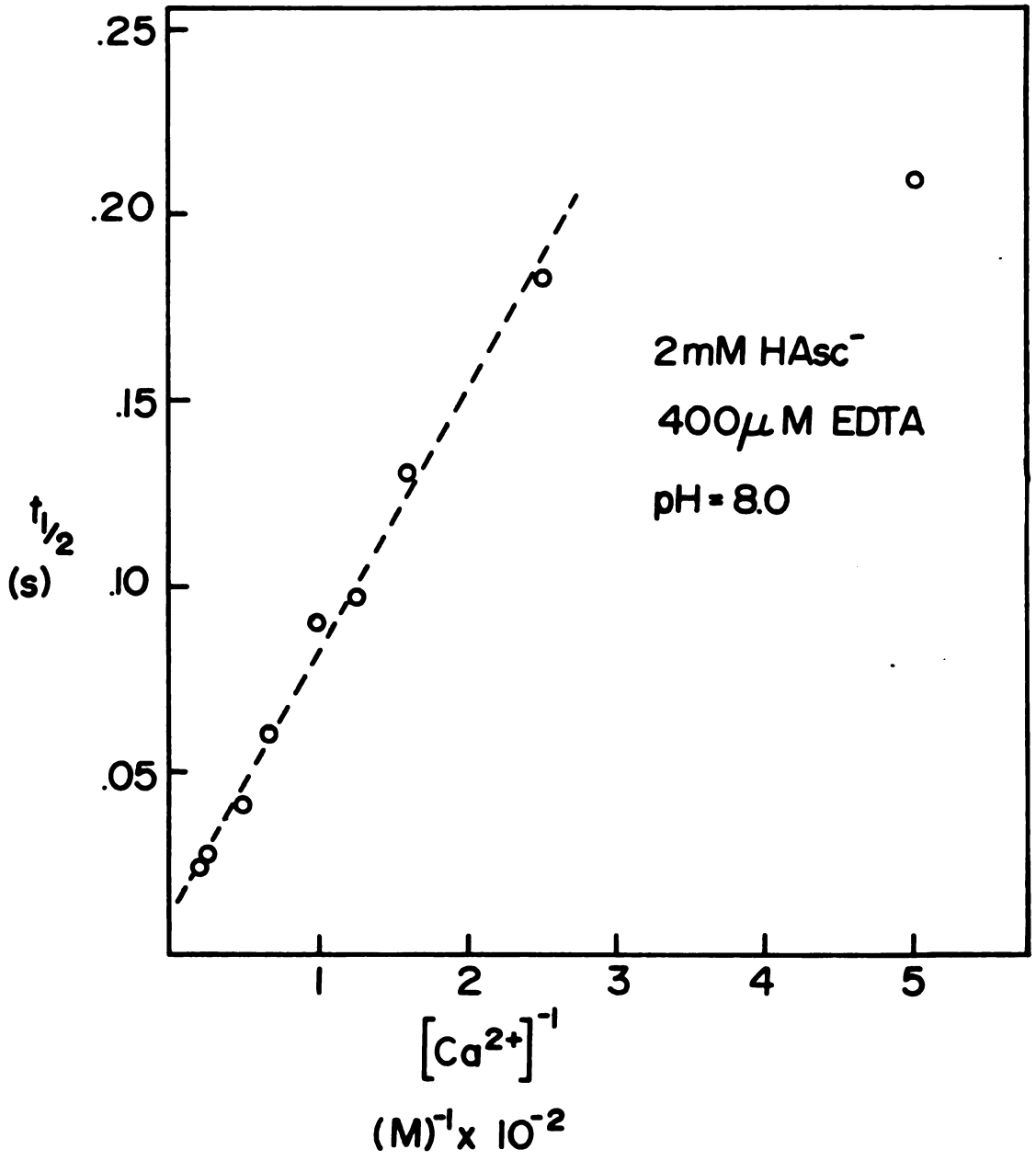
.25
.20
.15
.10
.05
$t_{1/2}$ (s)
2mM HAsc⁻
400μM EDTA
pH = 8.0
1
2
3
4
5
$[Ca^{2+}]^{-1}$
$(M)^{-1} \times 10^{-2}$

FIGURE 29

possible explanation is that at low concentrations of Ca^{2+} (2 mM) and EDTA (400 μM), not all of the loosely bound manganese is removed from the membrane [119], leading to faster decay rates than predicted. This would be true if the site of the divalent cation effect had a higher affinity for Mn^{2+} than for Ca^{2+}. This is indicated by the decay traces of the Mn^{2+} and Ca^{2+} titration experiments. The Ca^{2+} decay kinetics are exponential, as predicted if $k_2 < k_{-6}$. The Mn^{2+} decay traces, however, are bi-phasic (Figs. 26 and 27), indicating that $k_2 > k_{-6}$ and that the Mn^{2+} may be binding at a site affecting the Z^{+} decay rate.

We have also explored the effects of CCCP on the decay of IIf. The decay traces are, as in the case of Ca^{2+}, exponential and lend themselves to the same analysis as that carried out for the Ca^{2+} experiments. Figure 30 is a plot of decay half-time versus $[CCCP]^{-1}$. In this case, $K_{CCCP} = 4 \times 10^4\ M^{-1}$. This may reflect the greater solubility of this lipophilic species in the membrane over that seen with Ca^{2+}. It is interesting to note that these experiments were carried out in the absence of exogenous donors, leading to the conclusion that CCCP must somehow facilitate the re-reduction of A_H between flashes (k_3) at concentrations too low to be explained by double layer effects.

Figure 31 shows the effect of EDTA (b) and Ca^{2+} (c) on Tris-washed chloroplasts in the presence of 50 mM KI (a).

Figure 30 -- A plot of observed decay half-time versus inverse concentration of CCCP.

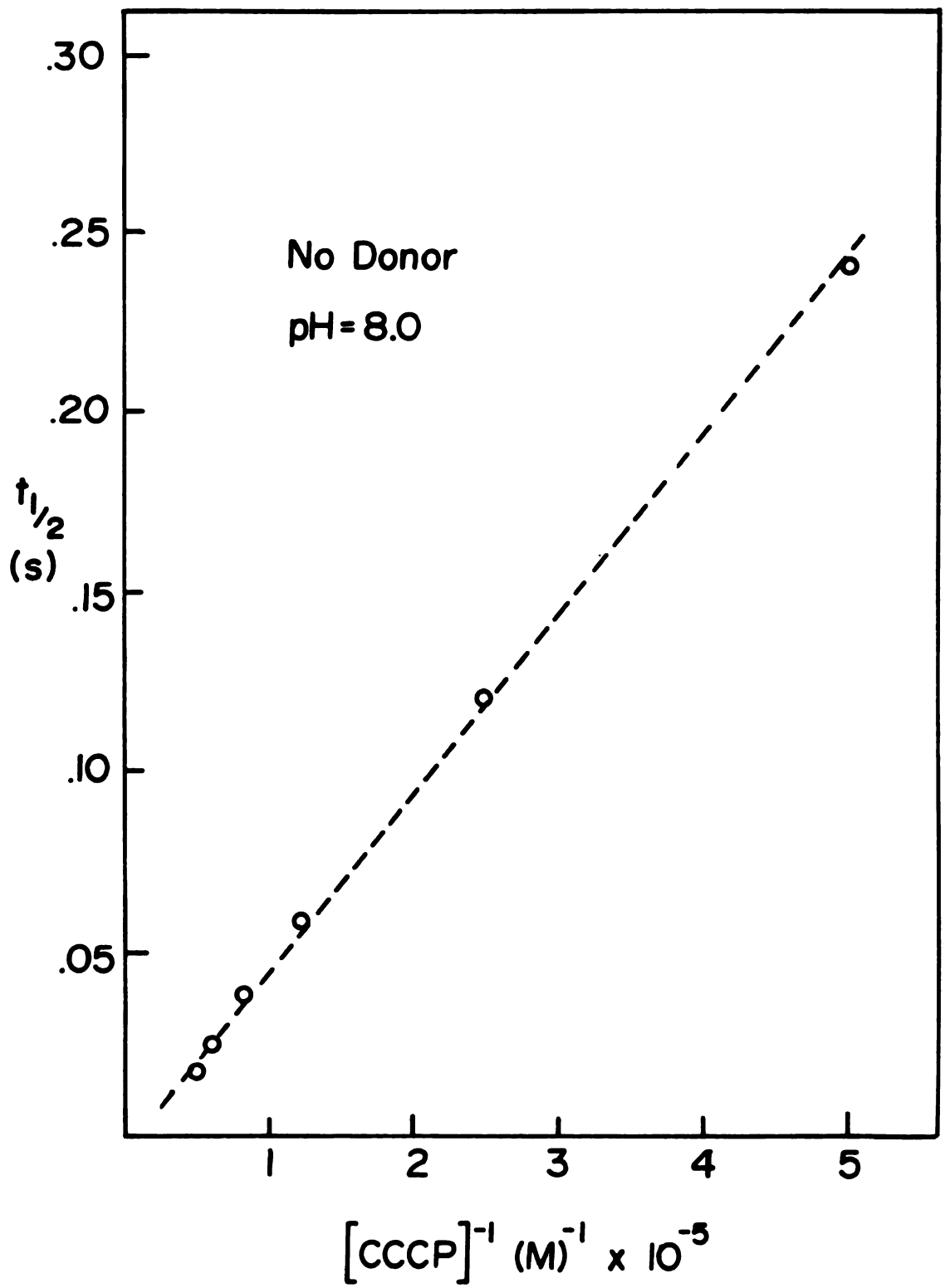

FIGURE 30

Figure 31 -- The effects of 50 mM KI on the decay kinetics of Tris-washed chloroplasts (pH = 8.0) (a), with 1 mM EDTA (b), with 50 mM Ca^{2+} (c) and with 2 mM $HAsc^-$ (d) as compared to 2 mM $HAsc^-$ alone (e). Time constant = 1 ms, 150 scans averaged.

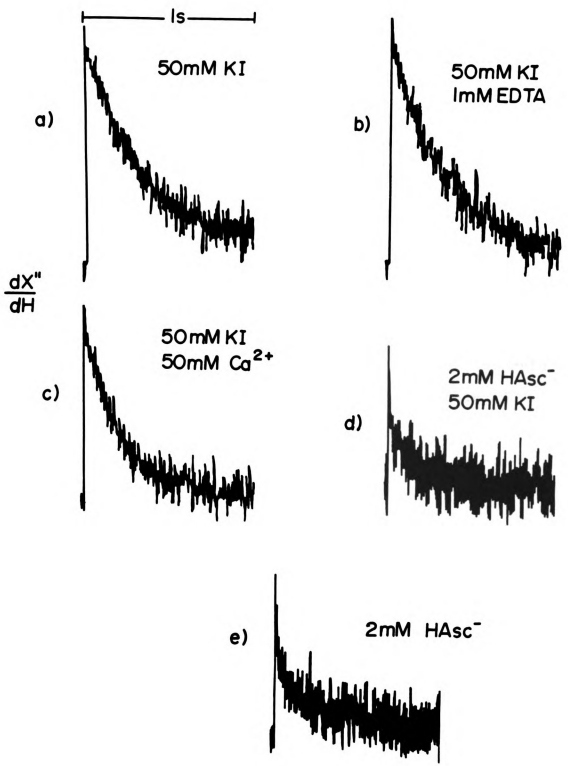
1s
50mM KI
a)
50mM KI
1mM EDTA
b)
dX"/dH
50mM KI
50mM Ca2+
c)
2mM HAsc-
50mM KI
d)
e)
2mM HAsc-

FIGURE 31

It has been shown previously that I^- is an electron donor to PS II [121] and specifically to Z^+ [89]. As the experimental results show, the decay of IIf is not dramatically enhanced by addition of 50 mM Ca^{2+} (Fig. 31c) nor slowed by the addition of 1 mM EDTA (Fig. 31b). As I^- has been used as a chaotrope in photosynthetic systems [25] we have added 2 mM $HAsc^-$ (pH = 8.0) (Fig. 31d) to a suspension already 50 mM in I^- (Fig. 31a) and observe essentially the same trace as in the presence of $HAsc^-$ alone (Fig. 31e) demonstrating that I^- does no irreversible damage to the system in the concentration range used. Because the I_2/I^- couple is of a substantially higher potential (E_m° = +.536 V) than the dehydroascorbate/ascorbic acid couple (E_m' = +.058 V) [122], the results of Fig. 31 suggest that the I_2/I^- couple may not be capable of maintaining A_H in the reduced state (4.4 and 4.5). We have, therefore, done preliminary experiments on the potential dependence of the fast, endogenous donor to Z^+, A_H.

b. Potential Effects

Figure 32 is a collection of experimental traces showing the effects of Ca^{2+} (a,b) and EDTA (c,d) on the decay kinetics of Signal IIf at different redox potentials (E_M = +0.480 V and +0.380 V, pH = 8.0). The poise was maintained with a 10 mM $Fe(CN)_6^{3-}/Fe(CN)_6^{4-}$ couple, titrated with 0.1 M $HAsc^-$ (pH = 8.0) in STN. At +0.48 V, addition of 1 mM EDTA (Fig. 32c) gives a mono-phasic decay with an

Figure 32 -- The effect of suspension potential (2 mM $HAsc^-$, pH = 8.0) on the decay kinetics of Signal IIf with (a,b) 50 mM Ca^{2+} and (c,d) 1 mM EDTA. Time constant = 1 ms, 150 scans averaged.

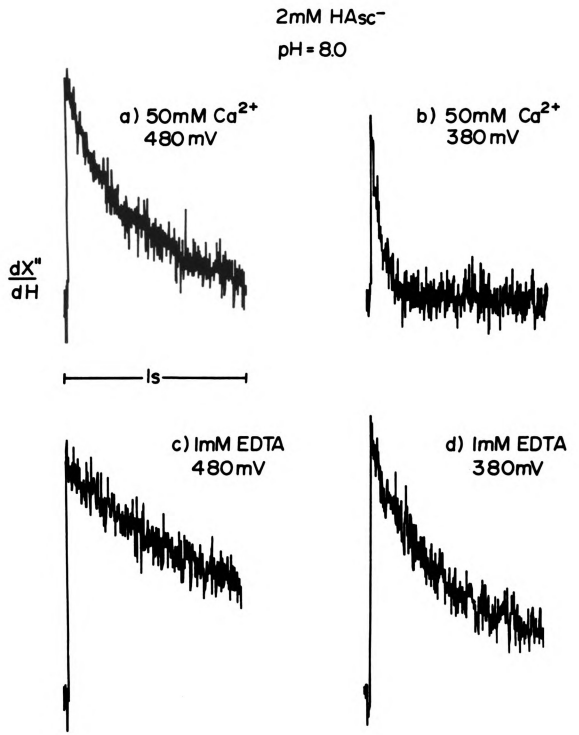
2mM HAsc⁻
pH = 8.0
a) 50mM Ca2+
480 mV
b) 50mM Ca2+
380 mV
dX''/dH
1s
c) 1mM EDTA
480mV
d) 1mM EDTA
380mV

FIGURE 32

apparent rate constant of 0.7 s^{-1}, a rate that correlates fairly well with that observed for Signal IIf decay in the absence of exogenous donors. In contrast, addition of Ca^{2+} at this same potential (Fig. 32a) gives a bi-phasic decay trace. About 30% of the signal decays with an apparent rate constant of 11 s^{-1} and the remainder at about 1.6 s^{-1}. The observation of bi-phasic decay kinetics was unexpected, as the addition of Ca^{2+} at lower potentials, such as with the donors $HAsc^-$ and DPC, leads to a rapid and monotonic decay of the $Z^{+\cdot}$ radical. The same is true at lower potentials with the $Fe(CN)_6^{3-}/Fe(CN)_6^{4-}$ couple (Fig. 32b) which demonstrates a single exponential decay at a rate of about 16 s^{-1}. The mixed kinetics at 0.48 V may be an indication of a mixed redox population, with some fraction of the centers, determined by the poise of the system, behaving as all of the centers do at lower potentials.

At 0.38 V, the $Fe(CN)_6^{4-}$ concentration should be roughly 10^{-2} M. From Table 1, this should give a decay rate of 0.24 s^{-1}, whereas the observed rate is 1.2 s^{-1}. This discrepancy may be a reflection of the rate of donation of A_H^- to $Z^{+\cdot}$ in the absence of an associated metal cation (Ca^{2+}, Mn^{2+}) or CCCP. This would make $k_5 \sim 1$ s^{-1}. These kinetics would predominate at $Fe(CN)_6^{4-}$ concentrations below about 40 mM ($k_5 > k_1$ as discussed above).

These data suggest the existence of a relatively high potential donor ($E_m' \sim 400$ mV) to PS II in Tris-washed chloroplasts and that its involvement in the reduction of the photo-induced $Z^{+\cdot}$ radical depends on the association of either Mn^{2+} or Ca^{2+} with the reaction center. The system must also be poised at a sufficiently low potential to maintain A_H in its reduced form, A_H^-. The same kinetics are seen in the presence of low concentrations (μM) of the ADRY reagent, CCCP. However, under these conditions, the re-reduction of A_H between flashes is somehow facilitated. The divalent cations may serve a structural role in allowing the endogenous donor to reduce $Z^{+\cdot}$ efficiently or, they may serve to alter the potential of the donor. A more complete potential dependence study is planned to resolve this question.

2. Oxidizing Conditions

Addition of the herbicide, DCMU, to chloroplast suspensions significantly alters the electron transfer processes of PS II. DCMU blocks the electron transfer from Q, the primary stable electron acceptor to B, the two electron acceptor that links PS II to the plastoquinone pool. This inhibition leads to a loss of photochemistry after a single, saturating flash. The inhibition can be relieved by maintaining a high redox potential in the system. This effect has been studied by a number of

groups, using a variety of experimental techniques [30-35]. The common explanation has been the proposal of a high potential acceptor ($E_m' > 400$ mV) for PS II.

Babcock and Sauer [36] have studied the decay kinetics of EPR Signal IIf under similar experimental conditions. At low potentials ($E_m < 400$ mV) and under signal averaging conditions, no Signal IIf was seen in Tris-washed, DCMU inhibited chloroplasts. Upon increasing the potential, an increase was seen in the amplitude of IIf. This effect had a midpoint potential of about 480 mV at pH = 8.0. They reported a IIf decay half-time of about 300 ms and showed that above 400 mV, this decay rate was largely independent of the suspension potential.

We have extended these EPR experiments and the results are shown in Fig. 33. The Mg^{2+} traces (Fig. 33b) show decay half times at pH = 8.5 (280 ms) and pH = 7.5 (270 ms) which correspond well to the decay half-time measured by Babcock and Sauer at pH = 8.0 (300 ms), and may reflect the rate of donation of A_H^- to Z^+ in the absence of Ca^{2+} or Mn^{2+} ($k_5 = 2\ s^{-1}$). This is assuming that donation to Z^+ in DCMU inhibited chloroplasts proceeds via A_H. This contention is strengthened by the traces in Fig. 33a and c which again show specific Ca^{2+} and CCCP effects on IIf. Addition of 50 mM Ca^{2+} or 8 μM CCCP (with 50 mM Mg^{2+}) leads to an almost three fold enhancement in the decay rate over that observed with 50 mM Mg^{2+}. At corresponding pH values, the Ca^{2+} and CCCP decay half-times

are very nearly the same. Again, by analogy, this suggests that the donor to Z^{+} is A_H. The most striking effect of pH occurs between the traces taken at pH = 6.5 and those at 5.5. In all three cases (Ca^{2+}, Mg^{2+} and CCCP) there is a decrease in the decay half-times, to rates approaching those we have previously attributed to donation by the endogenous donor.

The pH = 8.5 trace in Fig. 31c shows another interesting effect we have observed, the loss in Signal IIf amplitude in Tris-DCMU chloroplast suspensions of low ionic strength, here, CCCP alone. This signal loss was also seen in EDTA treated samples and in samples that were 50 μM in Mn^{2+} (data not shown). This can be interpreted in terms of surface charge effects (Sections I and II). At low ionic strengths, the rapid equilibration of the potential of membrane components with that imposed by the charged redox couple may be hampered by the membrane potential. This surface potential would be lowered by inclusion of salts in the reaction mixture permitting a more rapid equilibration. Addition of 50 mM Mg^{2+} to the CCCP sample (Fig. 33c, pH = 7.5) does restore full signal height.

Initial experiments have been carried out to determine if the addition of Ca^{2+} or CCCP changes the potential dependence of the cyclic reaction (data now shown). These compared Ca^{2+} to EDTA treated chloroplasts and the results were ambiguous, most likely due to the relatively low

Figure 33 -- The effect of pH on the decay kinetics of Signal IIf in Tris-washed chloroplasts with 100 μM DCMU, 10 mM $Fe(CN)_6^{3-}$ and (a) 50 mM Ca^{2+}, 50 mM Mg^{2+} and (c) 8 μM CCCP and 50 mM Mg^{2+} (except where otherwise noted). Time constant = 1 ms, 150 scans averaged.

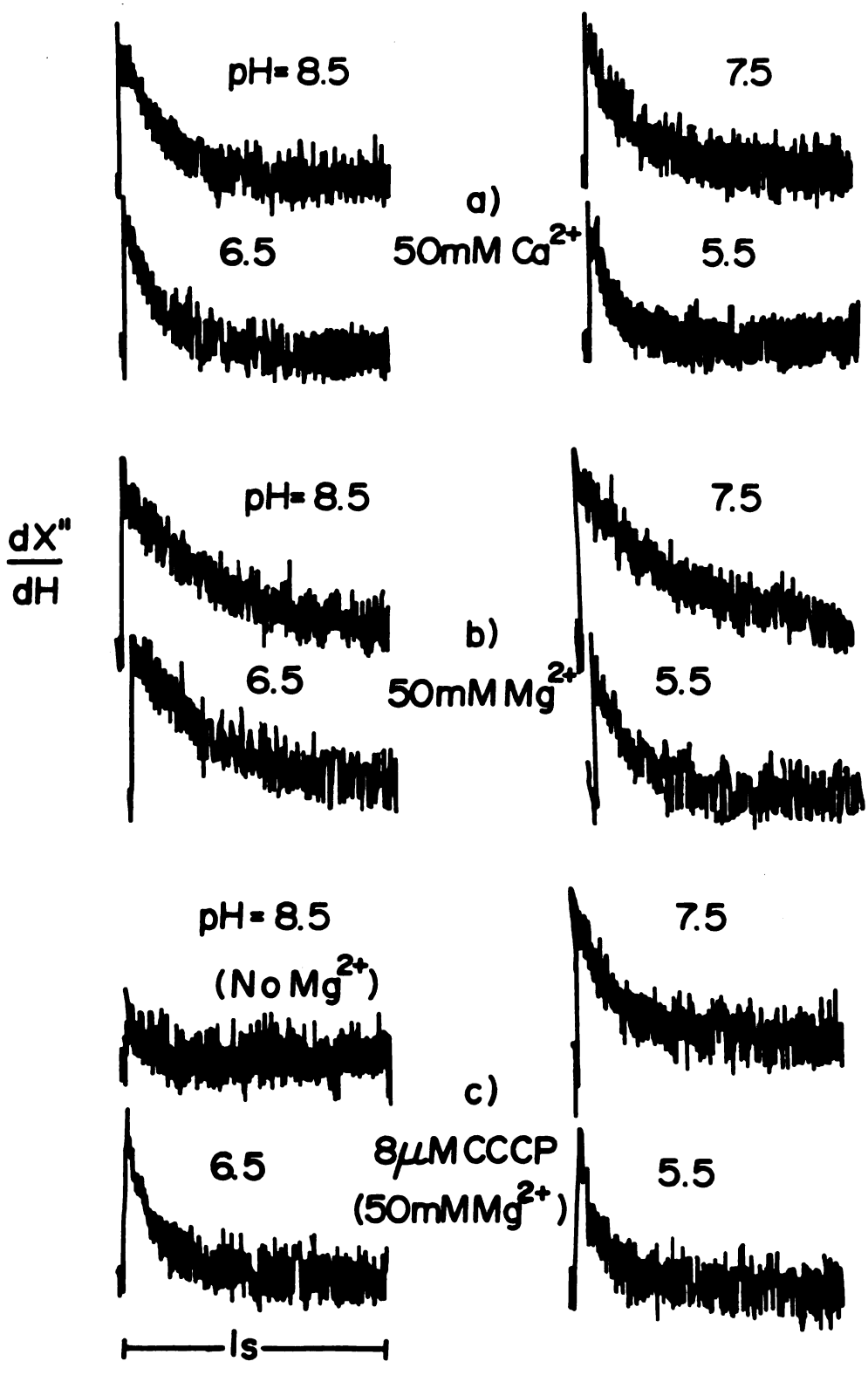
pH= 8.5
7.5
a)
50mM Ca^{2+}
6.5
5.5
$\frac{dX''}{dH}$
pH= 8.5
7.5
b)
50mM Mg^{2+}
6.5
5.5
pH= 8.5
(No Mg^{2+})
7.5
c)
8μM CCCP
(50mM Mg^{2+})
6.5
5.5
1s

FIGURE 33

signal observed in the EDTA case, as explained above. These experiments will be repeated, comparing Ca^{2+} to Mg^{2+} and Mg^{2+}/CCCP samples. The Ca^{2+} titration did appear to give a mid-point potential near 400 mV, demonstrating the participation of a high potential donor, at least in that case.

D. Discussion

The following model has been developed from the work presented here to explain the kinetics on the oxidizing side of Photosystem II in Tris-washed chloroplasts.

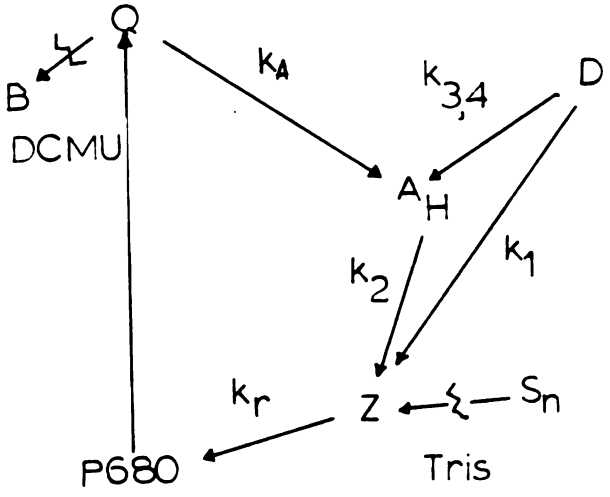

The photo-induced charge separation, described by the rate constant k_o, occurs within picoseconds following illumination. We have postulated that a membrane surface charge asymmetry in the vicinity of PS II may stabilize this forward reaction, over the charge recombination back reaction, by an additional factor of two in dark adapted

chloroplasts. This membrane field ($\Delta\psi_s \sim 20$ mV, 10 mM NaCl) will be dissipated as the inner thylakoid volume acidifies and the groups giving rise to the surface charge protonate. The re-reduction of $P680^+$, given by k_r, occurs in less than a microsecond in untreated chloroplasts and with a pH dependent half-time, ranging from 32 to 1.4 μs, in Tris-washed chloroplasts [124]. The $P680^+$ reduction times for Tris-washed chloroplasts correlate with data measuring the rise time of Signal IIf following flash illumination [53]. indicating that Z, the species giving rise to the EPR signal, is the primary electron donor to the reaction center chlorophyll radical.

Tris-washing blocks electron transfer between Z and the water oxidizing complex, S_n. This is reflected in the increase of the $Z^{+\cdot}$ decay time from less than a ms in oxygen evolving chloroplasts to half-times in excess of 1 s. We have made a comprehensive study of the k_1 donation kinetics ($A_HZ^+ + D \xrightarrow{k_1} A_HZ + D^+$) in Tris-washed chloroplasts (Section II). This rate varies with the nature of the exogenous donor, D, and ranges from $k_1 > 10^6$ M^{-1} s^{-1} for benzidine to $k_1 = 24$ M^{-1} s^{-1} for ferrocyanide. Table 1 is a summary of these results. We have also found that in the case of negatively charged donors, the rate of the reaction is mediated by the inner membrane surface potential.

We have recently observed a new decay pathway for the $Z^{+\cdot}$ radical, represented here by the A_H. These decay kinetics are given by $k_2 \sim 35$ s^{-1} and are seen when Mn^{2+}

or Ca^{2+} are associated with the reaction center. This is described by the reaction:

$$A_H^- Z^+ \; M \xrightarrow{k_2} A_H \; Z \; M$$

whre M can be either Mn^{2+} or Ca^{2+}. Their association with the A_H Z complex is given by the equilibrium reaction,

$$A_H \; Z^+ + M \underset{k_{-6}}{\overset{k_6}{\rightleftharpoons}} A_H \; Z^+ \; M \; , \quad K_M = k_6/k_{-6}$$

which is assumed to be rapid. When $k_2 < k_{-6}$, assuming that k_6 is fast, the decay of the state $A_H^- Z^+$ is given by:

$$\frac{-d[A_H^- Z^+]}{dt} = k'[A_H^- Z^+] \text{ where } k' = k_2 K_M [M]$$

Signal IIf decay should be exponential under these conditions. This is observed with Ca^{2+}. The equilibrium constant in this case is 50 M^{-1}.

Although the qualitative effects of Ca^{2+} and Mn^{2+} on the decay of IIf are similar, both introduce a rapid ($t_{\frac{1}{2}} \sim 20$ ms) decay phase, a different kinetic analysis is required in the two cases. As shown above, the decay of IIf, upon addition of Mn^{2+} (Figs. 26 and 27), is not exponential, but a convolution of k_1 and k_2 kinetics. This would be true if $k_2 > k_{-6}$. Thus, the fast phase can be titrated in. This implies a strong Mn^{2+} affinity site associated with A_H such that $k_{-6} < 35$ s^{-1}. The Mn^{2+} data also indicate that Mn^{2+} does not donate directly to $P680^+$ as has been previously suggested.

The effects of the ADRY reagent, CCCP, on the IIf decay rates were also examined. The mechanism is analogous to that shown for Ca^{2+} but the equilibrium constant is much higher, 4×10^4 M^{-1}. This may, in large measure, simply reflect the lipophilicity of CCCP as compared to Ca^{2+}.

The dark re-reduction time of A_H by exogenous donors has been inferred from flash frequency studies. It appears to be fairly slow in the presence of 2 mM $HAsc^-$ ($k_3 \sim 7 \times 10^{-2}$ s^{-1}) but appears to be faster upon addition of 50 mM Ca^{2+}, perhaps through a diminution of membrane surface potential. CCCP appears to facilitate the dark re-reduction of A_H, as decay rates by the k_2 pathway were observed with CCCP in the absence of exogenous donors, D. This suggests that CCCP may activate the k_4 pathway in the absence of DCMU.

In DCMU inhibited, Tris-washed chloroplasts, cyclic flow in PS II may occur by way of the A_H pathway if the redox potential is high enough to keep A_H oxidized in the dark. Under these conditions, we see fast decay kinetics (comparable to the k_2 rate) only at pH = 5.5 and in the presence of Ca^{2+} or CCCP. At pH = 6.5 and above, we see comparable decay half-times for Ca^{2+} and CCCP treated chloroplasts ($\sim$100 ms) which do not vary greatly with pH from 6.5 to 8.5. The half times for Mg^{2+} range from 280 ms at pH = 8.5 to 230 ms at pH = 6.5.

These are in agreement with the original work done by Babcock and Sauer [36]. At pH = 5.5, it decreases to 85 ms.

Because we can approach the k_2 rate constant in Tris-DCMU chloroplasts (pH = 5.5, 50 mM Ca^{2+} or 8 μM CCCP/50 mM Mg^{2+}), the longer half-times observed at higher pH values may reflect the rate of electron donation from Q^- to $A_H(k_A)$. A donation time of <5 μs has been reported by Bowes et al [35] for the $Q^- \longrightarrow Q_2$, DCMU insensitive reaction ($Em' \sim 400$ mV) in non-Tris-washed chloroplasts, which would not be rate limiting on our time scale. Velthuys and Kok [34] reported a similar donation rate for their $Q^- \longrightarrow C$ reaction, also DCMU insensitive. These reports suggest that the re-reduction of A_H (k_3, k_4) in Tris-DCMU chloroplasts is probably not by Q^-, as indicated by our model, but by an additional intermediate in the PS II cycle. Repetition of these experiments in which the time between illumination is varied may reveal the existence of this slower, rate limiting electron transfer reaction ($t_{\frac{1}{2}}$ = 300-100 ms).

Many other optical experiments are suggested by the work presented here. Our experiments have not been aimed at an identification of the molecular species which corresponds to A_H. It is interesting to speculate, however, on the striking correlation between the properties of our donor, A_H, and those of the enigmatic PS II component, cytochrome b_{559}. It has a mid-point potential

at pH = 7.5 of about +370 mV, unusually high for a b-type cytochrome. One explanation for this high potential is that it is a consequence of a local positive environment (Mn^{2+}) near the heme [110]. Indeed, EDTA effects on its photooxidation have been reported [112]. Addition of low concentrations of CCCP lead to the photooxidation of cyt b_{559} by PS II [124]. Its mid-point potential is pH independent from 6.0 to 8.0 but increases at 5.5 [125].

These similarities are tantalizing. The recent observation that cyt b_{559} can be photooxidized by very low light intensities, including the measuring beam in spectrometers (personal communication, H.H. Robinson and A.R. Crofts) may explain some of the ambiguities in the cyt b_{559} literature and suggests that careful optical measurements made under conditions under which we observe the $Z^{+}\cdot$ decay pathway given by k_2, may reveal a 20 ms photooxidation of cyt b_{559} and tie it, at last, to a pathway in PS II.

LIST OF REFERENCES

LIST OF REFERENCES

1. Sauer, K. (1978) Acc. Chem. Res. 11, 257.

2. Emerson, K. and Arnold, W. (1932) J. Gen. Physiol. 15, 391.

3. Van Gorkom, H.J., Tamminga, J.J. and Haveman, J. (1974) Biochim. Biophys. Acta 347, 417.

4. Davis, M.S., Forman, A. and Fajer, J. (1979) Proc. Nat. Acad. Sci. U.S.A. 76, 4170.

5. Rutherford, A.W., Paterson, D.L. and Mullet, J.S. (1981) Biochim. Biophys. Acta 635, 205.

6. Klimov, V.V., Klevanic, A.V., Shuvalov, V.A. and Kravsnovsky, A.A. (1977) FEBS Lett. 82, 183.

7. Rockley, M.G., Windzor, M.W., Cogdell, R.G. and Parson, W.W. (1975) Proc. Nat. Acad. Sci. U.S.A. 72, 2251.

8. Stiel, H.H. and Witt, H.J. (1969) Z. Naturforsch. 24b, 1588.

9. Bouges-Bocquet, B. (1973) Biochim. Biophys. Acta, 314, 250.

10. Mitchell, P. (1966) Biol. Rev. 41, 445.

11. Jagendorf, A.T. and Neumann, J. (1966) J. Biol. Chem. 320, 3210.

12. Joliot, P., Barbieri, G. and Chabaud, R. (1969) Photochem. Photobiol. 10, 309.

13. Joliot, P., Bouges, B. and Barbieri, G. (1971) Photochem. Photobiol. 14, 287.

14. Kok, B., Forbush, B. and McGloin, M. (1970) Photochem. Photobiol. 11, 45.

15. Babcock, G.T., Blankenship, R.E. and Sauer, K. (1976) FEBS Lett. 61, 286.

16. Cheniae, G.M. and Martin, I.F. (1966) in Energy Conversion by the Photosynthetic Apparatus, Brookhaven, Symp. Biol., 19, 406.

17. Blankenship, R.E. and Sauer, K. (1974) Biochim. Biophys. Acta 357, 252.

18. Wydrzynski, T., Zumbulyadis, N., Schmidt, P.G., Gutowsky, H.S. and Govindjee (1976) Proc. Nat. Acad. Sci. U.S.A. 73, 1196.

19. Siderer, Y., Malkin, S., Poupko, R. and Luz, Z. (1977) Arch. Biochem. Biophys. 179, 174.

20. Wydrzynski, T. and Sauer, K. (1980) Biochim. Biophys. Acta 589, 56.

21. Robinson, H.H., Sharp, R.R. and Yocum, C.F. (1981) Arch. Biochem. Biophys. 207, 1.

22. Saphon, S. and Crofts, A.R. (1977) Z. Naturforsch. 32c, 617.

23. Erixon, K., Lozier, R. and Butler, W.L. (1972) Biochim. Biophys. Acta 267, 275.

24. Horton, P. and Croze, E. (1977) Biochim. Biophys. Acta 462, 86.

25. Cox, R.P. and Bendall, D.S. (1972) Biochim. Biophys. Acta 283, 124.

26. Knaff, D.B. and Arnon, D.I. (1969) Proc. Nat. Acad. Sci. U.S.A. 63, 963.

27. Velthuys, B.R. (1980) Proc. 5th Int. Congr. Photosyn., Haldikidi, 1980, in press.

28. Ben-Hayyim, G. (1972) FEBS Lett. 28, 145.

29. Heber, U., Kirk, M.R. and Boardman, N.K. (1979) 546, 292.

30. Glaser, M., Wolff, C. and Renger, G. (1976) Z. Naturforsch. 31c, 712.

31. Ikegami, I. and Katoh, S. (1973) Plant Cell Physiol. 14, 829.

32. Diner, B.A. (1978) Proc. 4th Int. Congr. Photosyn., Reading, 1977 (Hall, D.O., Coombs, J. and Goodwin, T.W., eds.), pp. 359-372, The Biochemical Society, London.

33. Joliot, P. and Joliot, A. (1978) Biochim. Biophys. Acta 462, 559.

34. Velthuys, B.R. and Kok, B. (1978) Proc. 4th Int. Congr. Photosyn., Reading, 1977 (Hall, D.O., Coombs, J. and Goodwin, T.W., eds.), pp. 397-407, The Biochemical Society, London.

35. Bowes, J.M., Crofts, A.R. and Itoh, S. (1979) Biochim. Biophys. Acta 547, 320.

36. Babcock, G.T. and Sauer, K. (1975) Biochim. Biophys. Acta 375, 339.

37. Bouges-Bocquet, B. (1980)

38. Junge, W., Renger, G. and Auslander, W. (1977) FEBS Lett. 79, 155.

39. Bowes, J.M., Crofts, A.R. and Itoh, S. (1979) 547, 336.

40. Duysens, L.N.M. and Sweers, H.E. (1963) in Studies in Microalgae and Photosynthesis Bacteria (Jap. Soc. Plant Physiologists, ed.), pp. 353-372, Univ. of Tokyo Press, Tokyo.

41. Butler, W.L., Visser, J.W.M. and Simons, H.L. (1973) Biochim. Biophys. Acta 325, 539.

42. Sonneveld, A., Rademaker, H. and Duysens, L.N.M. (1979) Biochim. Biophys. Acta 548, 536.

43. Lavorel, J. (1975) in Bioenergetics of Photosynthesis (Govindjee, ed.), pp. 225-314, Academic Press, New York.

44. Duysens, L.N.M., denHaan, G.A. and vanBest, J.A. (1974) in Proc. 3rd Int. Congr. on Photosyn., Rehovet (Avron, M., ed.), pp. 1-12, Elsevier, Amsterdam.

45. Arnold, W.A. and Azzi, J. (1971) 14, 233.

46. Babcock, G.T., Yerkes, C.T. and Buttner, W.J. (1980) Proc. 5th Int. Congr. on Photosyn., Halkidiki, in press.

47. Floyd, R.A., Chance, B. and DeVault, D. (1971) Biochim. Biophys. Acta 226, 103.

48. Van Gorkom, H.J., Tamminga, J.J., Haverman, T. and van der Linden, I.K. (1974) Biochim. Biophys. Acta 347, 417.

49. Van Best, J.A. and Mathis, P. (1978) Biochim. Biophys. Acta 503, 178.

50. Robinson, H.H., Sharp, R.R. and Yocum, C.F. (1980) Biochim. Biophys. Acta 593, 414.

51. Dismukes, G.C. and Siderer, Y. (1981) Proc. Nat. Acad. Sci. U.S.A. 78, 274.

52. Babcock, G.T. and Sauer, K. (1975) Biochim. Biophys. Acta 376, 315.

53. Blankenship, R.E., Babcock, G.T., Warden, J. and Sauer, K. (1975) FEBS Lett. 51, 287.

54. Beinert, H. and Kok, B. (1964) Biochim. Biophys. Acta 88, 278.

55. Kohl, D.H. (1972) in Biological Applications of ESR (Schwartz, H.M., ed.) p. 213, John Wiley and Sons, New York.

56. Malkin, R. and Bearden, A.J. (1975) Biochim. Biophys. Acta 396, 250.

57. Visser, J.W.M., Rijgersberg, C.P. and Gast, P. (1977) Biochim. Biophys. Acta 460, 36.

58. Kohl, D.H., Townsend, J., Commoner, B., Crespi, H.L., Dougherty, R.C. and Katz, J. (1965) Nature 206, 1105.

59. Kohl, D.H. and Wood, P.M. (1969) Plant Physiol. 44, 1439.

60. Kohl, D.H., Wright, J.R. and Weissman, M. (1964) Biochim. Biophys. Acta 180, 536.

61. Babcock, G.T. and Sauer, K. (1973) Biochim. Biophys. Acta 325, 504.

62. Blankenship, R.E., McGuire, A. and Sauer, K. (1977) Biochim. Biophys. Acta 459, 617.

63. Van Best, J.A. (1977) Disseration, University of Leiden.

64. Yamashita, T. and Butler, W.L. (1969) Plant Physiol. 44, 435.

65. Sun, A.S.K. and Sauer, K. (1971) Biochim. Biophys. Acta 234, 483.

66. Yerkes, C.T. (1979) M.S. Thesis, Michigan State University.

67. Etienne, A.L., Boussac, A. and Lavergne, J. (1980) in Proc. 5th Int. Congr. on Photosyn., Halkidiki, in press.

68. Babcock, G.T. and Sauer, K. (1975) Biochim. Biophys. Acta 396, 48.

69. Ben-Hayyim, G. and Avron, M. (1970) Eur. J. Biochem. 15, 155.

70. Bohme, H. and Trebst, A. (1969) Biochim. Biophys. Acta 180, 137.

71. Good, N.E. (1977) in Encyclopedia of Plant Physiology, New Series (Trebst, A. and Avron, M., eds.) Vol. 5, pp. 429-436, Springer-Verlag, Berlin.

72. Nakatani, H.Y., Barber, J. and Forrester, J.A. (1978) Biochim. Biophys. Acta 504, 215.

73. Itoh, S. (1978) Biochim. Biophys. Acta 504. 324.

74. Barber, J. (1972) Biochim. Biophys. Acta 275, 105.

75. Itoh, S. (1978) Plant Cell Physiol. 19, 149.

76. Mukerjee, P. and Mysels, K.J. (1971) Critical Micellar Concentrations in Aqueous Surfactant Systems, National Bureau of Standards, NSRDS-NBS 36, Washington.

77. Saha, S., Outrakul, R., Izawa, S. and Good, N.E. (1971) J. Biol. Chem. 24b, 3204.

78. Handbook of Chemistry and Physics (1968) 49th ed. Weast, R.C., ed.), The Chemical Rubber Co., Cleveland.

79. The Merck Index (1976) 9th ed. (Windholz, M., ed.) Merck and Co., Inc., Rahway.

80. Crofts, A.R. (1967) J. Biol. Chem. 25, 3352.

81. Itoh, S. (1979) Biochim. Biophys. Acta 548, 596.

82. Akerlund, H.E., Andersson, B., Persson, A. and Albertsson, P.A. (1979) Biochim. Biophys. Acta 552, 238.

83. Duniec, J.T. and Thorne, S.W. (1979) FEBS Lett. 105, 1.

84. Itoh, S. and Nishimura, M. (1977) Biochim. Biophys. Acta 460, 381.

85. Overbeek, J.T.G. (1950) in Colloid Science (Kruyt, H.R., ed.) Vol. 1, pp. 115-193, Elsevier, Amsterdam.

86. Barber, J., Mills, J. and Love, A. (1977) FEBS Lett. 74, 174.

87. Itoh, S. (1977) Biochim. Biophys. Acta 548, 579.

88. Laitinen, H.A. and Harris, E.W. (1975) in Chemical Analysis, 2nd edition, pp. 9-16, McGraw Hill, New York.

89. Yerkes, C.T. and Babcock, G.T. (1980) Biochim. Biophys. Acta 590, 360.

90. De Grooth, B.G., Van Gorkom, H.J. and Meiburg, R.F. (1980) Biochim. Biophys. Acta 589, 299.

91. Duysens, L.N.M. (1954) Science 120, 353.

92. Junge, W. and Witt, H.T. (1968) Z. Naturforsch. 23b, 244.

93. Witt, H.T. (1971) Q. Rev. Biophys. 4, 365.

94. Reich, R. and Schmidt, S.R. (1972) Ber. Bunsenges. Phys. Chem. 76, 589.

95. Reinwald, E., Stiehl, H.H. and Rumberg, B. (1972) Z. Naturforsch. 236, 1616.

96. Amesz, J. and De Grooth, B.G. (1976) Biochim. Biophys. Acta 440, 301.

97. Jackson, J.B. and Crofts, A.R. (1969) FEBS Lett. 4, 185.

98. Schmidt, S.R., Reich, H.T. and Witt, H.T. (1971) Naturwiss. 58, 414.

99. Reich, R. and Sewe, K.-U. (1977) Photochem. Photobiol. 26, 11.

100. Sewe, K.-U. and Reich, R. (1977) Z. Naturforsch. 32c, 161.

101. Holten, D., Windsor, M., Parson, W.W. and Gouterman, M. (1978) Photochem. Photobiol. 28, 951.

102. Blankenship, R.E. and Parson, W.W. (19) in Topics in Photosynthesis, Vol. 3 (Barber, J., ed.) Elsevier, Amsterdam.

103. Yerkes, C.T. and Babcock, G.T. (1981) Biochim. Biophys. Acta 634, 19.

104. Gross, E.L. and Hess, S.C. (1974) Biochem. Biophys. Acta 339, 334.

105. Fredericks, W.W. and Jagendorf, A.T. (1964) Arch. Biochem. Biophys. 104, 39.

106. Brand, J.J. (1977) FEBS Lett. 103, 114.

107. Piccioni, R.G. and Mauzerall, D.C. (1976) Biochim. Biophys. Acta 423, 605.

108. Piccioni, R.G. and Mauzerall, D.C. (1978) Biochim. Biophys. Acta 504, 398.

109. Cramer, W.A. and Horton, P. (1975) Photochem. Photobiol. 22, 304.

110. Ikegami, I., Katoh, S. and Takamiya, A. (1970) Plant and Cell Physiol. 11, 777.

111. Fujita, Y. (1974) Plant and Cell Physiol. 15, 861.

112. Renger, G. (1872) Biochim. Biophys. Acta 256, 428.

113. Cramer, W.A., Fan, H.N. and Bohme, H. (1971) Bioenergetics 2, 289.

114. Satoh, K. and Satoh, S. (1972) Plant and Cell Physiol. 13, 807.

115. Maroc, J. and Garnier, J. (1979) Biochim. Biophys. Acta 548, 374.

116. Poole, C.P. (1967) Electron Spin Resonance, pp. 404-410, Interscience Publishers, New York.

117. Ulmgren, P. and Wahlberg, O. (1973) Chem. Scr. 3, 193.

118. Yocum, C.F., Yerkes, C.T., Blankenship, R.E., Sharp, R.R. and Babcock, G.T. (1981) Proc. Nat. Acad. Sci. U.S.A., in press.

119. Lozier, R., Baginsky, M. and Butler, W.L. (1971) Photochem. Photobiol. 14, 323.

120. Izawa, S. (1970) Biochim. Biophys. Acta 194, 328.

121. Izawa, S. and Ort, D. (1974) Biochim. Biophys. Acta 357, 127.

122. Handbook of Biochemistry (1970) 2nd. Edition.

123. Reinman, S., Mathis, P., Conjeaud, H. and Stewart, A. (1981) Biochim. Biophys. Acta 635, 429.

124. Garnier, J. and Maroc, J. (1975) Proc. 3rd Int. Congr. Photosyn., Rehovet (Arnon, M., ed.) pp. 547-556, Elsevier, Amsterdam.

125. Knaff, D.B. (1975) FEBS Lett. 60, 331.

126. Schapendonk, A.H.C.M., Hemrika-Wagner, A.M., Theuvenet, A.P.R., Sang, H.W.W.F., Vredenberg, W.J. and Kraayenhof, R. (1980) Biochim. 19, 1922.

127. Chow, W.S. and Barber, J. (1980) Biochim. Biophys. Acta 589, 346.